1995-12

Drifter-based velocity statistics in the vicinity of the Azores Front

Brown, John E. M.

Monterey, California. Naval Postgraduate School

NAVAL POSTGRADUATE SCHOOL
MONTEREY, CALIFORNIA

THESIS

DRIFTER-BASED VELOCITY STATISTICS IN THE VICINITY OF THE AZORES FRONT

by

John E. M. Brown

December, 1995

Thesis Advisor: Jeffrey D. Paduan

Approved for public release; distribution is unlimited.

REPORT DOCUMENTATION PAGE

Form Approved OMB No. 0704-0188

1. AGENCY USE ONLY *(Leave blank)*	2. REPORT DATE December 1995	3. REPORT TYPE AND DATES COVERED Master's Thesis

4. TITLE AND SUBTITLE DRIFTER-BASED VELOCITY STATISTICS IN THE VICINITY OF THE AZORES FRONT

5. FUNDING NUMBERS

6. AUTHOR(S) John E. M. Brown

7. PERFORMING ORGANIZATION NAME(S) AND ADDRESS(ES)
Naval Postgraduate School
Monterey CA 93943-5000

8. PERFORMING ORGANIZATION REPORT NUMBER

9. SPONSORING/MONITORING AGENCY NAME(S) AND ADDRESS(ES)

10. SPONSORING/MONITORING AGENCY REPORT NUMBER

11. SUPPLEMENTARY NOTES The views expressed in this thesis are those of the author and do not reflect the official policy or position of the Department of Defense or the U.S. Government.

12a. DISTRIBUTION/AVAILABILITY STATEMENT
Approved for public release; distribution is unlimited.

12b. DISTRIBUTION CODE

13. ABSTRACT *(maximum 200 words)*

Surface velocity observations from the Canary Basin of the northeast Atlantic Ocean are studied with emphasis on the region of the Azores Current. Data are based on trajectories of 155 WOCE-standard Lagrangian surface drifters drogued at 15 m depth. Over 52,000 daily velocity estimates are available for the region 45° W, 25° N and 5° W, 45° N for July 1991 through March 1995. A clear view of the mean Azores Current emerges around 34° N with average speeds of ~10 cm/s and eddy kinetic energy ~181 cm^2/s^2. The Current moves eastward beyond Madeira Island to join the southwestward flowing Canary Current. Part of the flow bifurcates west of the Madeira Plateau around 23° W. Eddy kinetic energy in the Canary Current region is only ~80 cm^2/s^2 even though mean speeds are similar to those in the Azores Current.

Zonal averages of the flow show significant convergence in the meridional velocity north of the Azores Front. A time history of the frontal locations is developed based on SST and drifter information. A methodology is presented for converting drifter observations into along-front and cross-front coordinates. Although these frontal locations do not faithfully track the location of the main subsurface front, particularly in the eastern portion of the domain, mean velocities in frontal coordinates support the hypothesis that large-scale subduction of surface waters in this region is concentrated in a region of convergence associated with the Azores Front, particularly from the north.

14. SUBJECT TERMS Drifting Buoys, Lagrangian Drifters, Azores Current, Azores Front, ARGOS System, Eddy kinetic energy, Frontal coordinate system.

15. NUMBER OF PAGES 169

16. PRICE CODE

17. SECURITY CLASSIFICATION OF REPORT	18. SECURITY CLASSIFICATION OF THIS PAGE	19. SECURITY CLASSIFICATION OF ABSTRACT	20. LIMITATION OF ABSTRACT
Unclassified	Unclassified	Unclassified	UL

NSN 7540-01-280-5500

Standard Form 298 (Rev. 2-89)
Prescribed by ANSI Std. 239-18 298-102

Approved for public release; distribution is unlimited.

DRIFTER-BASED VELOCITY STATISTICS IN THE VICINITY OF THE AZORES FRONT

John E. M. Brown
Lieutenant, United States Navy
B.S./B.A. Purdue University, 1987

Submitted in partial fulfillment
of the requirements for the degree of

MASTER OF SCIENCE IN METEOROLOGY AND PHYSICAL OCEANOGRAPHY

from the

NAVAL POSTGRADUATE SCHOOL
December 1995

Author: [redacted]
John E. M. Brown

Approved by: [redacted]
Jeffrey D. Paduan, Thesis Advisor

[redacted]
Robert H. Bourke, Second Reader

[redacted]
Robert H. Bourke, Chairman, Department of Oceanography

ABSTRACT

Surface velocity observations from the Canary Basin of the northeast Atlantic Ocean are studied with emphasis on the region of the Azores Current. Data are based on trajectories of 155 WOCE-standard Lagrangian surface drifters drogued at 15 m depth. Over 52,000 daily velocity estimates are available for the region 45° W, 25° N and 5° W, 45° N for July 1991 through March 1995. A clear view of the mean Azores Current emerges around 34° N with average speeds of ~10 cm/s and eddy kinetic energy ~181 cm^2/s^2. The Current moves eastward beyond Madeira Island to join the southwestward flowing Canary Current. Part of the flow bifurcates west of the Madeira Plateau around 23° W. Eddy kinetic energy in the Canary Current region is only ~80 cm^2/s^2 even though mean speeds are similar to those in the Azores Current.

Zonal averages of the flow show significant convergence in the meridional velocity north of the Azores Front. A time history of the frontal locations is developed based on SST and drifter information. A methodology is presented for converting drifter observations into along-front and cross-front coordinates. Although these frontal locations do not faithfully track the location of the main subsurface front, particularly in the eastern portion of the domain, mean velocities in frontal coordinates support the hypothesis that large-scale subduction of surface waters in this region is concentrated in a region of convergence associated with the Azores Front, particularly from the north.

TABLE OF CONTENTS

LIST OF FIGURES

ACKNOWLEDGMENT

The author would like to thank his Thesis Advisor, Prof. Jeffrey D. Paduan, for his outstanding support and counsel. It has been an awesome experience working with such a talented and ambitious investigator. He kept me motivated and focused on my objectives when I felt lost and problems started to become insurmountable.

An incredible debt of gratitude is owed to Mike Cook, resident MATLAB expert and all-round cool guy, for his rescuing me from the depths of programming despair! Half this thesis belongs to him for the amount of assistance he gave me in debugging my code and preparing figures. No matter what government shutdowns and furloughs may say, Mike Cook is definitely an "essential" person!

Remote sensing assistance and guidance came from Prof. Toby Garfield, of the Oceanography Department, and Prof. Phil Durkee, of the Meteorology Department. It was from their classes that I became excited in pursuing this multi-discipline thesis. Special thanks goes to University of Miami technician, Geoffrey Samuels, for preparing the GAC composite image data base and drifter trajectory file.

A final acknowledgment goes to the Office of Naval Research for providing the financial support for the SUBDUCTION Experiment and related activities.

I. INTRODUCTION

A. BACKGROUND

The advent of satellites has opened up a whole new dimension in our ability to observe, study, and acquire detailed synoptic information about the Earth's land, sea, and atmosphere environments. The development of satellite-tracked drifting buoys has enabled us to gain basic information on ocean surface currents and other properties and how they vary on a regional basis. The combination of these two technologies has given the oceanographic research community powerful new tools to analyze and describe many oceanic features remotely. Simultaneous wide area coverage is now possible, thus saving the great expense of ship operations. However, remotely sensed data from satellites and drifting buoys can only provide information about the surface of the ocean and its uppermost mixed layer.

The depth of this mixed layer varies with season and location but is on the order of tens of meters thick. It is here that momentum and buoyancy are exchanged between the atmosphere and the deeper ocean below. Many oceanographic field programs have been conducted with the specific aim of describing the growth and decay of the mixed layer under various air-sea interactions (e.g., Tabata, 1965; Davis et al., 1981; Paduan and deSzoeke, 1986; Paduan et al., 1988). Even more studies have attempted to model the evolution of mixed layer depth, temperature, and velocity. The simplest of these models consider bulk mixed layers in which velocity and temperature are constant. Parameterizations of turbulent kinetic energy at the mixed layer base are then responsible for mixing (e.g., Kraus and Turner, 1967; Niiler and Kraus, 1977). Other models use Richardson number dependent mixing (e.g.,

Pollard et al., 1973; Price et al., 1986). In all cases, one-dimensional assumptions limit the usefulness of these models over long time periods.

Important links between the processes in the mixed layer and deep ocean circulation have been found and modeled theoretically by Luyten et al. (1983) (Figure 1.1a). These links occur in specific ocean areas where deep (subsurface) isopycnals are known to intersect the bottom of the mixed layer or the sea surface. This process is known as outcropping. The northeast Atlantic Ocean is an area where deep isopycnals extending from points south of the region outcrop at the surface. This observation is critical in light of the theory of Luyten et al. (1983). They have shown how south of the outcropping latitude, water motion within isopycnal layers can be predicted based on the conservation of potential vorticity, which is determined by the layer thickness and latitude. Thus, given a distribution of deep isopycnal layers, the corresponding deep ocean circulation can be simply modeled.

The collection of deep ocean density data is quite difficult to obtain, however. A more practical starting point would be based on observations at the ocean surface, particularly in the forcing regions of the outcropping isopycnals. If a predictive link can be made between mixed layer processes in the outcrop region and the thickness of deep isopycnals, then the deep ocean circulation can be forecast without the need for deep ocean in situ measurements.

B. AREA OF INTEREST

Understanding the link between mixed layer processes and the distribution of deep isopycnals in an outcrop area was the purpose of an oceanographic field program sponsored by the Office of Naval Research (ONR) in the Canary Basin region of the northeast Atlantic.

The program was referred to as the SUBDUCTION Experiment. The name reflects the belief that, according to the theory of Luyten et al. (1983), water from the mixed layer must be descending, finding its way into the upper thermocline in this area, and setting the thickness properties of isopycnal layers. This process of downwelling water making its way into the thermocline is referred to as subduction (Figure 1.1b.). In other words, subduction can be thought of as the ventilation of mid-depth waters. (In this context, thermocline refers to the permanent thermocline below 100 m and not to the seasonal thermocline, which is expected to incorporate and release water from the mixed layer during the course of the seasonal cycle.)

Many time series and survey measurements were made in the SUBDUCTION region, which extends from the Azores Islands southward to the Canary Islands and from the west coast of North Africa westward to the Mid-Atlantic Ridge. For the purposes of this thesis our area of interest is defined by a box extending from 25° N to 45° N and 5° W to 45° W (Figure 1.2).

The Canary Basin is a likely area for subduction because the region of interest spans the latitude band where, climatologically, wind stress curl is negative as a result of westerlies in the northern portion of the area giving way to easterlies in the southern portion of the area. This wind forcing produces Ekman convergence and downwelling currents. Therefore the surface wind-driven currents are expected to be convergent on average. Furthermore, most of the convergence is expected to result from north-south currents given the smaller east-west variability in the wind forcing. In such an area, zonal (east-west) averages of current should show a convergent pattern as a function of latitude.

The process of subduction is not fully understood. One major question that exists is whether the process is a distributed one spread over the entire region or whether the process is concentrated at oceanographic fronts as modelled by Niiler and Reynolds (1984) (Figure 1.3). A major oceanographic front, the Azores Front, is present in the SUBDUCTION region. Deployments of drifters were concentrated along latitude lines north and south of the frontal region in order to detect the presence of frontal convergence and possible asymmetry in the mean currents and eddy characteristics relative to the front.

C. AZORES FRONT

The path of the Gulf Stream appears to split into two branches, one turning north to form the North Atlantic Current (NAC) and the other turning southeast and south to the Newfoundland Rise. This branch of the subtropical North Atlantic gyre is the source region for the Azores Current (AC). The Azores Current flows across the Canary Basin at roughly 34° N and has three main southward recirculation branches which join the westward flowing North Equatorial Current (NEC). These branches, which vary seasonally and interannually (Stramma and Siedler, 1988), are found just east of the Mid-Atlantic Ridge, in the central Canary Basin, and near the western coast of North Africa (Klein and Siedler, 1989) (Figure 1.4).

Associated with the Azores Current is an oceanic front, the Azores Front. This narrow subtropical front (between 50 - 100 km) is characterized by strong Ekman convergence and a relatively large horizontal thermohaline gradient (Stramma and Müller,

1989). Temperature gradients of approximately 5 °C over a range of 200 km can be seen in the main subsurface front in accordance with geostrophic/thermal wind balance. Hydrographic surveys show salinity gradients to be on the order of 0.2 ‰ over 200 km (Gould,1985). Warm, salty water is found to the south, while colder, fresher water is found to the north. Thus, salinity is somewhat compensating in the density gradient. Historically, the front has been observed between 32° N and 36° N (Krauss and Käse, 1984; Gould, 1985; Stramma and Müller, 1989) (Figure 1.2). This region of the front is referred to as the Frontal Zone (FZ). West of 30° W, the front is limited to the south by the 18 °C water of the Sargasso Sea. Little variation of Mediterranean water properties through the front is noted. East of 30° W, the front is no longer bounded by the 18 °C water, and Mediterranean water has been observed only on its northern side (Gould, 1985).

Surveys in 1981 show that the frontal structure penetrates to a depth of 2000 m, with the main water contrasts being confined to the upper 400 m of the water column. In the mid-summer, the front is well-capped by a strong seasonal thermocline, while in the winter conditions permit a surface thermal expression (persistent cloud cover can prevent detection by satellite infra-red sensors) (Gould, 1985). However, it is doubtful whether a significant seasonal signal penetrates to depths greater than 300 m in the frontal area (Robinson et al., 1979).

Mesoscale circulations in the Azores-Madeira region are dominated by the meandering of the Azores Front/Current and its associated eddies (Käse and Siedler, 1982; Käse et al., 1985, 1986). A series of surveys conducted in 1980 by the Soviets also confirm the SW

Azores area to be one of high mesoscale activity and as a source for eddies which propagate into the western basin of the North Atlantic. They found that the interaction of near-surface flows with the complex bathymetry may be an important factor in the eddy generation process (Kort, 1981; Kort et al. 1983). Others have found some numerical and observational reasons to think that part of this mesoscale variability may result from the baroclinic instability of the Azores Current (Käse et al., 1985; Kielmann and Käse, 1987; Spall, 1990).

Measurements of mesoscale variability were made by Richardson (1983) who calculated the eddy kinetic energy (EKE) distribution for 2° lat/long boxes from satellite-tracked drifting buoys. His analysis showed high energy (> 200 cm^2/s^2) around 40° N, 40° W and at 32° - 34° N, 32° - 34° W, close to the frontal zone. The surface currents implied by these values are 15 - 20 cm/s.

Precise surveying of the Azores Front has been recently analyzed by Rudnick and Luyten (1995). They used the tracers of potential density and potential vorticity to show dense water from the north side of the front sliding down beneath the surface outcrop. Their horizontal velocities were nearly parallel to the isopycnals, indicating that the time rate of change and vertical advection must be small. The importance of vertical circulation at fronts has been demonstrated by numerous studies. Pollard and Rieger (1990; 1992) also examined vertical circulation through tracers and by solution of the omega equation. Their studies of the subtropical front in the western North Atlantic have inferred vertical velocities as strong as 40 m/day. Rudnick (1995) uses one of the first fully three-dimensional versions of the omega equation (assuming quasigeostrophic dynamics) to solve for vertical velocities and

rates of subduction at the Azores Front. Maximum vertical velocities on the order of 2 x 10^{-4} m/s (approximately 20 m/day) were found at a depth of 200 - 300 m. The resulting ageostrophic circulation cells were found to be potentially important mechansisms of stratification and subduction in the upper ocean of the Azores Front.

Environmentally, the Azores region is an area of great biological productivity evidenced by its rich fishing ground (Parfit, 1995). The frontal concentration of subducting waters is hypothesized to be responsible for the vertical transport of large volumes of nutrients and oxygen, and associated planktonic life, to deeper depths below the euphotic zone (1% light level). Previous studies conducted off the northern California coast as part of the Coastal Transition Zone (CTZ) program show the occurrence of layers of high concentrations of phytoplankton at these depths due to frontal subduction (Washburn et al., 1991; Kadko et al., 1991). These studies support the frontal subduction hypothesis by a variety of physical, biological, and geochemical indicators including ^{222}Rn, dissolved O_2, and chlorophyll. Kadko et al.'s (1991) geochemical data indicate that this transport was rapid with vertical velocities on the order of 20 - 30 m/day. These vertical motions are similiar to the magnitudes measured by Rudnick (1995). Vertical subduction is evidenced by high levels of chlorophyll, deficiencies of ^{222}Rn, and a local maxima of dissolved oxygen. Thus, we can safely assume these same physical processes are happening along the Azores Front and can explain its biological productivity.

In subsequent analyses, the drifter data are divided into regions as a function of latitude. For continuity with Giannetti (1993), zonal averages are investigated and the Frontal Zone is considered to extend between 33° N and 35° N.

D. APPROACH, SCOPE, AND OBJECTIVES

This thesis is a follow-on study to that conducted by Giannetti (1993). His work concentrated on characterizing the mean currents of the mixed layer in the SUBDUCTION Experiment. He provided a complete suite of Lagrangian statistics which would be useful to numerical modelers needing such statistics to parameterize and validate global ocean circulation models. Data collected from 36 surface drifters deployed from July 1991 to May 1993 in the Northeast Atlantic Ocean were analyzed. Statistical parameters calculated included mean currents, mean eddy kinetic energies, mean Lagrangian integral time and length scales and mean diffusivity. Investigators from Scripps Institution of Oceanography (SIO) are also actively developing a set of drifter statistics using a Cartesian latitude/longitude box binning process (Paduan et al., 1995). They are using National Meteorological Center (NMC) weekly mean sea surface temperature (SST) data to calculate vertical heat fluxes and horizontal advection.

For this thesis a larger and longer drifter data set was analyzed than that of Giannetti (1993). Seasonal deployments of five to ten drifters continued to be done as part of the SUBDUCTION experiment through 1993. The drifter deployments were conducted within the context of the larger-scale World Ocean Circulation Experiment (WOCE) Surface Velocity Program (SVP). A larger release of 40 surface drifters was made in October 1993 in conjunction with the French SEMAPHORE Experiment. In all, over 52,000 buoy days (based on daily interpolated drifter positions) are available for analysis from a total of 155 separately deployed drifters. Chapter II describes these drifters and their dataset.

The problem of using at Cartesian box averages for drifter statistics is apparent when the oceanographic feature of interest, the Azores Front, moves in and out of the boxes. Separating out eddy kinetic energy (EKE) due to actual eddies, jets and meanders versus EKE due to the migration of the front becomes very difficult. This migration can effectively "contaminate" data meant to describe motion relative to the front. Computed areas of convergence or divergence, positive or negative vorticity are more suspect since frontal spatial evolution could account for all the derived statistics. Motion due to drifters following converging, subducting currents would be blended in these values. Results from this method of averaging could then be biased.

The original approach taken for this thesis was to examine the spatial and temporal evolution of the Azores Front using weekly composited satellite images of SST, drifter trajectories, and isolated hydrographic surveys. The goal was to see if the combination of sea surface temperature gradients, "characteristic" temperatures, and drifter trajectories could be used to track the front's location. Our goal then was to produce an orthogonal curvilinear coordinate system to be used in computing multi-year statistics. Given the location of the Azores Front, along-front and cross-front velocities of the drifters should provide a clearer, more focused picture of eddy kinetic energy, convergence, subduction, and other associated processes. An estimated frontal location was derived by combining the standard 1° by 1° weekly mean SST product from NMC with interpolated drifter velocities for drifters in the area during the same week. This rough frontal location was then used to calculate the multi-year statistics.

This thesis is organized as follows: Chapter II describes the Lagrangian drifters and the processing of the dataset they produced. Chapter III covers aspects of oceanographic satellite data and image processing used to obtain the SST dataset. Chapter IV focuses on how the Azores Front was located and fixed. It also details the methodology for producing a frontal, curvilinear orthogonal coordinate system given an established front. Chapter V provides the results and interpretation of the statistical analysis. Conclusions and recommendations for further work are presented in Chapter VI.

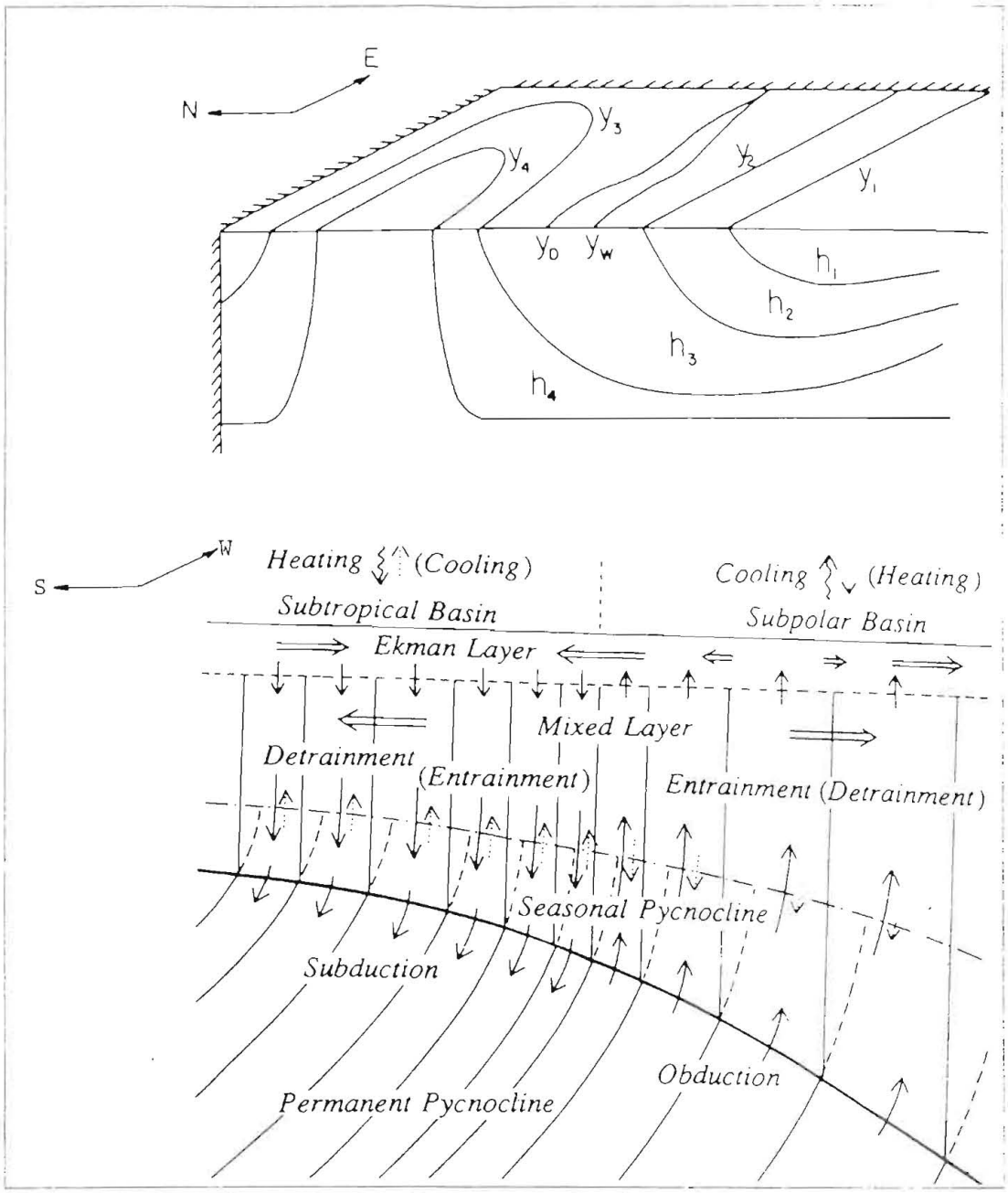

Figure 1.1a (top) Schematic of the five layer ventilated thermocline model, after Luyten et al. (1983). Outcrops of the deep layers are indicated as y_1, y_2, y_3, and y_4. The zero wind stress curl is y_w, the zero Sverdrup forcing (D_0^2) is y_0. Looking east. From Talley (1985).

Figure 1.1b (bottom) Schematic of subduction in the subtropical gyre and obduction in the subpolar gyre. Looking west. From Qiu and Huang (1995).

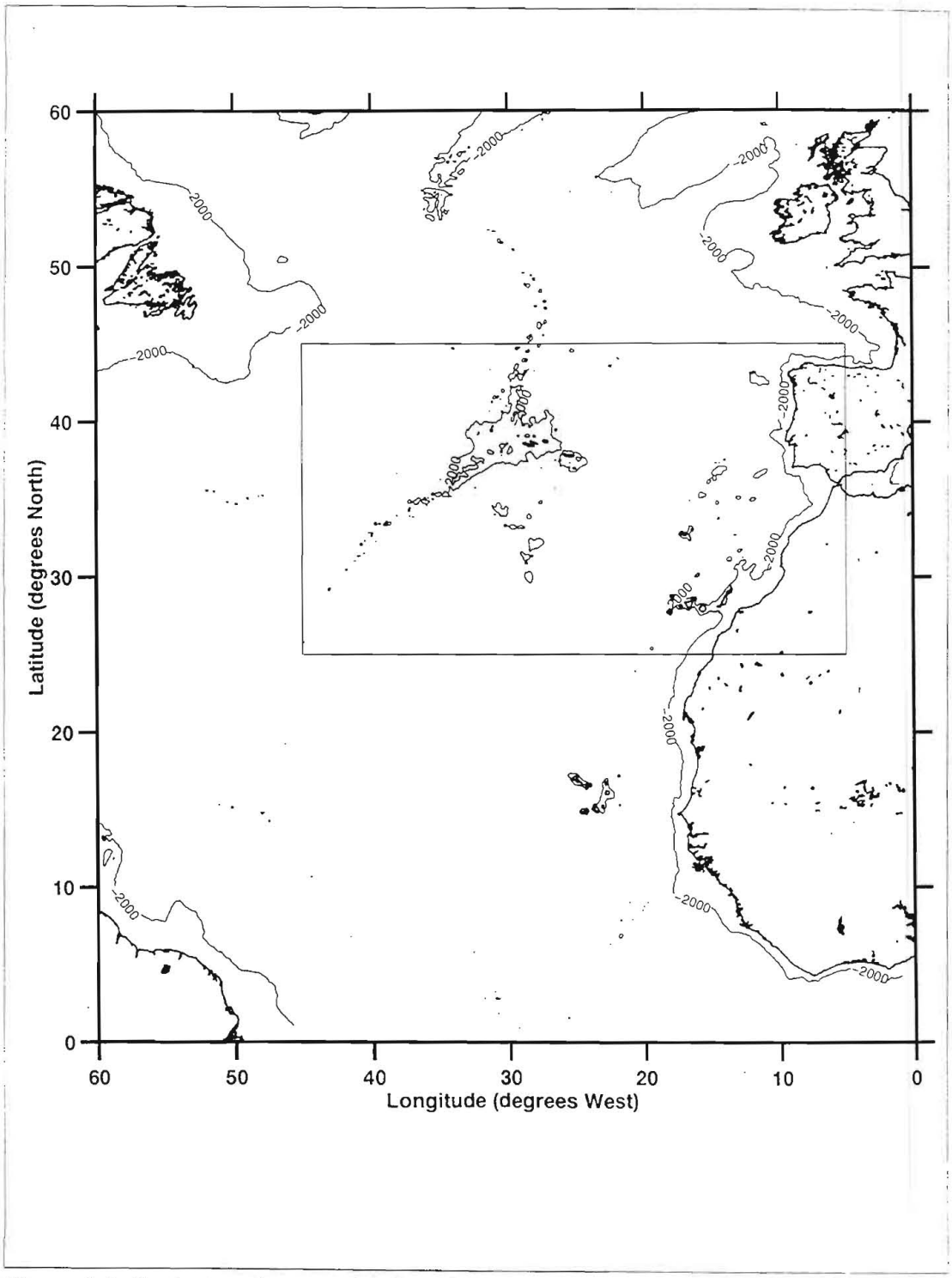

Figure 1.2 Study domain area with 0 and 2000 m isobaths. Box denotes area used in analyses.

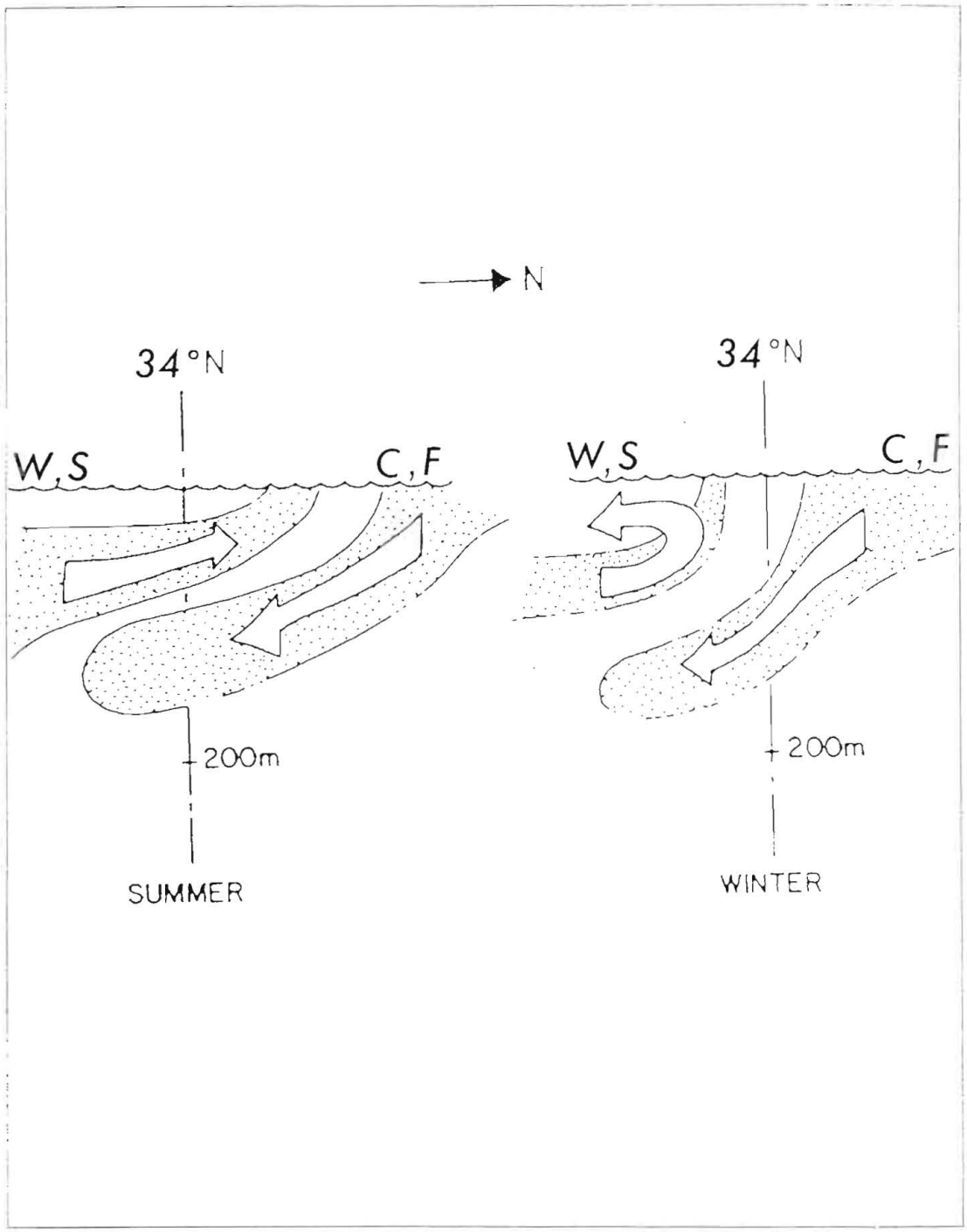

Figure 1.3 Schematics of the Summer (left) and Winter (right) circulation patterns in the vertical and meridional direction. Hypothesized circulation around subtropical front adapted from Niiler and Reynolds (1984) showing cold, fresh (C,F) water subducting beneath warm, salty (W,S) water.

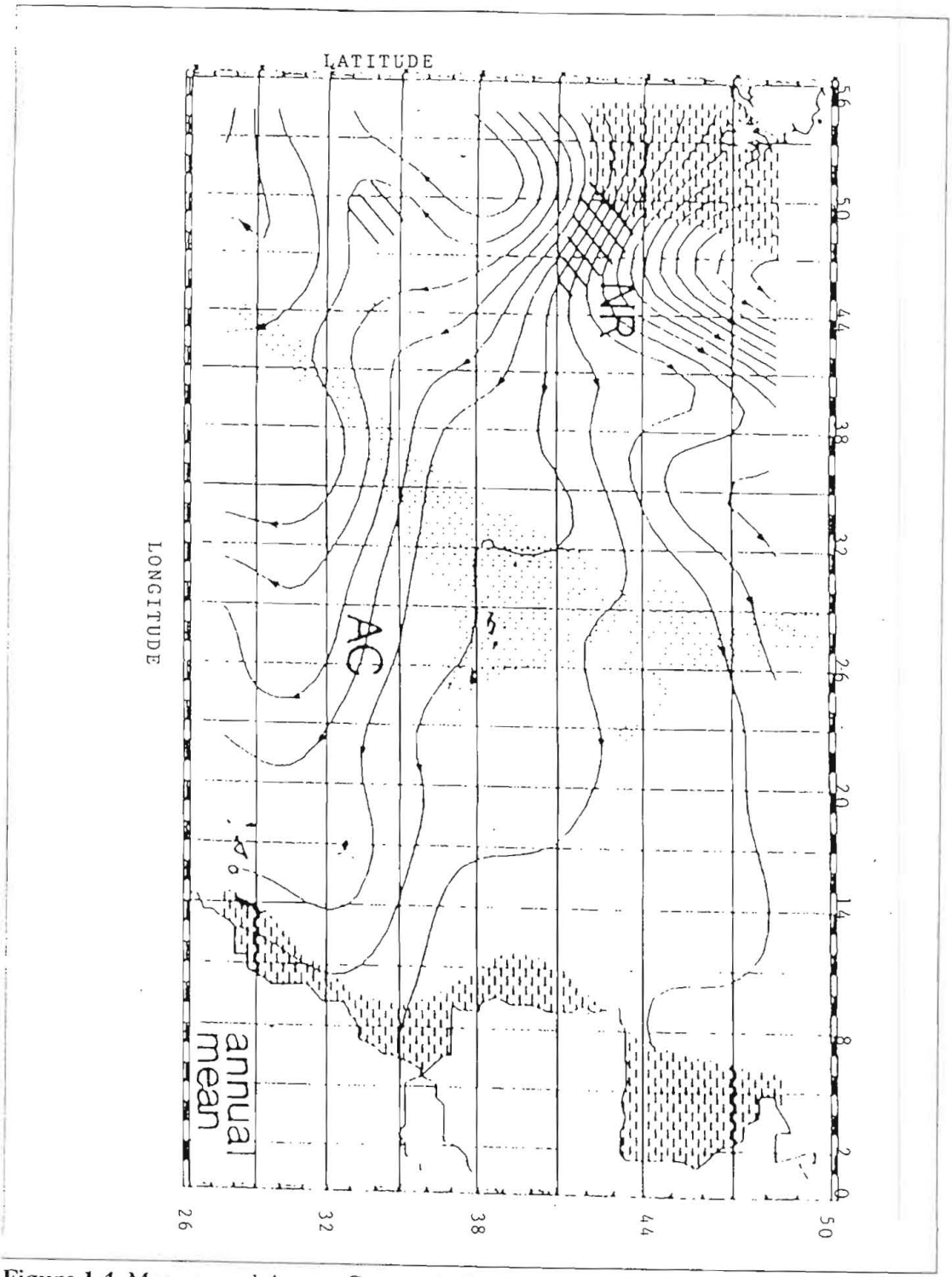

Figure 1.4 Mean annual Azores Current (AC) being fed from the North Atlantic Current over the Newfoundland Rise (NR). From Klein and Siedler (1979).

II. DRIFTER DATASET

A. SATELLITE-TRACKED SURFACE DRIFTERS

Low earth-orbit satellites with positioning sensors have made it possible to remotely track the position of drifting buoys on the surface of the ocean. The time rate of change of drifter position gives estimates of the surface currents. Such measurements can be used to gain new information about the ocean mixed layer. Current measurements from drifting buoys are particularly well-suited to provide spatial information, although they usually do not provide measurements at more than one depth (Paduan and Niiler, 1995). Early deployments of satellite-tracked drifters provided basic information about surface currents and their variability in many regions (Kirwan et al., 1976; Kirwan et al., 1978; McNally, 1981; Krauss and Böning, 1987; Richardson, 1983).

More recently, it has been shown that the performance of drifting buoys as water followers depends critically on the design of the instrument (Niiler and Paduan, 1995). Niiler et al. (1987, 1995) describe actual measurements of slip past drogue elements for various drogue designs and wind conditions. They show that both the shape of the drogue and its drag area relative to the drag area of the surface float plus tether are important parameters. The shape of the drogue must be rigid and symmetric so that the drogue does not produce an airfoil effect that could move it at an angle to the direction of the current. The drag characteristics of a drifter are characterized by the drag area ratio, R, which gives the ratio of the drag of the drogue to the combined drag of the surface float plus tether. For properly constructed drifters with drag area ratios greater than 40, the current slip past the drogue (the

error) is less than 2 cm/s for wind speeds up to 20 m/s. Early-generation drifters with low drag area ratios (R $<$ 10) had significant downwind slip, which led to some incorrect interpretations of the Ekman response in the mixed layer (McNally, 1981; McNally et al., 1989). Niiler and Paduan (1995) show that properly constructed drifters approximate much more closely the theoretical motion in an Ekman boundary layer where water moves at right angles to the wind.

The primary goal of drifter measurements during the SUBDUCTION and SEMAPHORE Experiments was to study the currents in the Ekman layer and, with the advantage of many thousands of observations over several years, attempt to observe the expected surface convergence during a period when extensive meteorological and deeper hydrographic and float measurements were obtained. Drifters are a good way to attempt this difficult measurement because they have much shorter integral time scales than do moored instruments and they are also relatively inexpensive. In fact, since late 1990, the half-life of drifters has increased to 400 days. Projected costs in 1996 will be about $2600 per unit and by 1998, $2200 per unit (Niiler, 1995). These factors mean that a large number of independent observations of surface velocity can be obtained from an array of drifting buoys. Large numbers of observations are required to measure mean currents and their divergence field in the mixed layer because of the large contributions by mesoscale eddies. (Mixed layer velocity variability is usually many times greater than the mean current.)

The instruments used consist of ARGOS-tracked surface drifters with "holey sock" drogue elements. They were constructed according to specifications of the WOCE SVP. "The WOCE/TOGA Lagrangian Drifter Construction Manual" (Sybrandy and Niiler, 1991)

describes the drifter manufacturing procedures, which are now used in at least ten countries. These drifters have a drag area ratio of 41. Figure 2.1 shows a scale drawing of the drifter illustrating the relative sizes of the surface and subsurface floats and the drogue element. The midpoint of the drogue element is 15 m below the water line. The surface float houses the antenna, ARGOS transmitter, batteries, and a through-hull sea surface temperature sensor. A drogue-on sensor was also mounted in the surface floats to detect whether the drogue remained attached or not. The sensor failed to produce useful data for these drifters during the first year of the experiment. The sensor did work successfully in the later years. For this first year, then, no direct measure of whether the drogues remained attached or not is available. For the purposes of this study, drifter position data from that first year was treated as drogued data. Indirect evidence, such as the overall lack of downwind motion, suggests that the drogues were, in fact, in place during the whole period. Position data from later years for which drogues were known to be missing were not used.

B. DRIFTER DATA COLLECTION AND LOCATION

1. Overview of ARGOS System

The drifters were remotely tracked using the ARGOS Data Collection and Location System (DCLS). The ARGOS DCLS provides an operational satellite-based means to collect, locate, and disseminate environmental data. Development of the system was achieved through a cooperative effort among Centre National d'Etudes Spatiales (CNES), NOAA, and NASA and became operational in October 1978. The ARGOS DCLS is administered by Service Argos, Inc., within the United States, and by CLS/Service Argos, S. A., in France.

The ARGOS DCLS has four subsystems:

(1) The Platform Transmitter Terminal (PTT) used on the surface drifter .

(2) The Data Recovery Unit (DRU) package aboard two NOAA polar orbiters.

(3) The telemetry receiving stations, data ingest and decommutation system, and communication links to the data processing centers.

(4) Two data processing centers, located at Landover, Maryland, and Toulouse, France. Each center processes platform location and sensor data and disseminates the data through communication networks.

There are two basic PTT categories: the locator type, equipped with good quality oscillators used for both location and data collection; and the data collection only type, equipped with lower quality oscillators. The characteristics of ARGOS PTT can be found in the Service Argos manual. The accuracy of PTT positions depends on many factors, including the stability of the transmitter oscillator, but is usually better than 0.5 km (Rao et al., 1990).

The space segment of the ARGOS DCLS consists of two NOAA polar-orbiting satellites. Onboard DRUs receive messages transmitted by PTT within the satellite's area of coverage (a swath approximately 2500 km either side of the subsatellite track). Each satellite is capable of making its own determination of drifter position each time the drifter is in view of the sensors for a sufficient length of time (on the order of minutes). Doppler shift of transmitter frequency with time observed by the satellite, together with accurate knowledge of the satellite's position, places the drifter within a half cone of possible locations with the

satellite at the apex of the cone. The intersection of that location cone with the ocean surface limits the possible locations to just two positions symmetrically located with respect to the satellite ground track (Figure 2.2). Prior known locations plus a range of realistic drifter velocities is used to resolve the final ambiguity.

Since there are normally two satellites in operation, a minimum of four positions per day are obtained from a PTT in Equatorial regions and up to 28 positions per day in polar areas. In temperate latitudes, such as the Canary Basin domain, eight positions per day are typical. This assumes a full time operating PTT.

Each time a satellite passes over one of three telemetry receiving stations (Wallops Island, Virginia; Fairbanks, Alaska; and Lannion, France) all recorded data are transmitted. All ARGOS data received by these stations are sent via the NOAA/NESDIS facility at Suitland, Maryland, to the ARGOS Data Processing Centers at Toulouse and Landover where the following operations are performed (Figure 2.3):

(1) Decoding of PTT messages and conversion of data into physical units.

(2) Very accurate computation of satellite orbits.

(3) Computation of PTT positions from orbital data and Doppler shifts.

(4) Computer storage of all results for user access.

Since each transmission is also rebroadcast by the satellite as soon as it is received, anyone with a downlink receiver within the range of the satellite can receive data from drifter PTTs in view of the satellite at the same time.

Data collected by the ARGOS DCLS is then obtained from Service Argos. They are available on computer files accessible by telephone, telex, or communication networks,

generally within four hours after receipt of data. Processed data are available on computer compatible tapes, print outs, or floppy disks every two to four weeks. Formatted data are distributed over the Global Telecommunication System (GTS). The user can access three types of files:

(1) The "AJOUR" file containing the past 24 hours of location and sensor data for each PTT.

(2) The "TELEX" file, containing, in chronological order for the past 100 hours, one sensor message and corresponding location per satellite pass for each PTT.

(3) The "DISPOSE" file containing, in chronological order for the past 100 hours, all location data and all sensor messages for each satellite pass and each PTT. (Rao et. al., 1990).

2. Global Drifter Center and Data Assembly Center

Lagrangian surface drifter data is processed further once it is collected by the ARGOS DCLS. From Service Argos in both Landover and Toulouse, drifter data are sent monthly to the newly consolidated Global Drifter Center (GDC) and Data Assembly Center (DAC) at the NOAA Atlantic Oceanographic and Meteorological Laboratory (AOML) in Miami, Florida. The GDC is responsible for shipping and deploying the drifters, while the DAC is responsible for creating a research quality dataset of surface velocity and SST. Data from 26 different ARGOS programs, 25 scientists, and 12 countries are presently acquired at the DAC (Bushnell, 1995).

Raw data (from Service Argos on nine track tapes) are quality controlled by removal of outliers, primarily by using rate of change constraints. A uniform time series of position and sensor data at six hour time steps is then created using optimum interpolation (OI) logic.

Uncertainty estimates are included for each value (Bushnell, 1995). Data processing procedures and the optimum interpolation logic are more fully described by Hansen and Poulain (1995). Finally, the DAC provides the dataset to the Canadian Marine Environmental Data Service (MEDS) for permanent archive and public dissemination.

3. Argos Drifter Error

Error in drifter position data occurs from two sources: 1) error in the positions derived from the ARGOS system as described above and 2) error due to slippage of water past the drogue element. This latter error is discussed in the next section. Errors in the ARGOS positions themselves are well documented. The operators of the system specify the accuracy of position fixes in terms of the standard deviation of positions about a known point. This means that, assuming a normal distribution of the error, 68% of the calculated values fall inside a radius equal to the standard deviation from the real position. Each fix includes an indicator of the position confidence based on the length of time the satellite was able to track the drifter on the ocean surface. These indicators (classes) are 1, 2, or 3. The standard deviations for these classes are 1000 m, 450 m, or 150 m, respectively.

The data in this study is derived from positions with a mixture of location classes. An opportunity to estimate the position accuracy and precision for the geographical location of this study was given by a drifter that apparently stuck on land (São Jorge Island), or was abandoned on land. It continued to broadcast for over one year from the same location. The standard deviations of the locations were 383 m in the east-west direction and 359 m in the north-south direction relative to the year-long mean position (Giannetti, 1993). These values

provide the best measure of the ARGOS system position accuracy for the dataset used in this study.

C. QUASI-LAGRANGIAN NATURE OF THE DRIFTERS

The second source of error in the drifter position data is caused by the slippage of water past the drogue elements. This is due to the effect of wind and waves on the surface float and tether components as well as the effect of vertical shear on the drogue itself. For the particular drifters used in this study, field tests have been conducted to calibrate the slip past the drogue elements as a function of wind speed and velocity shear (Niiler et al., 1987; 1995). The calibration was accomplished by attaching current meters to the top and bottom of the drogue elements for various sizes of drogues under varying wind conditions. Niiler et al. (1995) present the best-fit model for correcting drifter motion as a function of wind speed, shear, and the drifter drag area ratio. For the holey-sock drifters used in this study, the velocity error due to slippage past the drogue element is less than 2 cm/s for wind speeds up to 20 m/s. For typical wind speeds the error due to slip is less than 1 cm/s, which is comparable to the error of modern moored current meters (Weller and Davis, 1980). It is important to note that earlier-generation drifters with small drag ratios experienced significantly more error due to slip (Niiler and Paduan, 1995). The drifters used in this study are also quasi-Lagrangian tracers of water motion because they are confined to one level (approximately 15 m) and do not follow water motions in three dimensions. This two-dimensional aspect of the instruments does not, however, affect the study of horizontal currents.

D. OVERVIEW OF DATA RETURNED

1. Spatial Coverage

A summary of the spatial coverage obtained by the drifter data is presented in Figure 2.4, which shows the trajectories of all SUBDUCTION and SEMAPHORE drifters passing through the study area during the period investigated in this study. One hundred and fifty-five separate drifters are represented in the figure. The trajectories are based on daily interpolated positions. (The interpolation procedure is described below.) The drifter coverage extends approximately over a 1000 km x 1000 km portion of the northeast Atlantic Ocean between the Azores Islands and the Canary Islands. The distribution peaked in the vicinity of 34° N and 25° W (Figure 2.4). The distributions are more concentrated along a southwest axis extending from this center to 25° N and 35° W. The non-uniform nature of the data distribution could effect drifter-derived velocity averages in the presence of turbulent diffusion. This error is known as array bias and is described in detail in Davis (1993). This thesis does account for array bias. Paduan et al. (1995) compensate for array bias using this same drifter dataset and find it to be typically < 2 cm/s for the mean current calculation.

Initial deployment locations for the 155 drifters analyzed in this study are shown in Figure 2.5. Most of these instruments were deployed by volunteer observing ships traveling, primarily, between Miami and Gibraltar. The deployment locations are scattered throughout the data area but there are also high concentrations along latitude lines on the northern and southern side of the climatological latitude of the Azores Front.

Mesoscale eddies are reflected in the drifter trajectories of Figure 2.6. Despite this eddy activity, the striking part of the trajectory data is that very few drifters moved out of the area of the Canary Basin, even though they drifted within the region for up to two years. This is in sharp contrast to observations based on earlier-generation drifters that were less effective water followers.

2. Temporal Coverage

Drifters were released at various times during the SUBDUCTION field program. They were generally deployed in groups of four or five from the volunteer ships. A larger release of 40 surface drifters was made from research vessels in October 1993 in conjunction with the French SEMAPHORE Experiment. The temporal extent of each of the drifters is shown in Figure 2.7. Also shown in Figure 2.7 is the total number of daily observations available each day. The deployment groupings of four or five drifters are clearly visible in the figure. Many of the instruments operated for a very long period with 73 drifters operating for at least 15 months. At the end of the study period (31 March 1995), 40 drifters were still operating within the study area.

In subsequent analyses, drifter data is divided into seasonal groupings in a manner similar to that described for the regional groupings by latitude. The number of daily observations available in each month is also shown in Figure 2.8. A continuous increase in available data is seen for the first nine months, after which the number of daily observations peaks by Autumn 1993 at around 1800. The seasonal grouping of data was actually done by combining data for a given season from all available years. Figure 2.8, shows the number of

available daily observations by month where multiple years have been combined. A fairly uniform number of observations is available for each month except for the month of June, which is under-represented because the observations used in this study began in July 1991 and ended in March 1995. The seasonal groupings were defined as three-month periods and referred to as Winter (Jan - Mar), Spring (Apr - Jun), Summer (Jul - Sep), and Autumn (Oct - Dec). The dataset covers four seasons for each of the three month-long seasonal divisions used in the study. Figures 2.9 shows the spatial distribution of observations for each of the seasons.

E. CONSIDERATION OF THE TRANSMITTER DUTY CYCLE

The utility of drifting buoy measurements as used in this study derives from the large number of independent velocity samples that can be obtained for a reasonable cost. Although the technological trend since the advent of satellite-based tracking has been toward less expensive and longer lived drifters, the tracking costs of the ARGOS system — as it has been operated to date — have remained relatively high. The cost to track one drifter for one full year is approximately $4000, which is larger than the approximate $3000 cost of the instruments themselves. In order to reduce tracking costs, the transmitters in these drifters were programmed to operate for 24 hours and then stop operating for 48 hours. This transmission schedule incurs charges of one third the full-on rate (approx. $1300/year) at the scientific expense of higher frequency observations of the surface currents.

During the day in which the drifter transmitters operate, several location fixes are typically received. Giannetti (1993) shows for a subset of the data a histogram of the number

of fixes per day during the days when the transmitters were operating for the SUBDUCTION drifter dataset available at that time. Typically, eight position fixes were received during a 24-hour period when the transmitters were operating. Giannetti (1993) also shows a histogram of the time separation between fixes for the dataset. Time between fixes were usually less than six hours. The most common separation was one and a half hours. Peaks in the histogram for time separations around 48 hours were found due to the preprogrammed 48-hour shutdown mode. Even though several locations per day are received when the transmitter is on, it is only possible to resolve motions with periods greater than 48 hours due to large gaps in the location data. All analyses in this study are confined to these "low-frequency" motions. This excludes, for example, motions at the inertial period, which is about 15 hours at the latitudes of this study.

F. DESCRIPTION OF THE INTERPOLATION PROCEDURES

Many of the statistical analyses performed in this study require evenly-sampled time series. The unprocessed dataset obtained from the ARGOS system consists of irregularly-spaced position data for each drifter. The majority of SUBDUCTION drifters were programmed to transmit for 24 hours and turn off for 48 hours. This was done strictly to save money on ARGOS tracking costs, not to conserve battery life nor to optimize the sampling. In fact, the transmitter duty cycle actually inhibits the ability to analyze high frequency motions in the drifter trajectories, such as inertial currents. The data used in this study were processed by the WOCE/DAC, which has the responsibility of quality controlling the raw fixes received from the ARGOS system and interpolating the unevenly sampled data

to a uniform six-hourly sample rate. WOCE/DAC receives drifter data from all WOCE-related projects around the world. (The SUBDUCTION Experiment, though funded by ONR, was managed as a process experiment within WOCE.)

Raw ARGOS drifter positions were preprocessed to remove obvious spikes in the data and then interpolated to uniform six-hourly positions at NOAA/DAC using the kriging interpolation procedure of Hansen and Herman (1989). Because of the two-day gaps in the raw position data, a further smoothing of the SUBDUCTION drifter data was accomplished by performing a two-day running average of the six-hourly data. This low-pass filtered data was sub-sampled daily to provide the drifter dataset used in this study.

Horizontal velocity estimates were produced for each drifter by center differencing the daily interpolated position data. Longitude and latitude data were converted into kilometers east and west of the average drifter position before the velocity calculations were made. The final processed dataset for this study were observations of position and horizontal velocity every day for each of the 155 drifters. These data were used to obtain the statistical descriptions presented in Chapter V.

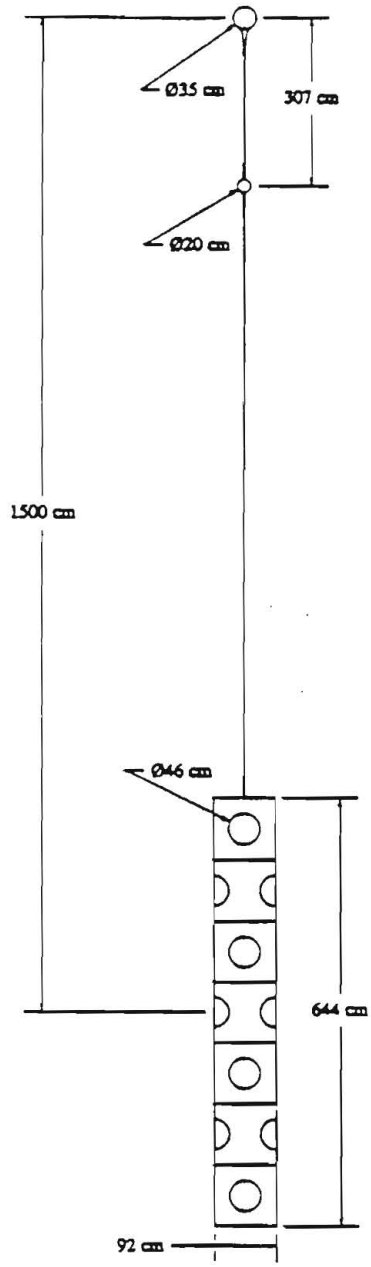

Figure 2.1 Scale drawing of the "holey sock" drifting buoy with Drag Area Ratio of 41.3.

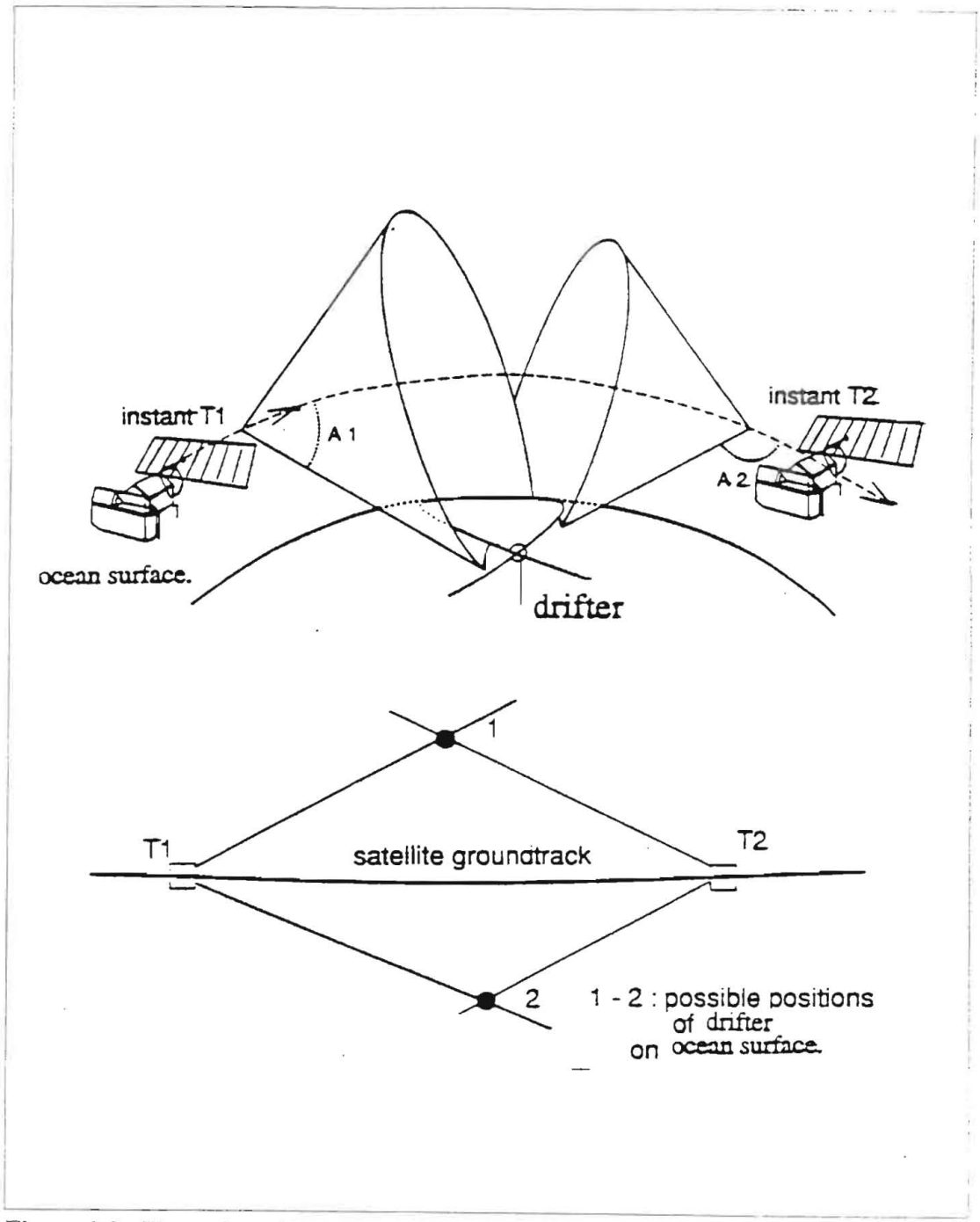

Figure 2.2 Illustration of buoy positioning using the ARGOS system. The ARGOS sensors monitor the Doppler frequency shift of the transmitter on the surface buoy. Knowledge of the satellite position determines the possible buoy positions at the intersections of the range cone and the ocean surface. Adapted from Service Argos System Guide (1989).

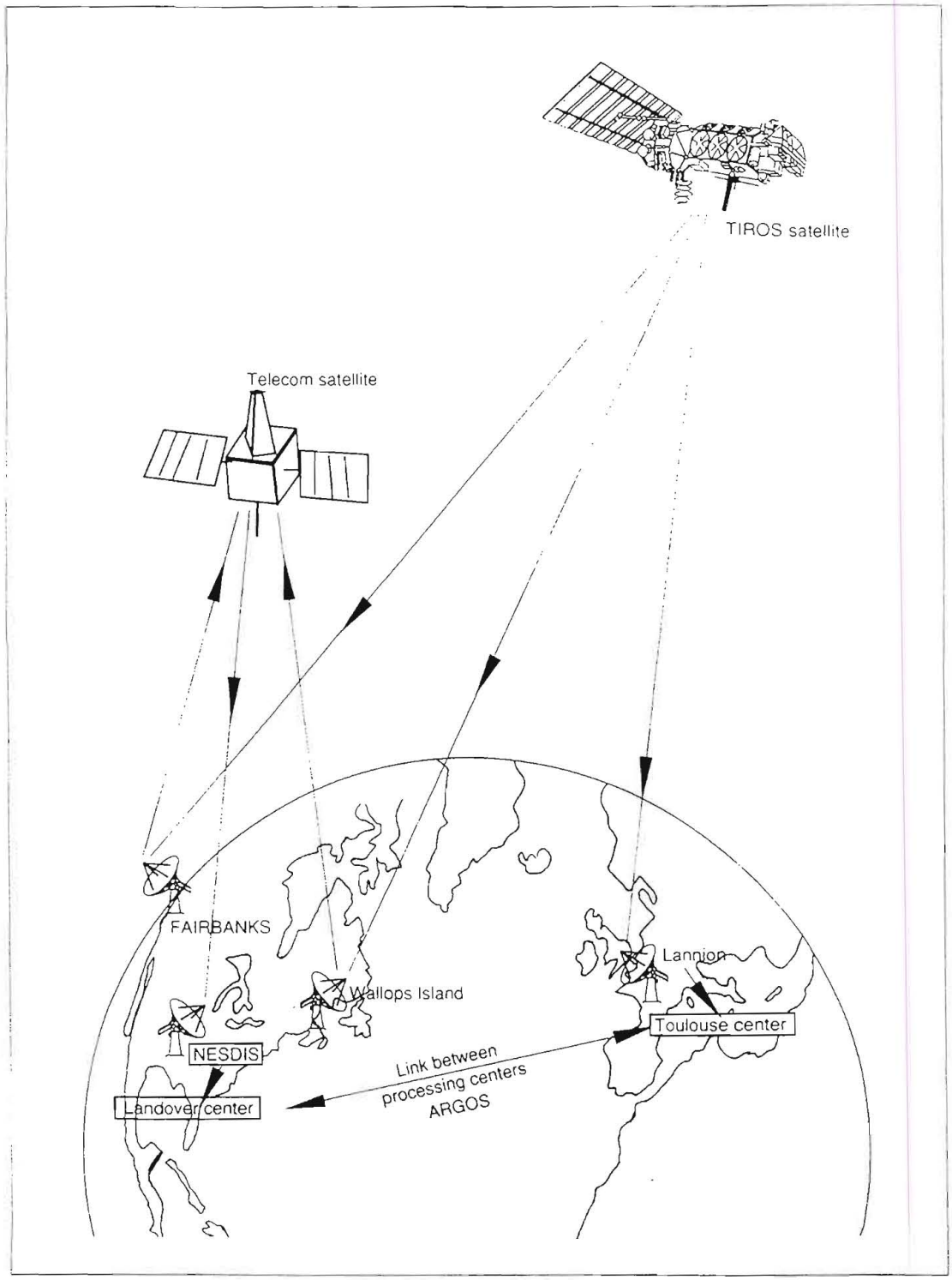

Figure 2.3 Telemetry and acquisition of data through the ARGOS data collection and location system. From Service Argos Service Guide (1989).

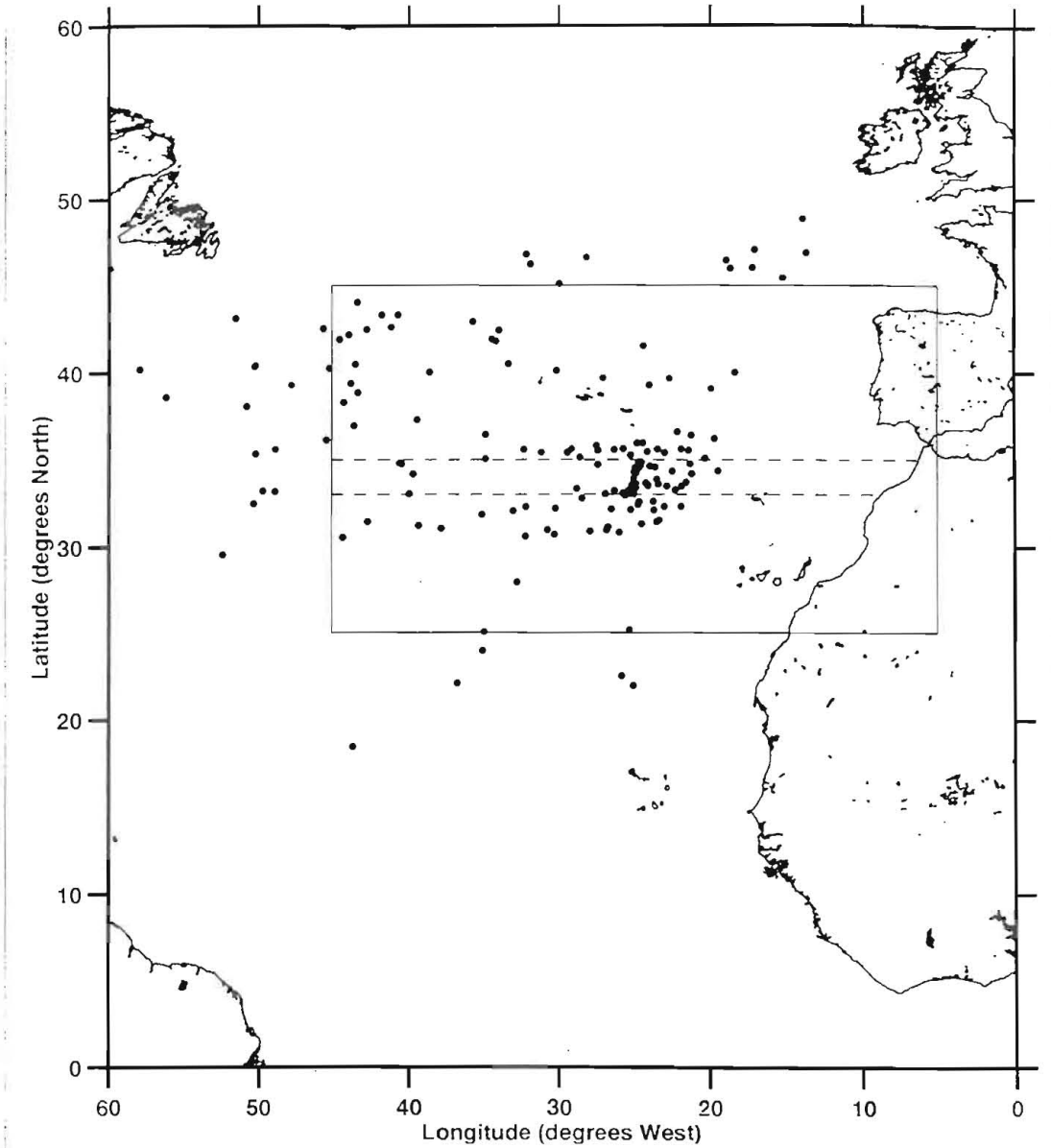

Figure 2.4 Initial deployment positions of surface drifters (dots) used in this study. The boundary for computation is shown by the box. Dashed lines separate Frontal Zone from the northern and southern regions.

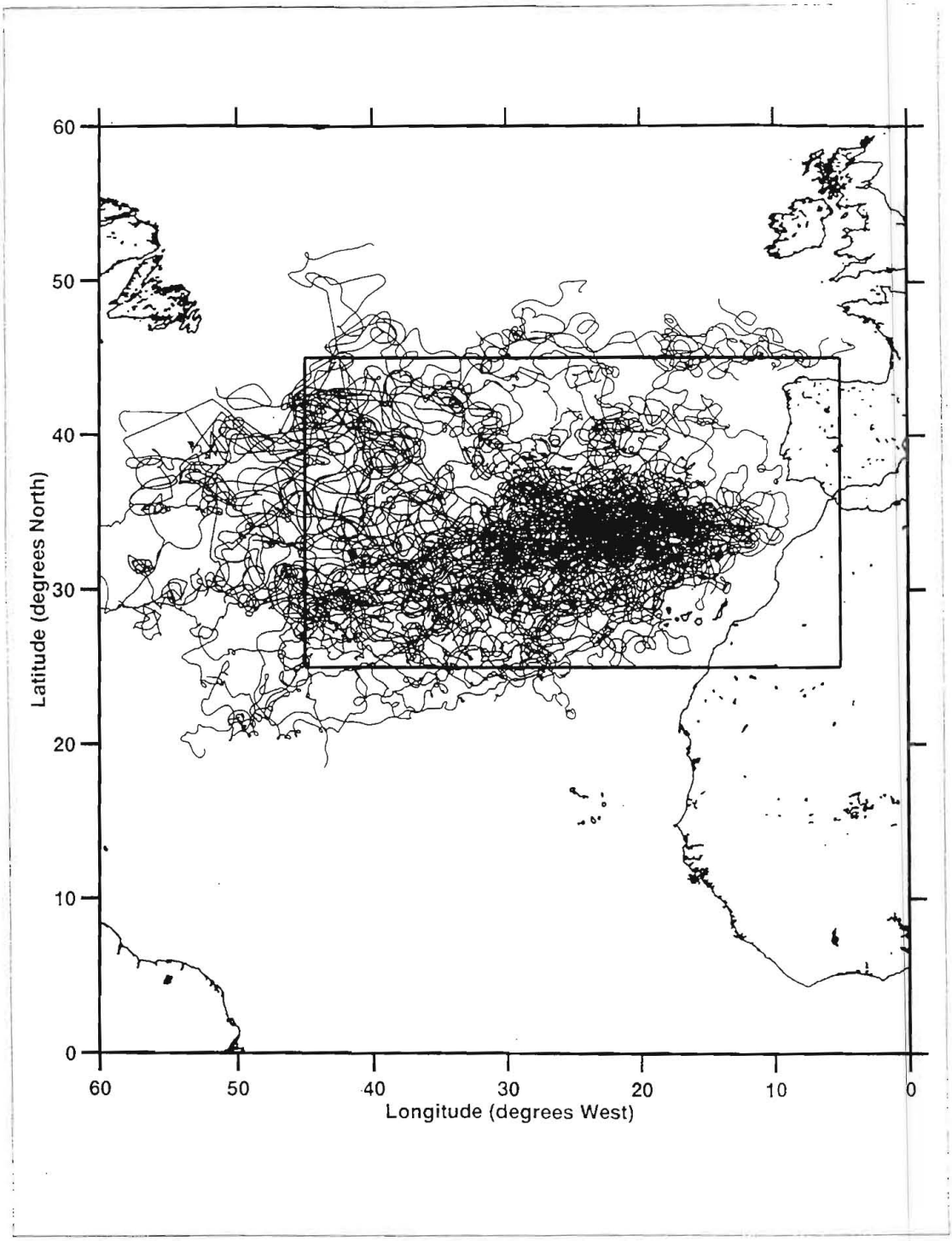

Figure 2.5 Trajectories of 155 surface drifters for the period from July 1991 through March 1995 that spent at least one day in the study area. Positions derive from the daily interpolated dataset.

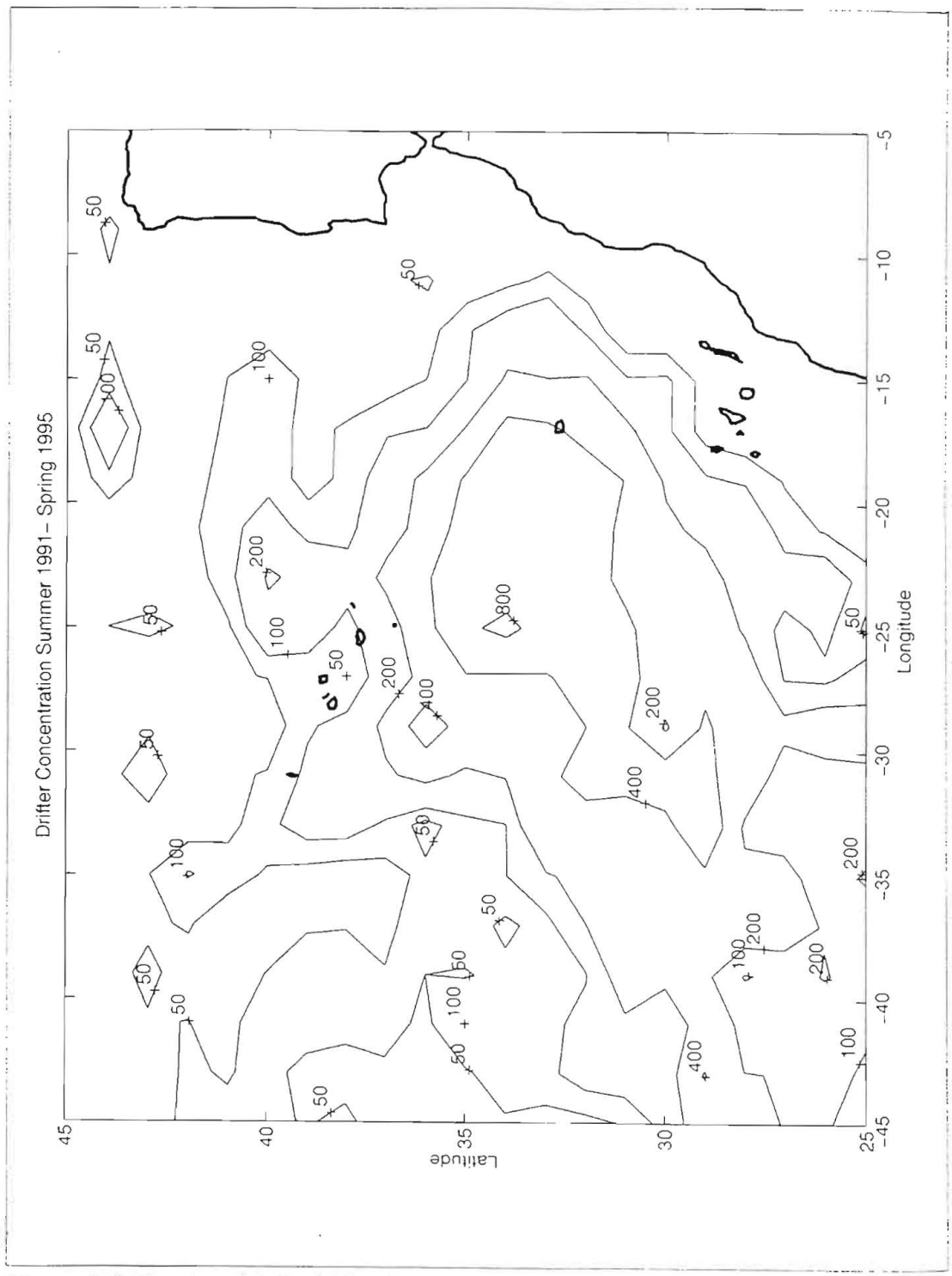

Figure 2.6 Density of daily drifter observations from July 1991 through March 1995. Note peak in the vicinity of 34° N, 25° W.

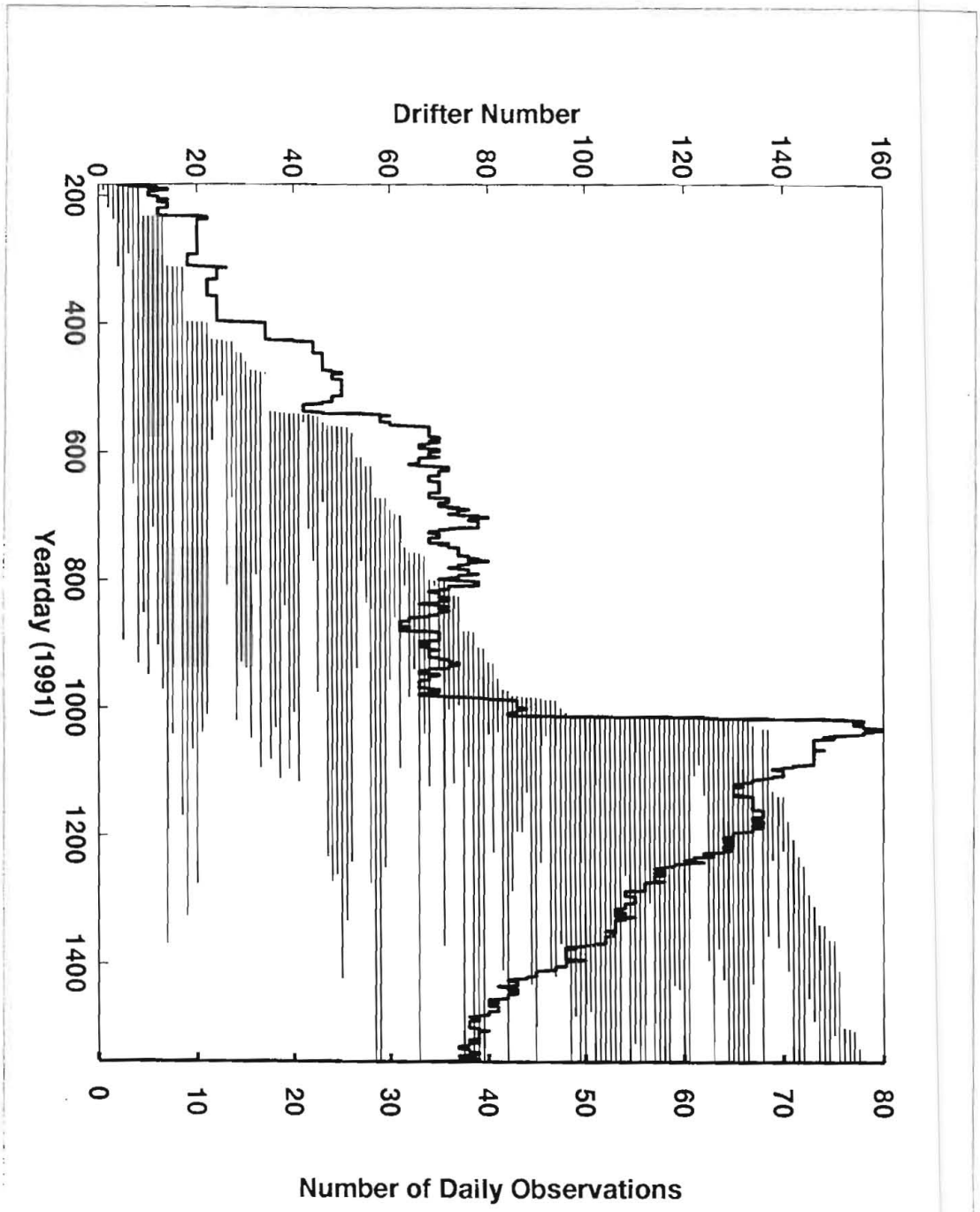

Figure 2.7 Time line of drifter performance from July 1991 through March 1995 in the study area. Forty drifters were still in operation at the end of this period. The bold line shows the number of daily observations.

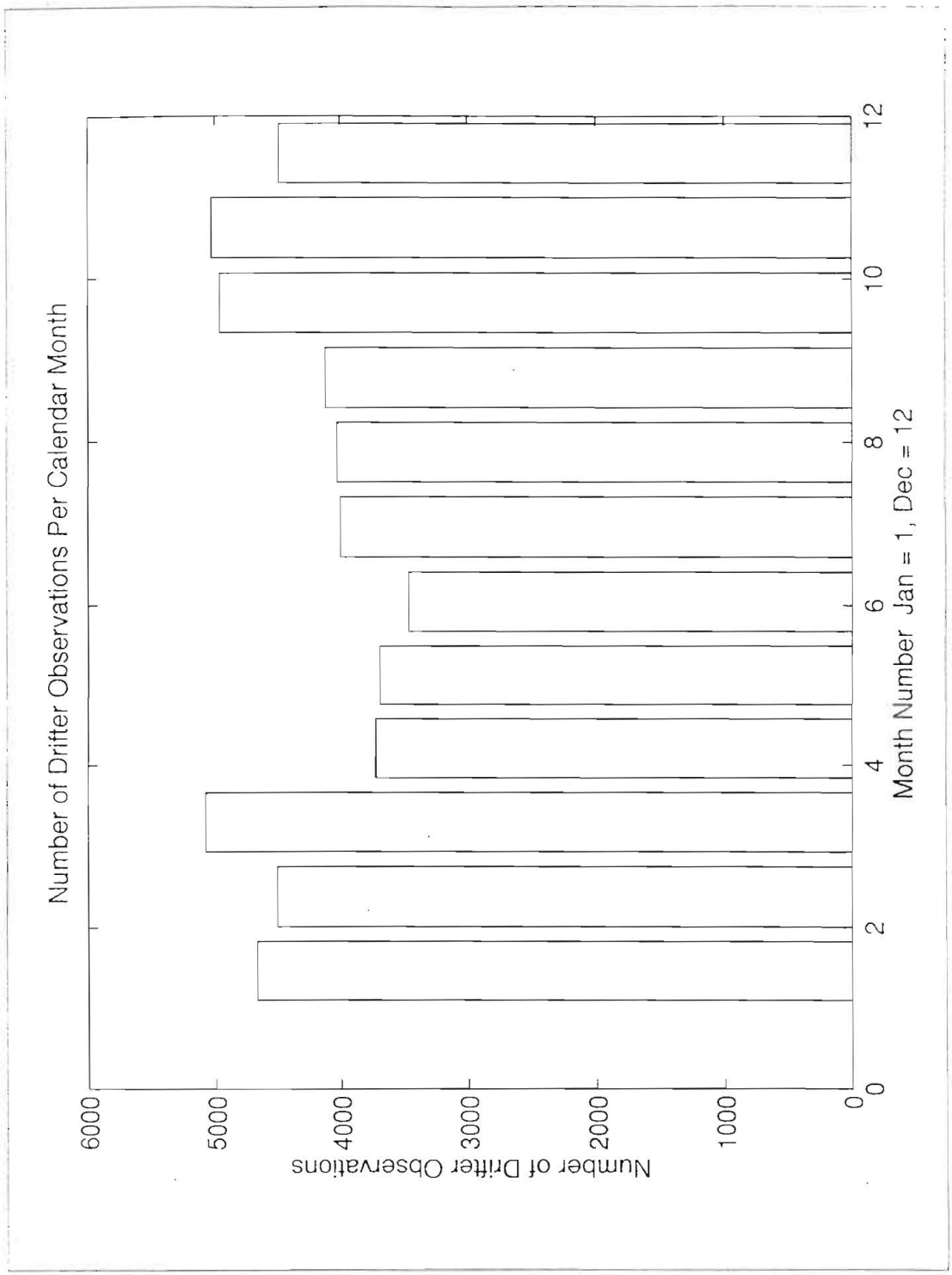

Figure 2.8 Histogram of the number of daily interpolated positions or velocity estimates available by month for all combined months.

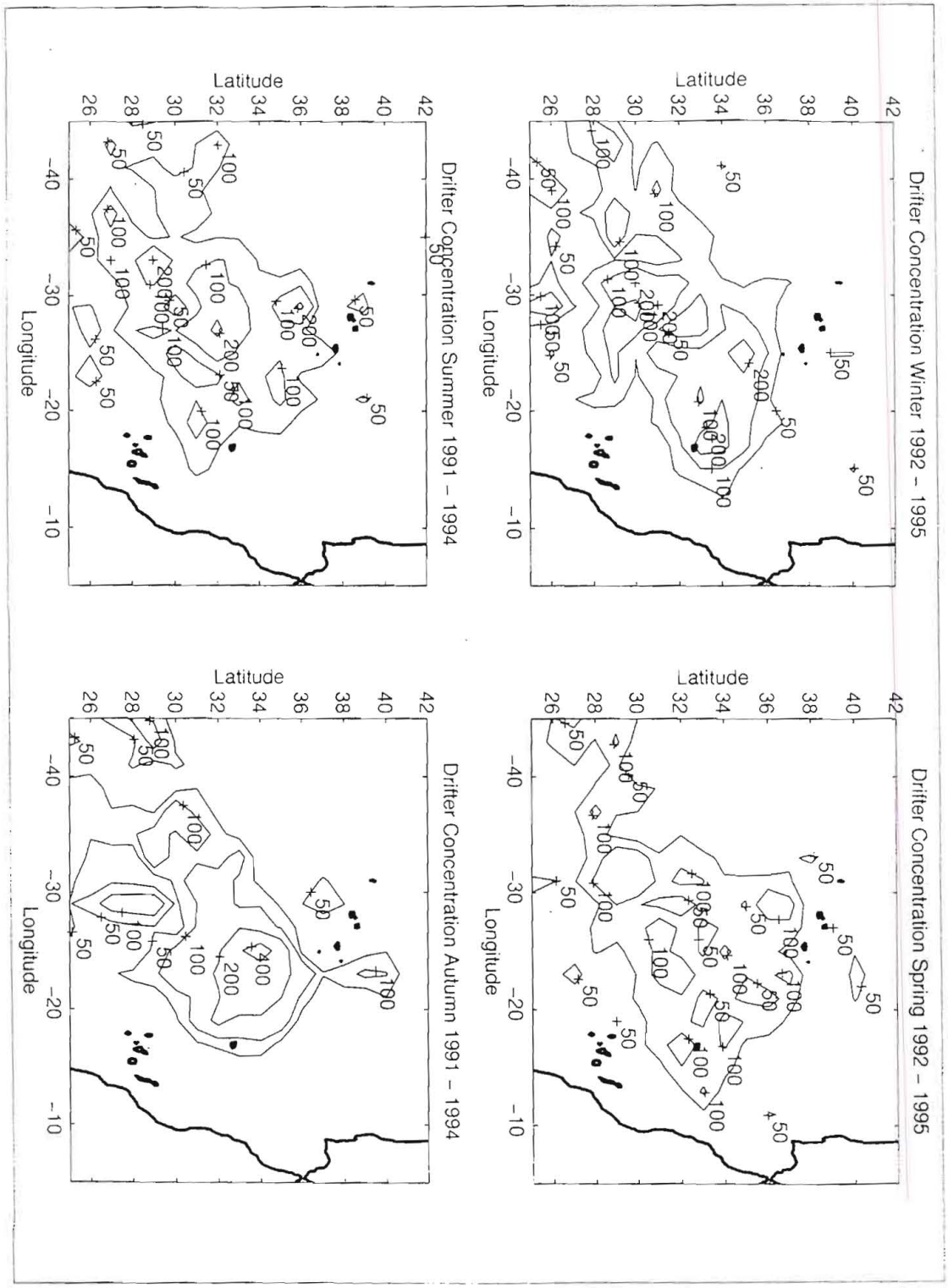

Figure 2.9 Four-panel seasonal distribution of daily drifter observations.

III. SATELLITE DATASET

Certain oceanographic features are well suited to study from space such as the western boundary currents of the Gulf Stream (east coast USA) and Kuroshio Current (Japan). Their strong horizontal temperature gradients are easily located in satellite infrared (IR) images. However, compared with the flows along the western boundary, the currents in the mid-Atlantic have relatively weak signals. These currents have not been studied in any detail until recently (Stramma and Müller, 1989).

A. OCEAN SURFACE TEMPERATURE MAPPING

Electromagnetic (EM) sensing of the ocean is limited to the ocean surface and the immediate subsurface. The presence of an atmosphere imposes limitations on the spectral regions that can be used to observe the surface . This is a result of EM interactions with atmospheric and ionospheric constituents leading to absorption or scattering in specific spectral regions. The ocean surface temperature affects the microwave and thermal emission of EM sensors, thus giving us a mechanism to remotely map the surface temperature. Both IR radiometers and passive microwave (MW) sensors are the satellite instruments used to observe sea surface temperature (SST) (Elachi, 1987). Details of how ocean surface temperature is measured can be found in Appendix A.

B. AVHRR DATA

1. Standard Product Resolutions

SST data from the Advanced Very High Resolution Radiometer (AVHRR) data are tape recorded onboard the NOAA Polar Orbiting Environmental Satellites (POES). The POES are owned and operated by the National Environmental Satellite, Data, and Information Service (NESDIS), a subunit of NOAA. POES AVHRR imagery and data are read out at the Fairbanks, Alaska and Wallops Island, Virginia Command and Data Acquisition (CDA) stations. These data can be recorded at 1.1 km resolution (the basic resolution of the AVHRR instrument) or at 4 km resolution. The stored high resolution (1.1 km) imagery is known as Local Area Coverage (LAC). Owing to the large number of data bits, only 11.5 minutes of LAC can be accommodated on the single recorders used at NESDIS. Temperature sensitivity at this resolution is 0.125 °C (Moshier, personal communication, 1995). In contrast, 115 minutes of the lower resolution (4 km) imagery, called Global Area Coverage (GAC), can be stored on a recorder, enough to cover an entire 102 minute orbit of data (Cotter, 1990). Four kilometers represents the best GAC resolution achieved at the center of the AVHRR sensor's scan.

2. GAC Image Compositing

For this thesis, composite GAC data was processed by the Remote Sensing Group of the Rosenstiel School of Marine and Atmospheric Science (RMAS), University of Miami, Florida. They used a unique software system especially designed to support oceanographic satellite data and image processing called DSP (described in the next section).

Focusing in on the Canary Basin region required remapping of the GAC composite images. The GAC composites were received in three month sets (January - March, April - June, etc) at the RMAS Remote Sensing Group after a delay of three to six months for initial processing by the National Aeronautics and Space Administration (NASA). The composites received from the Miami group came in "Sectors" which were 89.8° longitude by 89.8° latitude in extent. Composites containing the subduction region are in what the Miami group called the North-East Atlantic sector. A subimage of that sector was created and centered over the Azores frontal zone.

The compositing process is fairly simple: two images are taken and on a pixel by pixel basis one selects the warmer of the two pixels. Since cloud pixels are quite a bit cooler than even the coldest water pixels, the tendency is to select for cloud free pixels. This process is done for a week's worth of images (to screen out persistent clouds) to create the actual composite image. The result is now a collage of bits and pieces of several separate images, but it does not represent any kind of area average (Samuels, personal communication, 1995).

Remapping of images for the Azores Front area was completed by University of Miami research technician, Geoffrey Samuels. Pixel resolution now depends on the size of the remapped region. Since DSP images are 512 x 512 pixels, this comes to about 0.175 degrees per pixel, which is approximately 10.5 nautical miles or 19.5 km at the equator. This maps out to be about 7 km at the subduction latitudes. The pixel size of the images can be checked by using the DSP *dmphdr* function. Newer datasets are just now coming on line that have much better resolution (Olson, personal communication, 1995).

C. DSP SOFTWARE

DSP is a software package that is the user interface to the University of Miami image processing software (RMAS, 1990). For our purposes, DSP will include both the interface and the image processing software. The package can manage data among certain external and internal formats, mass storage, main memory, display memory, and the display monitor. It provides a means of geometric and radiometric correction for Coastal Zone Color Scanner (CZCS) and AVHRR image data. It has the ability to update ancillary navigation files based on user-defined refinements to satellite time and attitude parameters. This allows co-registration of images. The final products from DSP are earth-located, earth-gridded geophysical data files.

Graphically, DSP allows display of images on a color monitor with full user-defined mapping of 8-bit data values to any of 256 colors selectable at one time from a total palette of 32768 possible colors. Some automatic color mapping schemes are also provided. Color mapping schemes can be stored with an image or separately. Separate image planes may be combined for "true color" display. The system also provides separate color-mappable graphics and cursor (cross-hair) planes.

Two display resolutions are available, high and low. In low resolution, the display memory is organized into four memory planes, each containing 1024 x 1024 eight bit pixels, of which only 512 x 512 pixels are viewable on the screen at a time. Three of these planes are used to display images. These are called image planes 1, 2, and 3. Since data are scaled 0 - 255 (eight bit quantization), one complete image can be displayed in each plane. The fourth plane is reserved for graphics: lines, annotation, coastlines, etc. Each graphics plane

is one bit deep, for a total of eight planes. The one-bit depth means only "on" or "off" values are possible. The colors of the graphics planes are not set through the image plane palette but through separate commands. In high resolution, the display memory is organized into two memory planes, each containing 2048 x 1024 eight bit pixels, of which only 1024 x 1024 pixels are viewable on the screen at a time. Image plane 1 is used for the image, and plane 2 is usually used for graphics.

DSP supports hardware magnification and translation of the image. It can dump numerical values for individual pixels and rectangular regions as well as image transects. Programs are provided for adding graphics to an image such as arrows, transect lines, logos, etc.

Temperature calibration and navigation data can be found using the DSP command, *dmphdr*. Files used in this case study all have the same linear calibration:

$$T\,(^{\circ}C) = -2.1 + 0.2 \times \text{Pixel Value} \qquad (3.1)$$

D. NATIONAL METEOROLOGICAL CENTER (NMC) SST DATA

A second set of satellite data used in this thesis came from weekly composited SST fields from NMC. The major disadvantage of these fields is their resolution is limited to 1° by 1°. However, three advantages make them useful products for studying the Azores Front and as a starting point for the development of a new suite of drifter statistics based on a frontal coordinate system. One advantage is that all available data are blended into the final

product, making use of in situ measurements (from ships and buoys), satellite SST's, and SST's simulated by sea-ice cover. Another advantage is that there are no "gaps" in the analysis due to clouds, etc as encountered on the DSP analyzed images. This is a big problem during persistent cloudy periods such as winter. A third advantage comes from the resulting "smoother" temperature field (e.g., no loops, whirls, and filaments). Smoother fields help simplify the calculations relative to the curvilinear, orthogonal coordinate system.

Techniques used to blend all available observations were developed by Reynolds (1988) and Reynolds and Marsico (1993). A major advantage of their method is an objective, time dependent correction of any satellite biases relative to the in situ data. First, a preliminary large-scale spatial bias correction is calculated. This degrades the resolution of the monthly analysis to roughly 6° lat/long. Next, the corrected satellite data and the in situ data are reanalyzed both weekly and daily using optimum interpolation (OI) on a 1° lat/long spatial grid. This method retains the bias correction while improving the spatial and temporal resolution of the blend. A description of the OI analysis can be found in Reynolds and Smith (1994).

The bias correction improves the large scale accuracy of the OI. Examples of the effect of recent corrections can be found in Reynolds (1993). The bias correction does add a small amount of noise in time. Most of the noise can be eliminated by using a 1/4 - ½ - 1/4 binomial filter in time. An improved method of correcting the biases is currently being developed (Reynolds and Stokes, 1994).

For the period of this study (June 1993 - April 1995), the in situ data for the NMC SST fields were obtained from radio messages carried on the Global Telecommunication System (GTS). Satellite observations came from operational data produced by NESDIS. Analyzed weeks were defined to be centered on Wednesdays. This was done to agree with a definition used by ocean modelers. SST's were also generated for ice covered regions (not a factor for this study's domain) with any gridded SST values less than -1.8 °C set to -1.8 °C. All analyses are archived to the nearest 0.01 °C. Due to round off from movement between computers, this minimum value may change by up to +/- 0.02 °C (Reynolds and Stokes, 1994).

The OI analysis is done over all ocean areas. No analysis is done over land. Land values are filled in by Cressman interpolation to produce a complete grid for possible interpolation and use of high resolution coastline files. Ocean and land areas are defined by a simple land sea mask. The spatial grid of the land sea mask is defined identically to the grid used for the SST arrays. Values in the land sea mask are set to 1 over the ocean and 0 over land. Weekly OI fields are stored in yearly files at the NMC World Weather Building in Camp Springs, Maryland. These files plus the land sea mask data file can be accessed and transferred by file transfer protocol (FTP) in binary (IEEE) mode.

IV. FRONTAL ANALYSIS

A. INTRODUCTION

A fundamental question exists of how and where the process of subduction takes place. One school of thought theorizes that this process is concentrated along oceanographic fronts (Figure 1.3). The Azores Front in the Canary Basin was chosen as an ideal location to investigate this hypothesis. Drifters were deployed to the north and south of the frontal region to look for evidence of convergence. Because the actual front moves around with time, a knowledge of the frontal history and its evolution is necessary to relate data from Lagrangian drifters to any conclusions about subduction in the vicinity of this front.

Motions of the drifters themselves can provide an indication of location of the Azores Front. Other products and datasets, such as satellite imagery and hydrographic surveys, can further aid in the location of the front (Rudnick and Luyten, 1995). Once the front position has been determined, parameters such as convergence, heat flux, and eddy kinetic energy can be calculated relative to the front to establish the extent of subduction. Section B describes the methodology used to attempt the positioning of the front by (relatively) high resolution SST remote sensing imagery, pixel histograms, and high speed drifter trajectories. Section C describes the methodology in positioning the Azores Front given the low resolution NMC SST fields and interpolated drifter velocities and positions. Although the frontal analysis was done in a systematic way, procedures for both sets of data and the actual "choice" of a front position tended to be very subjective.

B. HIGH RESOLUTION ANALYSIS WITH DSP IMAGES

1. Description

To test the feasibility of using DSP software, AVHRR imagery, and Lagrangian drifters in tracking the location of the Azores Front, a limited time-frame case study was conducted. One of the first decisions to be made was concerning the time period for the case study. Previous investigators found detection of the front and associated eddies to be difficult due to weaker temperature contrasts and frequent cloud cover over the frontal region (Gould, 1985). The sharpest surface thermal expressions are expected to occur mainly in the winter months. However, this is a time when a substantial cloud cover is present south of the Azores. Observations in the summer are complicated by a strong seasonal thermocline, which may obscure the main dynamical front (Gould, 1985; Figure 4.1). Spring was chosen as being the best compromise to see clearly any frontal feature — based on the given temperature contrasts and the availability of clear, wide-area coverage for the region. Case study images started from Julian date 93062, 03 March 1993 to 93181, 30 June 1993. Sample DSP GAC weekly image composites from the beginning and end of this period are shown in Figures 4.2 - 4.4.

Histograms for each composite image were generated by DSP, showing the relative occurrence of each pixel value seen in the image (Figures 4.5). Relative minima in these histograms indicate a sharper temperature gradient. A subset of the Lagrangian surface drifter dataset was also created to help aid in the location of the Azores Front. The subset consisted of only those drifter positions where the drifter was moving with speed greater than 30 cm/s. The hypothesis here is that the greatest current speeds in the study area are associated with

the Azores Current and location of high speed regions, may therefore help locate the Azores Front.

Before this case study was undertaken, four major assumptions were made:

(1) The Azores Front fluctuates naturally north/south in periods of several weeks over a wide latitude range (32° N - 36° N). (2) The intensity of the front (as measured by the horizontal SST gradient) over the season might decrease as solar radiation (heating) increased. (3) If no clear SST expression of the front was visible in the DSP images, then high-speed drifter trajectories would indicate the Azores Front location. (4) Mesoscale phenomena such as the frontal boundary, eddies, jets, and meanders behave as a "frozen wave", varying their locations and shapes on time scales longer than the daily or weekly sampling in the drifter and satellite observations, respectively.

2. Procedure

Two graphical methods were used in attempting to fix the Azores Front. We name them the Pixel Method and the Gradient Method. These two methods utilize different functions of the DSP software. Due to the limitations of DSP, the graphical representations of the two methods could not be combined or overlaid. The Pixel Method is focused on using histograms of the relative occurrence of the pixel values making up an image. The Gradient Method is focused on using a built-in DSP function to find where the largest temperature gradients are. These two methods are described in step-by-step detail below.

To obtain weekly positions of the Azores Front, the following procedures were used:

a. The Pixel Method

(1) Load composite image.

(2) Choose complementary color palette scheme — warm colors (reds) for warm water and cold colors (blues) for cold water.

(3) Add in coastline and other navigation grids, using DSP command *troutc*. The information came from the Central Intelligence Agency's (CIA) World Database-II.

(4) Select a characteristic temperature band to highlight with DSP *slice* command. A band was defined from the histograms as one low relative occurrence pixel value to the next relative low occurrence pixel value. It may require several different *slices* depending on the corresponding weekly histogram. An example of such a temperature band is shown in Figure 4.2a based on the range of temperature values between the minima at pixel value 97 and 102 shown in Figure 4.5a.

(5) Overlay high speed (> 30 cm/s) drifter trajectories for a 60 day period centered on the composite image's Julian date. The 60 day window was selected to allow enough data to be shown to help locate the front.

(6) Estimate the frontal location with best correlations of drifter and SST data. To minimize confusion, only the north boundary was taken from the low temperature pixel minimum of the characteristic temperature band. When this characteristic (highlighted) pixel band migrated too far north past the Azores islands, the high temperature pixel low occurrence minimum value of the band became the new north frontal boundary (to keep consistent with climatology). If there were great differences between weekly positions

following a set characteristic pixel band (e.g. 92 - 97), the next band between relatively low occurrence pixel minima was tracked.

(7) Digitize position to output file for further studies (not done for this thesis). For this case study, weekly positions were transferred to overhead transparencies.

(8) Repeat process for each weekly Julian date using the prior week's pixel values as a first guess.

b. The Gradient Method

(1) Repeat steps (1) - (3) of the Pixel Method.

(2) Run DSP command *grad*. *Grad* calculates an estimate of the spatial gradient magnitude field for the specified area of the image display memory contents. This uses either a 2 x 2 pixel Roberts estimator, a 3 x 3 pixel Sobel estimator, or a 3 x 3 pixel Prewitt estimator. This highlights pixels with large value gradients. The least value gradient is colored blue, medium value gradients are colored green and yellow, and the maximum value gradient is colored red. An example of gradient information overlain on a weekly SST composite is given in Figure 4.2b.

(3) Repeat step (5) of the Pixel Method.

(4) Estimate frontal location with the best drifter correlations and SST data. Maximum gradients are expected to aid in location of the front.

(5) Repeat steps (7) (not done), and (8) of the Pixel method.

3. Case Study Analysis and Results

From each of these weekly images a high resolution frontal history evolved. The northern boundary of the characteristic temperature band from the Pixel Method was traced onto an overhead transparency. Frontal locations were traced for each month covered by the case study (March, April, May, June 1993). Each week shows the extent of meandering, looping, and pinching-off of eddies. Pockets of coastal upwelling could be seen along western North Africa. Where large areas of the image were black (void) of SST data, the front was extrapolated to rejoin the same characteristic band pixel values. The frontal history for April 1993 is shown in Figure 4.6.

The main results from this preliminary case study reveal some interesting points:

(1) Many surface SST frontal expressions are present in AVHRR imagery, confirming the results of Gould (1985). Correlating the correct SST front with the main submerged, dynamic frontal zone responsible for large volume transport is a problem. For example, only one of the many SST fronts visible in the XBT section in Figure 4.1 is associated with the actual sub-tropical front.

(2) Seasonal warming advances the SST fronts farther than the subsurface front is expected to move. The main dynamic front never really meanders far from its known climatological position between 32° N and 36° N latitude; rather it just takes on a warmer characteristic temperature.

(3) Mesoscale features of the front (eddies, jets, and meanders) can be seen developing and dissipating in one to three weeks (Figures 4.2 - 4.3).

(4) Surface drifters were very useful in correlating frontal location, particularly under cloudy images. Drifters, however, were often caught in mesoscale features such as eddies, filaments, and secondary fronts away from the main dynamic frontal zone and the amount of drifter information at any given time was usually not enough to locate the front over the entire study area.

(5) Gradient analysis helped distinguish frontal boundaries as separate features apart from the aforementioned mesoscale features. However, gradient analysis alone was insufficient to highlight along-front temperature gradients necessary to plot its meandering course.

The DSP gradient function, *grad*, uses a 3 x 3 pixel estimator to calculate magnitudes of variation in two dimensions. This worked well when highlighting looping fronts, eddies, and filaments, but was poor in highlighting one dimension cross-front gradients characteristic of more zonal-like flow. Using a larger sized estimator with a vector direction capability, such as the DSP function *gradan* (found after the case study), should improve frontal placement.

(6) Significant SST granularity occured on the north side of the front according to the *grad* analyses (Figures 4.2 - 4.4). Most of this granularity was in North-South bands associated with the North Atlantic Current extension and another recurring band around 30° W. Previous work has shown that mesoscale eddy kinetic energy (EKE) is higher to the south (Paduan et al., 1995), but it is not clear that the granularity in the DSP *grad* results is related to the same processes.

(7) The Pixel Method showed the best results, although there is a great deal of subjectivity in deciding which pixel band is representative of the actual front. Some histograms had four

or five relative pixel minima and choosing which band (e.g., pixel values 92 - 97, 97 - 102, or 102 - 107) was characteristic of the frontal zone was especially difficult during a transition time from the lower temperature band to the next higher temperature band. A sudden "jump" to the south from one week to the next was a common manifestation of this transition time. An example of this can be seen in the frontal history of April for the weeks of 7 April and 14 April 1993 (Figure 4.6). It reveals the effect of seasonal warming, with the "jump" probably being a byproduct of the seven day compositing process and the uncertainty associated with choosing a representative SST front to track the subsurface feature.

4. Case Study Conclusions and Recommendations

For this season, Spring 1993, the Azores Front can be reasonably tracked using AVHRR MCSST imagery. Correlating information such as surface drifters, XBT or CTD survey data, and image processing techniques are necessary to fine tune its location. High-speed surface drifter trajectories are too few to positively distinguish a frontal boundary from a propagating mesoscale eddy or filament.

Using drifter trajectories from a 60 day window centered on the composite Julian date allowed enough data to be shown to help locate the front. However, ambiguities did exist. One problem was deciding whether a trajectory segment was moving along the north side or south side of the front. Within those 60 days, the frontal boundary could have migrated north enough for the trajectory segment to fit both sides of the front during its evolution. On the other hand, it was possible to use a segment track as a "forecast" aid to see when the front would meet up with that segment.

One improvement would be to vary the criteria of the overlaying drifter data. For example, instead of using a 60 day window and > 30 cm/s segments, one could try a 30 day window centered on the Julian date and a speed criterion of > 20 cm/s segments. This should narrow the areas of frontal zone development. On the other hand, closer time spacing and slower threshold velocities might have the disadvantage of allowing too much noise in the data and thereby missing identification of the main dynamic front.

Seven day composite imagery allows greater area coverage than otherwise possible by eliminating some cloudy areas. Still, seven day composites do not guarantee complete area coverage. For very persistent cloudy periods, significant areas of the domain have no representative SST value from which to trace the frontal boundary. Resolution from the seven day composites (7 km) is adequate to track most mesoscale phenomena. These images could actually be redefined as high resolution when compared to the 1 $^{\circ}$ temperature averaging that is used by the National Meteorological Center's (NMC) Optimum Interpolation technique (Reynolds, 1994) .

Daily local area coverage (LAC) AVHRR data would give very fine resolution (1.1 km) capable of tracking small scale features, but it is limited by even greater susceptibility to any interfering clouds and its narrow regional focus. Only 11.5 minutes of LAC high resolution imagery can be stored as compared with an entire orbit for GAC. LAC must, therefore, be scheduled and timed carefully to meet the data needs of users with recording capability (Rao et al., 1990).

C. LOW RESOLUTION ANALYSIS WITH NMC WEEKLY SST DATA

1. Overview

Given the limitations in frontal analysis using DSP and high resolution GAC composite satellite imagery, an alternate approach was undertaken using National Meteorological Center (NMC) weekly analyzed SST fields. As mentioned in Chapter III, this dataset is considered low resolution ($1^{\circ} \sim 111$ km grid size), when compared to the DSP images whose individual pixels give a resolution of about 7 km (depending on latitude). Thus, many mesoscale features such as meanders, loops, and jet filaments generally are smoothed out by the optimum interpolation procedure and its incorporated decorrelation scales employed in the NMC analysis.

The first efforts with the NMC SST data were focused on comparing the weekly analyzed fields to the corresponding DSP images used in the preliminary case study of the Azores Front. Unfortunately, the weekly compositing process for the two datasets do not coincide. DSP images were centered on Sunday, while NMC data were centered on Wednesday making direct comparisons of frontal features not possible. However, using the "frozen wave" assumption of a slowly moving front, one can trace the evolution of the temperature fields and the shape of the frontal region.

The NMC analyzed SST fields for the time periods featured in the DSP images can be seen in Figures 4.7 - 4.9 together with drifter-derived velocity vectors for the respective weeks. In these figures, the NMC SST product has been plotted using an interpolating shading function. Some of the same characteristics that are present in the DSP images can be seen in the analyzed fields. In particular, the area-wide orientation of the SST isotherms

are similar. However, the interesting and important mesoscale features present in the DSP images are missing from the analyzed NMC SST images.

Processing of the analyzed NMC SST fields was conducted using MATLAB software. MATLAB, in fact, offers several advantages to a programmer manipulating these drifter and satellite datasets. Advantages can be found in such tasks as sorting, plotting, contouring, and shading. MATLAB's unique ability for matrix and vectorized computation allows fast and efficient processing of thousands of drifter observations involving various selection criteria and formulas. MATLAB's interpolated shading function, for example, gives a visual interpolation of the low resolution data, which definitely aids in selecting a frontal temperature.

2. Selection Criteria

The focus of the thesis is oriented to setting up a frontal curvilinear, orthogonal coordinate system for the purposes of describing drifter statistics. Only one ocean property, sea surface temperature, is remotely sensed and archived in data files; therefore, our front will be in terms of a characteristic temperature. Using a characteristic temperature to describe the boundary of an oceanographic feature is a common practice in this science. Gould (1985) shows part of an XBT section using the 18 $^{\circ}$C water mass temperature as a marker in describing the physical oceanography of the Azores Front (Figure 4.1). Temperature gradients have also been calculated but not used in determining the frontal location. Unfortunately, the temperature gradients in this region are comparatively weak, which means they are not very visually informative or distinguishable graphically to be used as aid in

selecting a front. Other ocean properties such as sea surface elevations from satellite altimetry or ocean color from the CZCS or other platform could be useful in pinpointing the front but these datasets were not available, or did not coincide with the time frame of this study.

The NMC SST data was loaded into a 21 x 41 matrix array, filling one temperature value for each 1° x 1° box of the domain. Zero values caused by the land-sea mask were then replaced by Not-a-Number (NaN in MATLAB), making contouring clear and simple next to the Iberian Peninsula and North African coast. Daily drifter observations were overlain on top of the temperature field. The temperature field was further interpolated using the MATLAB *interp* function to increase the density of temperature observations to a finer resolution of 0.1° degree of latitude and longitude. This helps the contouring of a specific characteristic temperature representative of the front.

Selection criteria were devised to help choose the characteristic temperature. Not all criteria could be kept for each selection. The following guidelines were used:

(1) Keep the characteristic temperature from wandering too far from 35° N latitude along the western boundary of the domain .

(2) Frontal position should be in general agreement with the climatology given by Klein and Siedler (1989; Figure 1.4). Their mean positions have the Azores Front and the Azores Current positioned mostly between 32° N and 36° N latitude. Gould (1985) in his XBT section shows the main dynamic front centered at around 34° N.

(3) The selected temperature should be biased toward observations which depict faster drifter speeds when oriented parallel to an isotherm. We expect faster trajectories along the front.

(4) Maintain temperature continuity from one week to the next. The maximum temperature change from one week to the next was 0.75 °C. This happened only during summer when maximum solar heating occurs. Most temperature fluctuations were between 0 to 0.5 °C.

(5) For the particular period of the DSP case study (e.g. Spring 1993), maintain consistency with the higher resolution DSP imagery. In that case frontal temperatures ranged from 16.3 °C to 19.3 °C.

A four year time series of frontal characteristic temperatures was collected and resulted in the seasonal frontal history. The time series of the subjectively chosen characteristic temperature for the entire study period is shown in Figure 4.10. The annual cycle of warming and cooling of the Azores Front can be seen clearly in the characteristic temperatures. The cycle ranges between 17.75 °C in the winter to 26.0 °C in the summer.

3. Frontal Position Digitizing Procedure

Once a characteristic temperature history was obtained, the process of digitizing weekly frontal positions was completely automated. The particular methodology used was optimized for the matrix functions in MATLAB. The NMC analyzed SST field was interpolated to provide spatial resolution ten times greater than the original 1° resolution

data. From this expanded temperature matrix array (210 x 410), the indecies for all temperatures +/- 0.1 °C from the chosen isotherm were found. The latitudes and longitudes corresponding to these indecies of the new "high" resolution array were then saved to a separate frontal file for post processing.

The MATLAB *find* command was used to extract frontal positions but it did not necessarily order the points in increasing along-front distance. (Frontal latitude/longitude pairs were ordered from west to east in terms of increasing longitude, not in terms of the order in which the front was continuously connected.) Cases that double back have two pairs of frontal points that share the same longitude, but different latitudes. Therefore, linear interpolation, or any other monotonic (one x for each y) interpolation scheme, cannot fit a smooth function to these points. An example of the frontal curve obtained by simply connecting the points, which results in a very jagged "sawtooth" front, is shown in Figure 4.11. To remedy this situation a sorting program was developed to find the shortest distance to the next adjacent point along the front beginning with the westernmost location. Other parts of the ocean with the same characteristic temperature, but not connected in any way to the front are discarded. This produces one, simple, continuous front that starts from the western boundary (45° W) and meanders east all the way to the North African coast or turns back south and west (e.g., Figures 4.11, 4.12).

For weeks with very weak temperature gradients there are sometimes wide areas of gaps that have no frontal location points (Figure 4.12). These gaps were as far apart as 300 km, but more often were on the order of 50 km (Figure 4.13). To apply the frontal

coordinate system distance calculations, high resolution (~ 10 km) frontal points are needed. A linear interpolation program was used to fit in more points between widely spaced adjacent locations. After passing through this interpolation program, the average spacing between adjacent frontal points was lowered to about 7 km (Figure 4.14).

The final weekly sorted and interpolated frontal files were saved for use in the curvilinear coordinate system to find the along-front distances, cross-front distances, along-front velocities, cross-front velocities, and other statistical quantities. The methodology for transforming the coordinate system is described in the next section. Sample fronts corresponding to the periods highlighted in the DSP images are shown in Figure 4.15. The seasonal NMC SST frontal history is shown in Figure 4.16.

D. FRONTAL COORDINATE SYSTEM

1. Overview

For standard Cartesian averages, the determination of the averaging box (bin) size is a balance dictated by the concentration of drifter observations occuring in each bin and the scale of the features to be studied. Mean values of velocity for each of these boxes thus end up giving us a picture of the average Eulerian circulation (Ollitrault, 1995). The problem of examining Cartesian (Eulerian) box averages for drifter statistics becomes apparent when the oceanographic feature of interest, such as the Azores Front, moves into and out of the boxes. Movement by the front can essentially mask any motion relative to the front. Are the EKE statistics due to individual eddies and meanders, or are they due solely to the migration of a relatively zonal front into and out of the averaging bin or a combination of both? Drifter

movement following converging, subducting currents are averaged together with the actual Azores Current. Establishing a coordinate system relative to the front then should aid in separating out these motions.

Given the location of a front, Cartesian u and v velocity components can be transformed into along-front and cross-front velocities. Regular latitude and longitude Cartesian boxes can be transformed into boxes of distances away from the front by distances along the front. The resulting boxes when viewed in Cartesian space would appear trapezoidal. The size of these trapezoidal boxes are still dictated by the same balance required of Cartesian boxes: drifter observation concentrations in each averaging bin, and the scale of the feature to be analyzed.

In order to increase the signal to noise ratio when computing secondary circulations around the Azores Front, a method was sought to transform the drifter velocity observations into along-front and cross-front coordinates. The method described in this setion was formulated using frontal location files generated from NMC SST data, interpolated drifter positions and velocities, and certain selection criteria resulting in a characteristic isotherm representing the Azores Front. However, this method should be flexible enough to handle any other frontal location file whether it was generated from hand-digitized positions, altimetry data, hydrographic surveys, etc. The two main requirements for this method are that the front starts at the western boundary (with along-front distance equalling zero) and that as the front wanders away from the western boundary its along-front distance increases continuously. The last point of the front would then have an along front distance equal to the total path length.

2. Methodology

The first step was to load in the master drifter observation file and search for all the drifters which met the selection criteria of the domain boundaries and weekly timeframe. This is very fast in MATLAB as it can be done in a vectorized form without the need for time consuming loops. The number of observations and the index of their position in the file matrix were recorded.

Next, the corresponding weekly frontal location data file, which had previously been sorted and interpolated for finer density of points, was loaded into a large matrix array. For each drifter observed in the domain during the weekly time frame a cross-front and an along-front distance was computed. Cross-front distances were calculated by computing the great circle distance from the drifter to every point on the front according to:

$$D = R \cos^{-1}(C) \tag{4.1}$$

where

$$C = \cos(\text{lat A}) \cos(\text{latB}) \cos(\text{lonA} - \text{lonB}) + \sin(\text{latA}) \sin(\text{latB}). \tag{4.2}$$

Locations A and B refer to the drifter and the frontal point, respectively, and R is the radius of the earth, which is assumed to be constant at 6370 km.

The minimum distance between the drifter observation and the front was then assumed to be aligned normal to the front and, thus, equal to the cross-front distance. This approximation will be valid if the separation between points along the front is much less than the distance to the drifter. A diagram visualizing the coordinate system and the techniques

involved is provided in Figure 4.17. The index defining the location of the minimum distance was also recorded. Due to the large distances involved for some drifters, great circle distances were used to take into consideration the curvature of the earth versus the straight-line distances obtained from the Pythagorean Theorem of Euclidian geometry. For even greater accuracy, complex geodesic formulas can be used that take into consideration the earth's eccentricity, but this level of accuracy is not justified by the measurements in this study.

Along-front distances were calculated incrementally starting from the western boundary to the end of the frontal path. Again, great circle distances were used between adjacent points of the front. This was done for consistency. Individually, Pythagorean Theorem distances are not very different from great circle distances for any two closely spaced adjacent points, but when these distances are totalled incrementally along the front, then a substantial difference can exist in total along-front distances from the two methods.

After these two calculations were completed each drifter had its location in terms of how far along the front it was from the western boundary and how far it was from its closest point of approach to the front (referred to as "along" and "cross", respectively). A very loopy front can have interesting affects on these new coordinates. For example, a drifter that lies at a vertex of an imaginary equilateral spherical triangle could very easily have its first day's position be located at 500 km along and 600 km cross and its second day's position be located at 1000 km along and 605 km cross despite it perhaps moving only a few kilometers from the first day to the second (Figure 4.17).

Because the front could loop back on itself, one cannot use simple tests such as north or south of the front to assign positive or negative cross distances. What is important is the maintenance of a right-hand coordinate system relative to increasing along-front distance. This can be accomplished by determining whether a point is "inside" or "outside" of the front as shown in Figure 4.17. For this thesis any drifter that was located above or "outside" of the front was considered to have positive "cross" distance, while drifters below or "inside" of the front were considered to have negative "cross" distance. Testing to find whether a drifter was inside or outside of the front was done by constructing a polygon made up of the first frontal point, the frontal points, the longitude of the front's end point and 24° N (below the southern boundary of the domain), 24° N and 46° W, and back to the first front point. A MATLAB function *inside1* took all the drifter positions and all the polygon positions and returned a value of 1 if the drifter was inside the polygon. All drifters that had an index value of 1 were then assigned negative cross distances.

The next few steps of the procedure were geared towards transforming each drifter's north (v) and east (u) velocities into along front and cross front velocities. Using techniques from plane analytic geometry and spherical trigonometry the appropriate angle to rotate a drifter's u and v components to make them front-parallel and front-normal was computed.

Frontal points of intersection (IP) were found by matching the front's latitude and longitude that corresponded to the minimum distance index found when calculating the cross distance. With two of the points of a spherical triangle, it was very easy to find the base vertex point (VP) by giving it the same longitude as the IP and the same latitude as the drifter

observation (DO). With the VP and IP identified we used the great circle function to determine the distance between the DO and the VP (base of the right spherical triangle) and the distance between the VP and IP (hypotenuse of the right spherical triangle; Figure 4.17). After the lengths of all three sides were known, we used the nonlogarithmic solution formulas to determine the angle between the DO latitude and the IP (Beyer, 1991):

$$\cos A = (b^2 + c^2 - a^2) / 2bc \tag{4.3}$$

where

A - angle between the DO latitude and the IP.
a - distance between DO and IP (cross distance)
b - distance between DO and VP (base distance)
c - distance between VP and IP (vertex distance).

This result gave a relative angle with which to rotate the east - west direction to the normal direction. It was still necessary to find the absolute angle needed to rotate the positive u component to be the positive along-front component. To find this actual rotation angle, we needed to know how the DO was placed with respect to the front, the slope of the front at the IP and the direction of the front. Figure 4.18 diagrams a few sample orientations.

Slopes at the IP of the front were calculated by taking a centered difference of neighboring latitudes (rise) over a centered difference of associated longitudes (run), except for the degenerate cases where the IP also happens to be a frontal endpoint. For these two cases we used a forward difference and a backward difference. Slopes of infinity were assigned a specific high number, +/- 1e10. Slopes that were NaN were assigned zero (for

points DO directly on the front). Better slope criteria could be developed by correlating how a front is generally sloping to how far away the DO is from the front.

The next important front parameter to be considered was the front's direction or orientation. Did the front's incremental along-distance component increase heading east (most cases), west (during summer and fall with bent back fronts), south (as a front turns from east to west), or north (when it loops back up)? A front was heading east when the next incremental point from the IP was farther east. It was heading west when the next incremental point from the IP was farther west. If there was no change from the IP's longitude and the next incremental point's longitude, then the front was heading south if the latitude of next incremental point was farther south and heading north if the latitude of the next incremental point was farther north.

The final criteria for determining the absolute rotation angle was whether a DO was inside or outside of the front. All three criteria were placed in a complex nested "if-then" algorithim to find this angle. For example, if the front was heading east, the DO was above or outside of the IP, and the slope at the IP was negative, then the rotation angle necessary to bring the positive u component to be the positive along-front component would have been - (90 - angle A). In all a total of 20 different possibilities were examined. Given this absolute rotation angle, α, the velocity components were rotated according to (Thomas, 1972):

$$u' = u\cos(\alpha) + v\sin(\alpha) \quad (4.4)$$

$$v' = -u\sin(\alpha) + v\cos(\alpha). \quad (4.5)$$

At this point, each drifter had an identifying along-front and cross-front distance and its motion was in terms of movement parallel to the front and normal to the front. The final step was to save all this data to a new master drifter file for use later in statistical analysis. The code used to transform the coordinates can be found in the Appendix B. The results of the statistical analysis are covered in Chapter V.

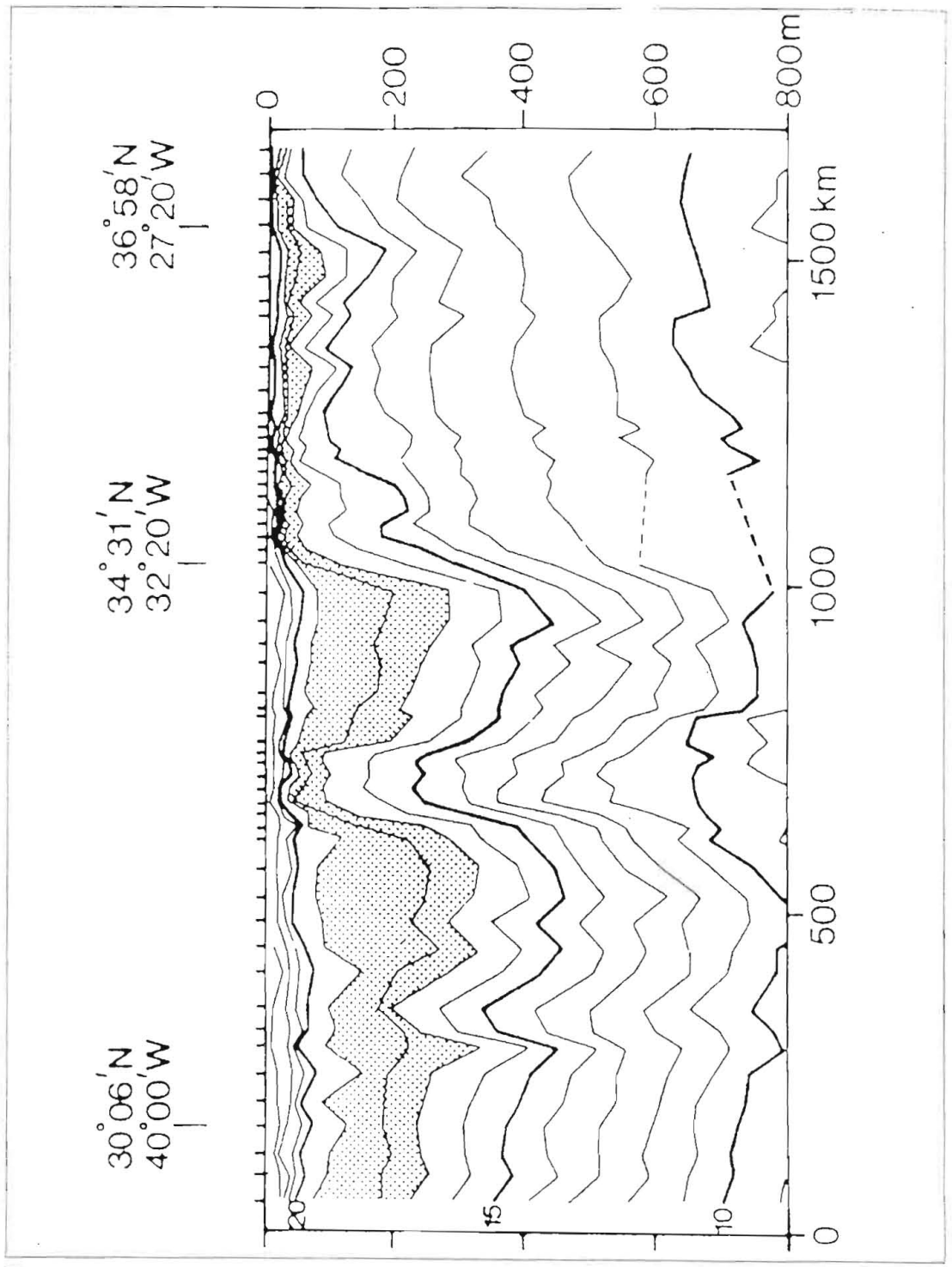

Figure 4.1 Meridional XBT section through the Azores Front. The water mass between 17 and 19 °C is marked with stippling. From Gould (1985).

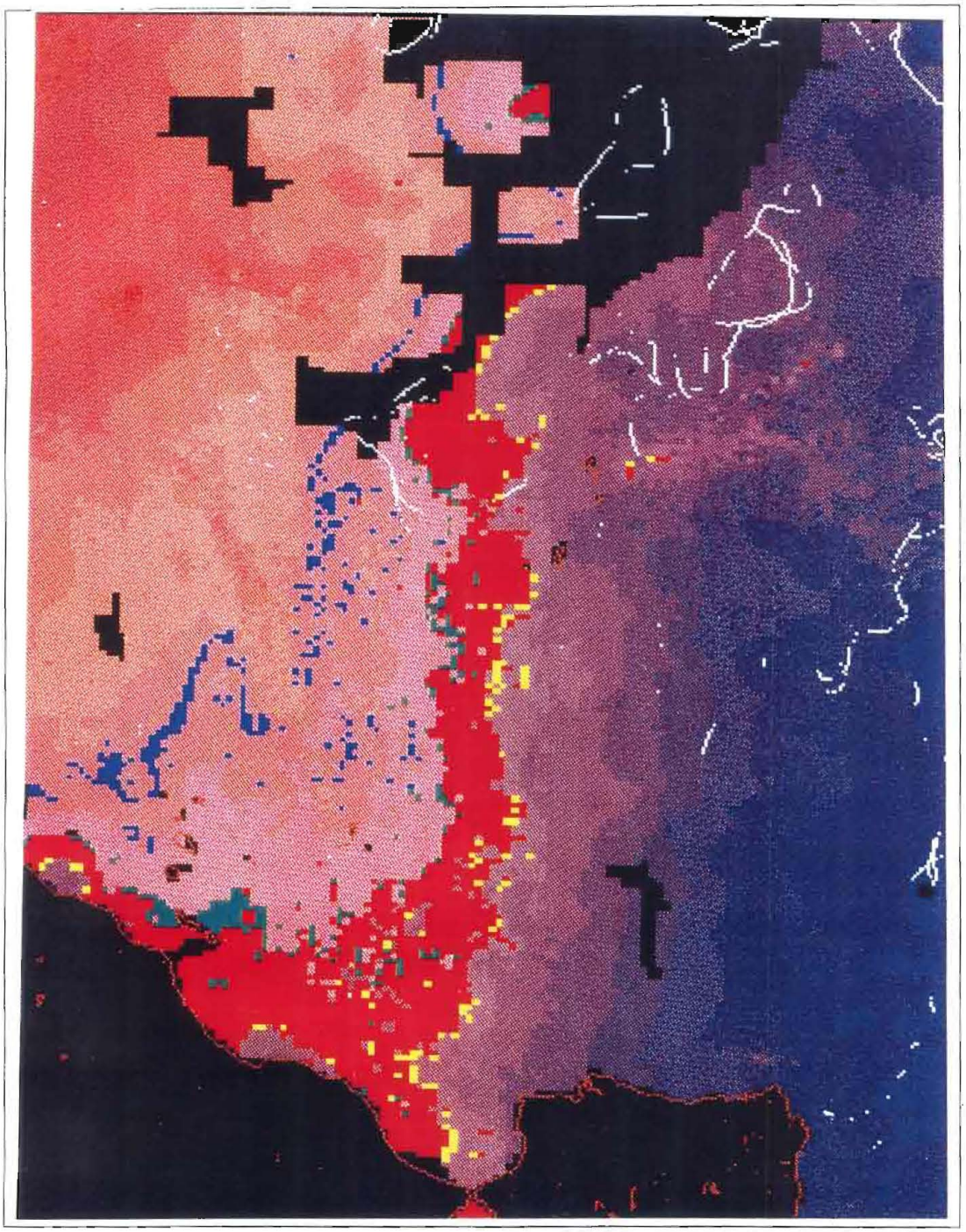

Figure 4.2a DSP SST image for 14 April 1993 (93104). Pixel values 97 (yellow), 102 (green), and 107 (blue) are highlighted along with high-speed (> 30 cm/s) drifter trajectories for 60 days centered on the image time (white). Estimate of the frontal band (red) is also shown.

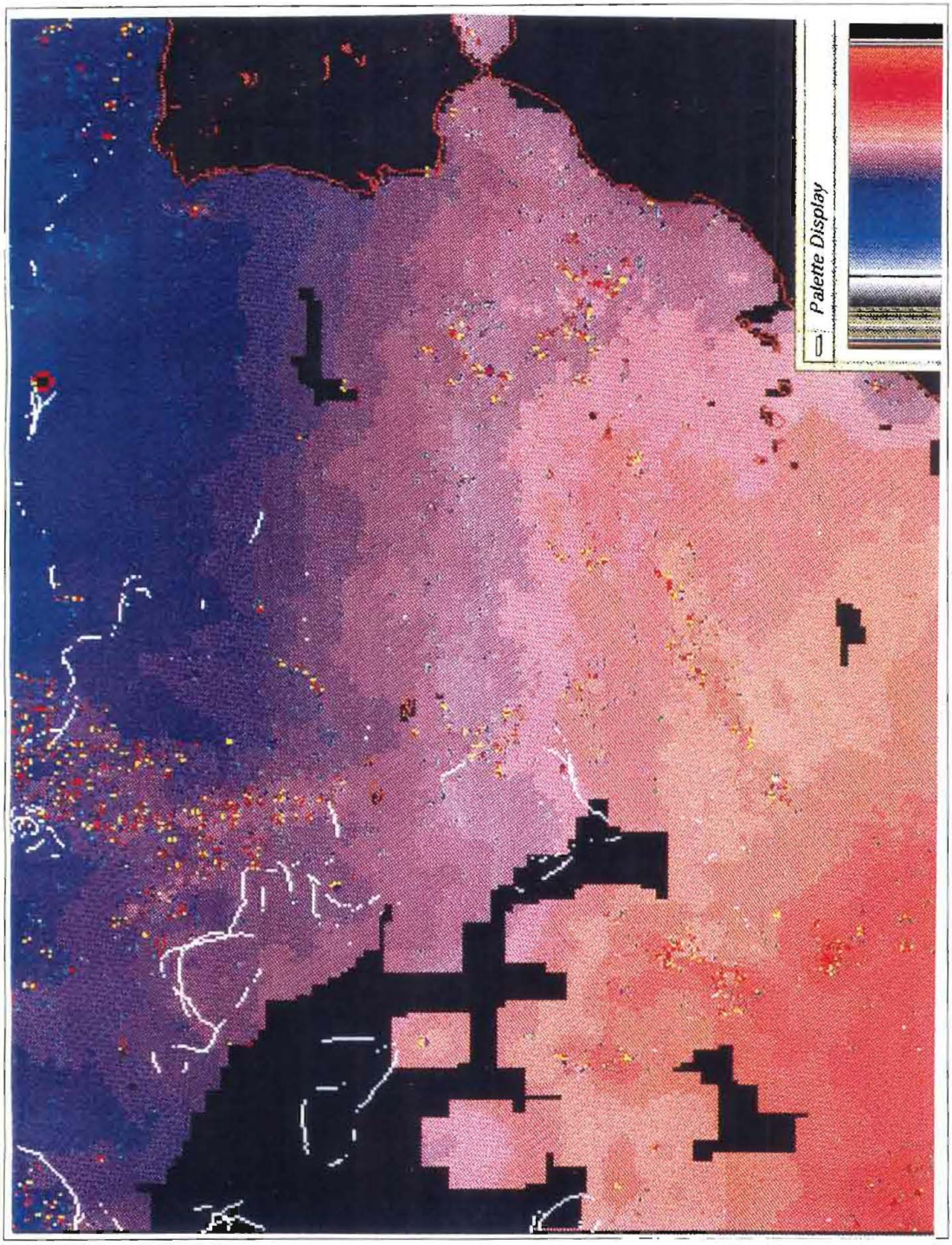

Figure 4.2b DSP SST image for 14 April 1993. High (red), intermediate (yellow), and low (green) temperature gradients are highlighted along with high-speed drifter trajectories for 60 days centered on the image time (white).

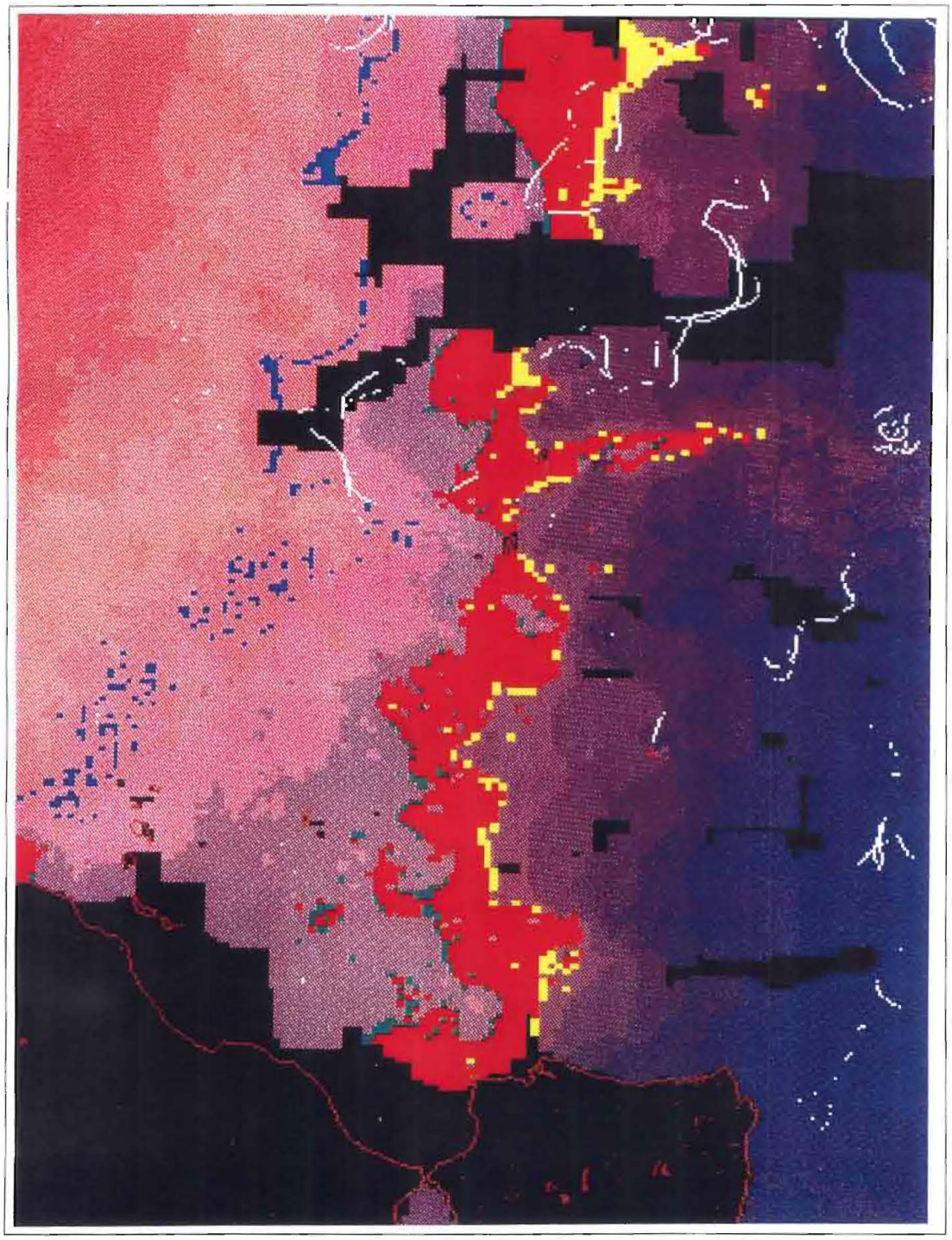

Figure 4.3a DSP SST image for 21 April (93111). Pixel values 97 (yellow), 102 (green), and 107 (blue) are highlighted along with high-speed (> 30 cm/s) drifter trajectories for 60 days centered on the image time (white). Estimate of the frontal band (red) is also shown.

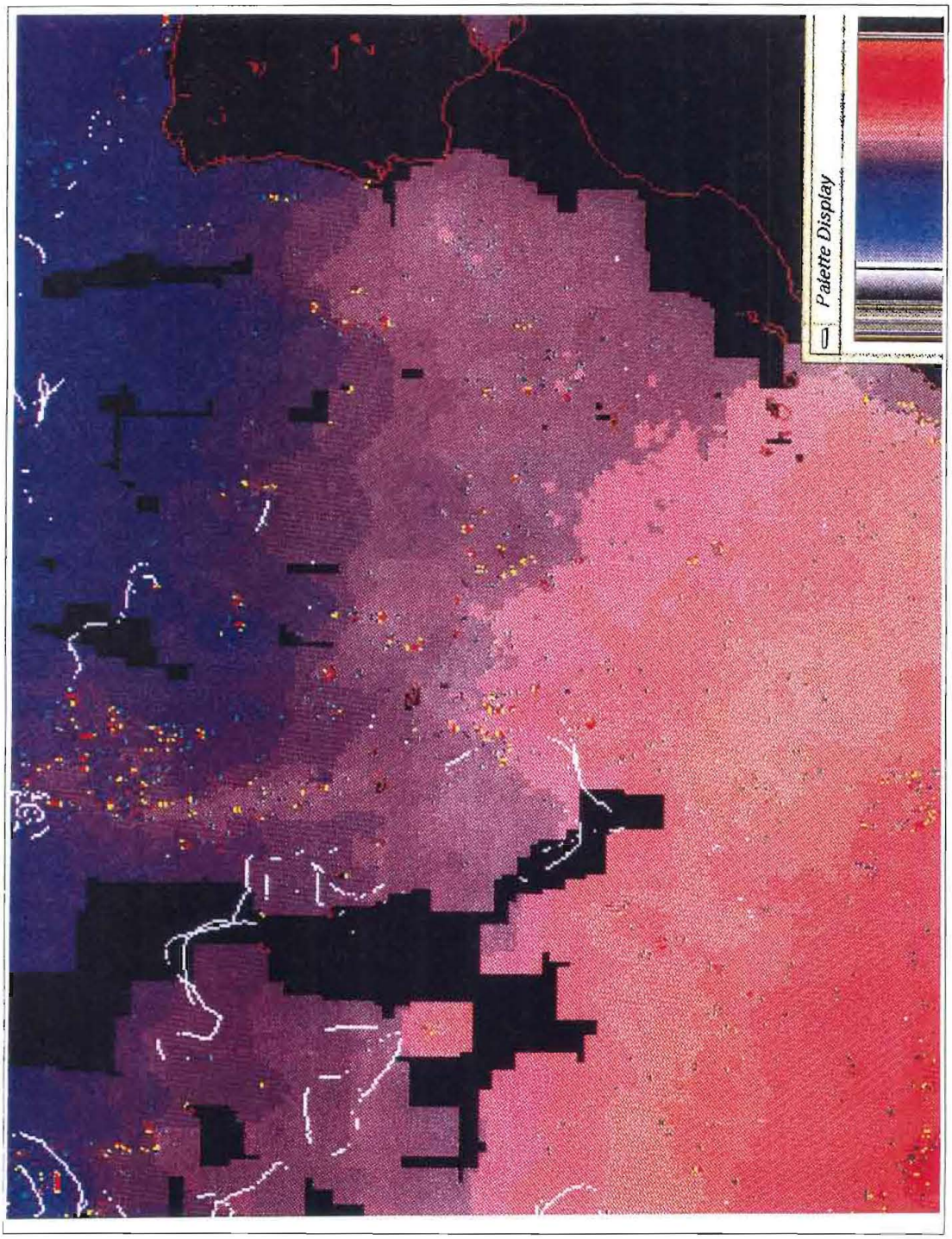

Figure 4.3b DSP SST image for 21 April 1993. High (red), intermediate (yellow), and low (green) temperature gradients are highlighted along with high-speed (> 30 cm/s) drifter trajectories for 60 days centered on the image time (white).

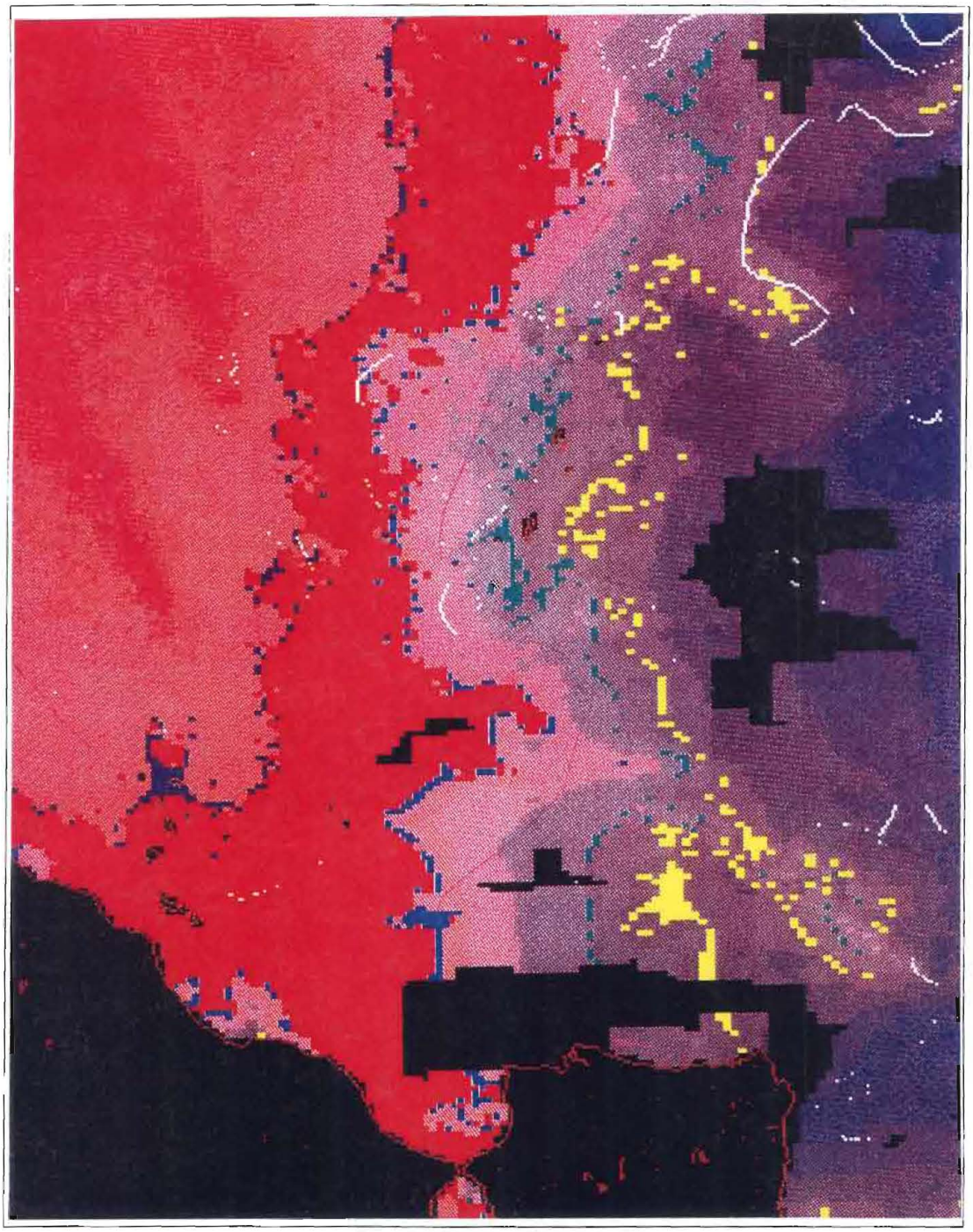

Figure 4.4a DSP SST image for 9 June 1993 (93160). Pixel values 97 (yellow), 102 (green), 107 (blue), and 112 (dark blue) are highlighted along with high-speed (> 30 cm/s) drifter trajectories for 60 days centered on the image time (white). Estimate of the frontal band (red) is also shown.

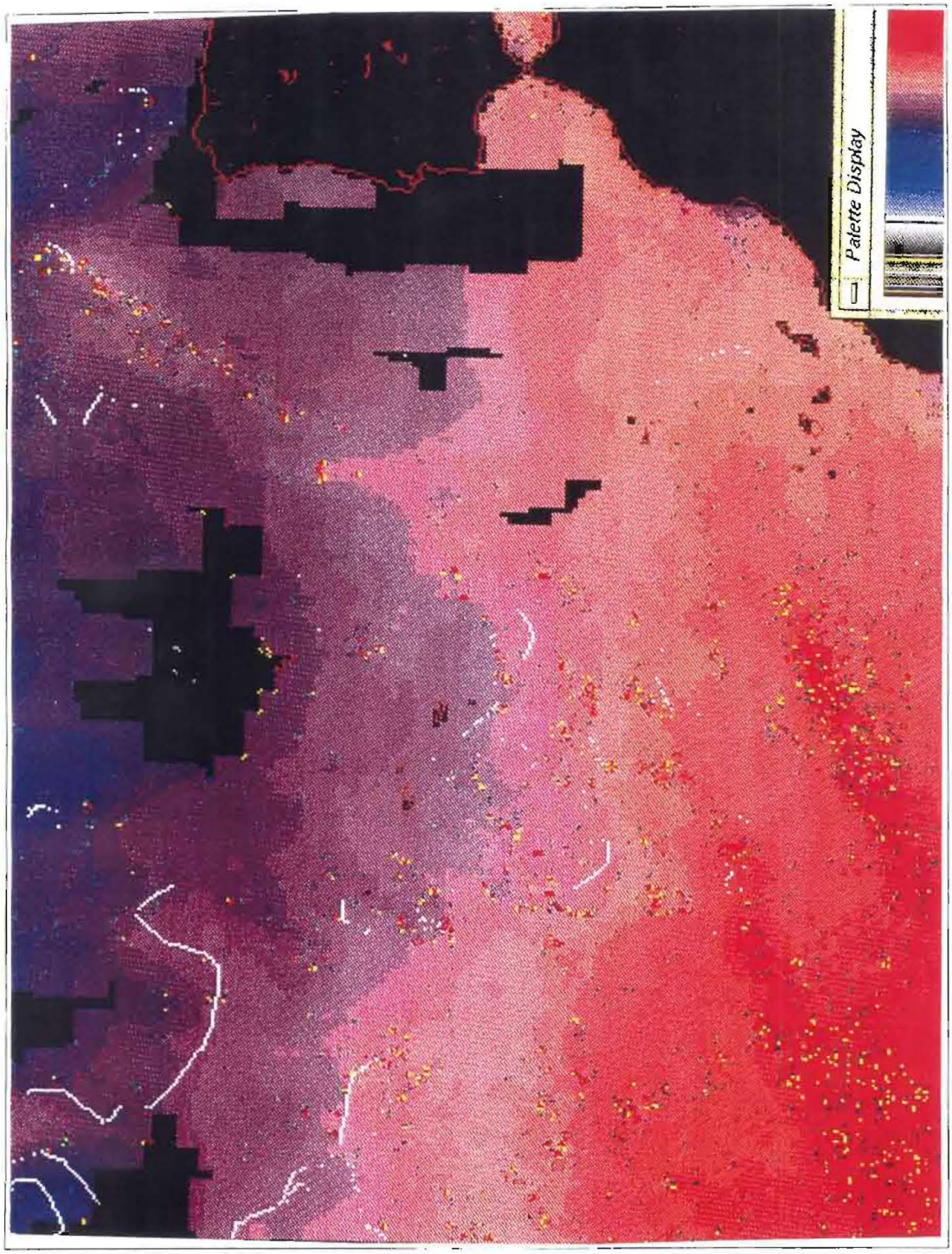

Figure 4.4b DSP SST image for 9 June 1993. High (red), intermediate (yellow), and low (green) temperature gradients are highlighted along with high-speed (> 30 cm/s) drifter trajectories for 60 days centered on the image time (white).

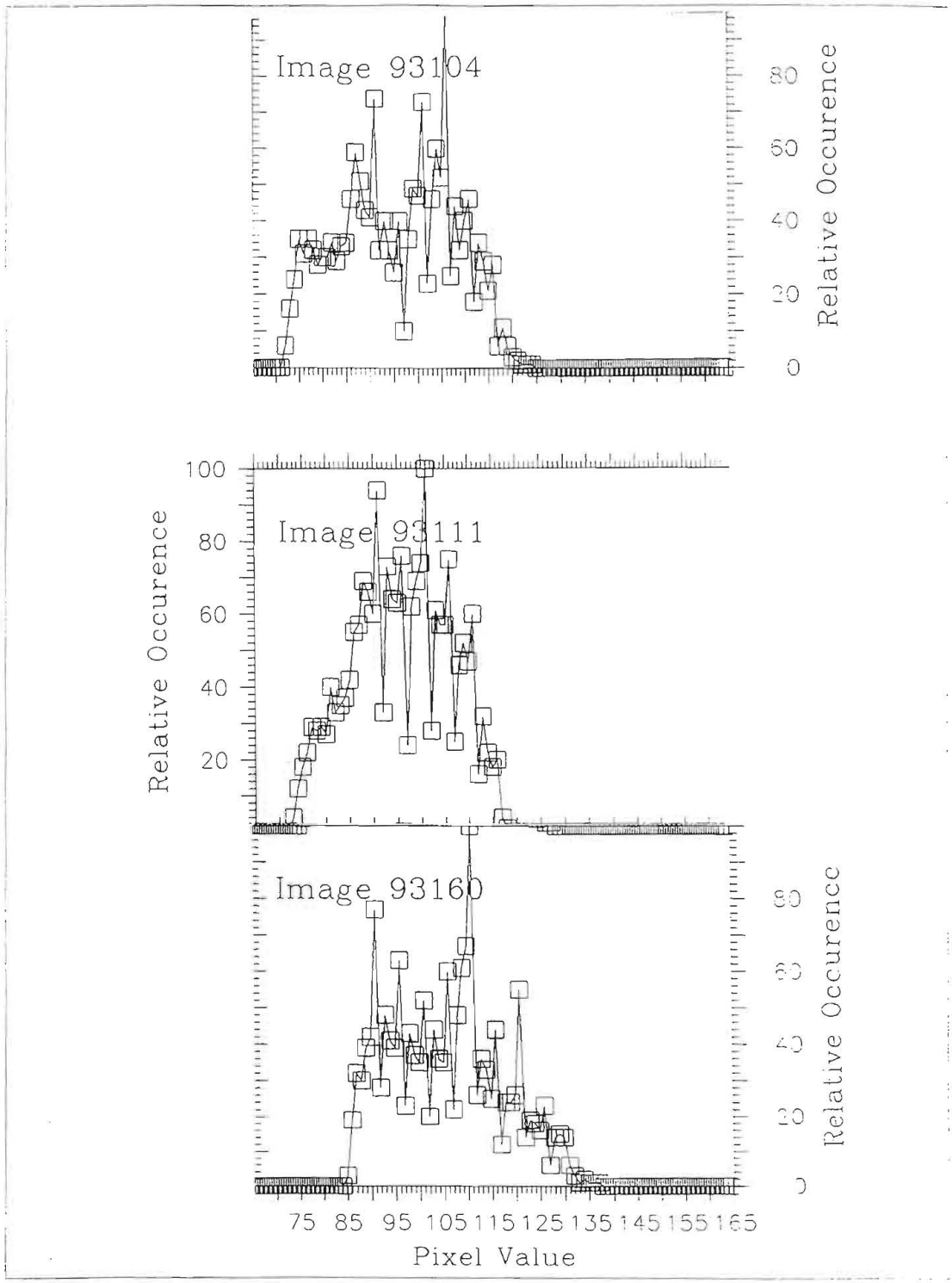

Figure 4.5 Histograms of percent occurrence of pixel values in DSP SST images from 14 April 1993 (93104), 21 April 1993 (93111), and 9 June 1993 (93160).

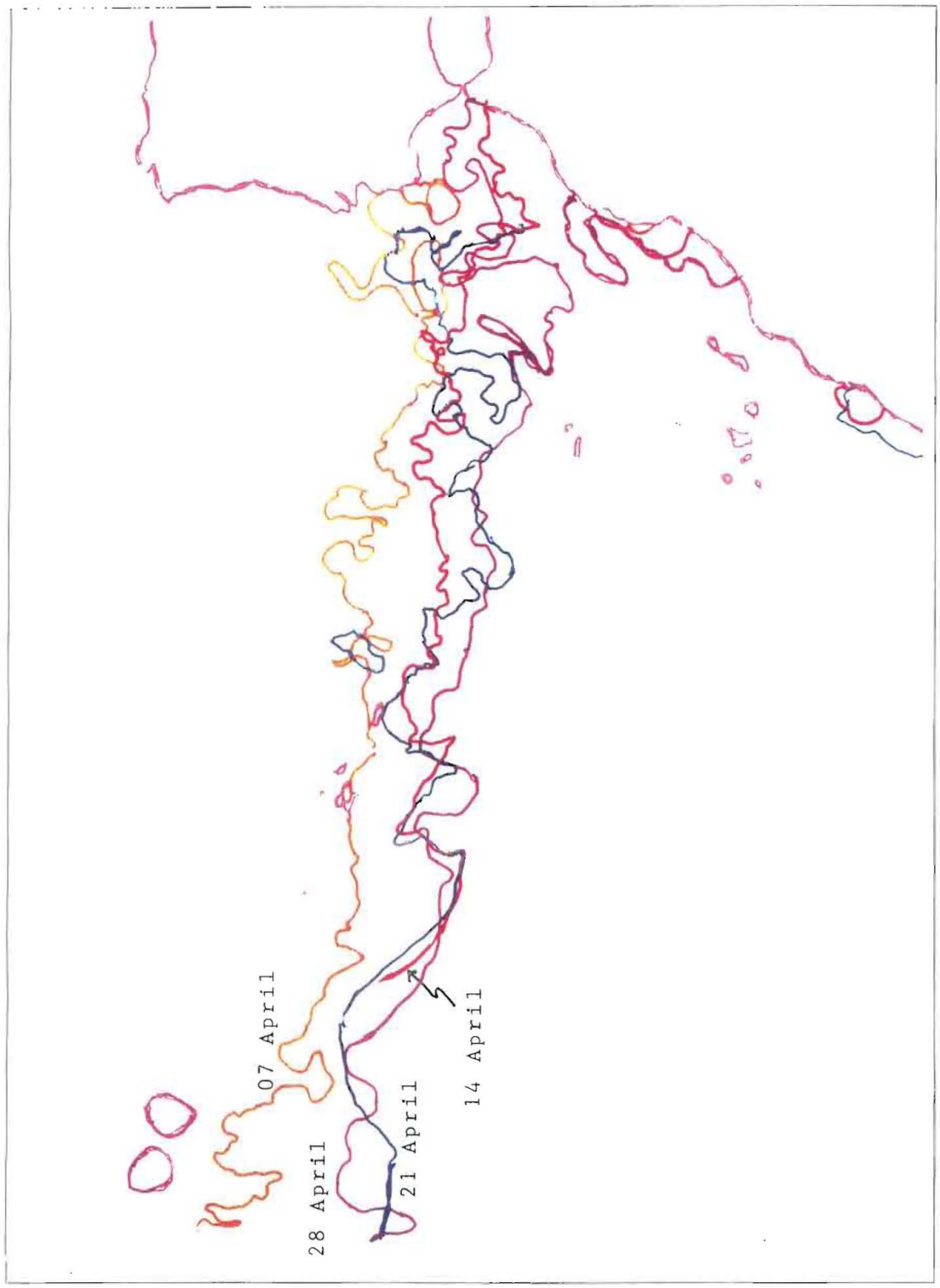

Figure 4.6 Weekly frontal locations for April 1993 from the Pixel Method.

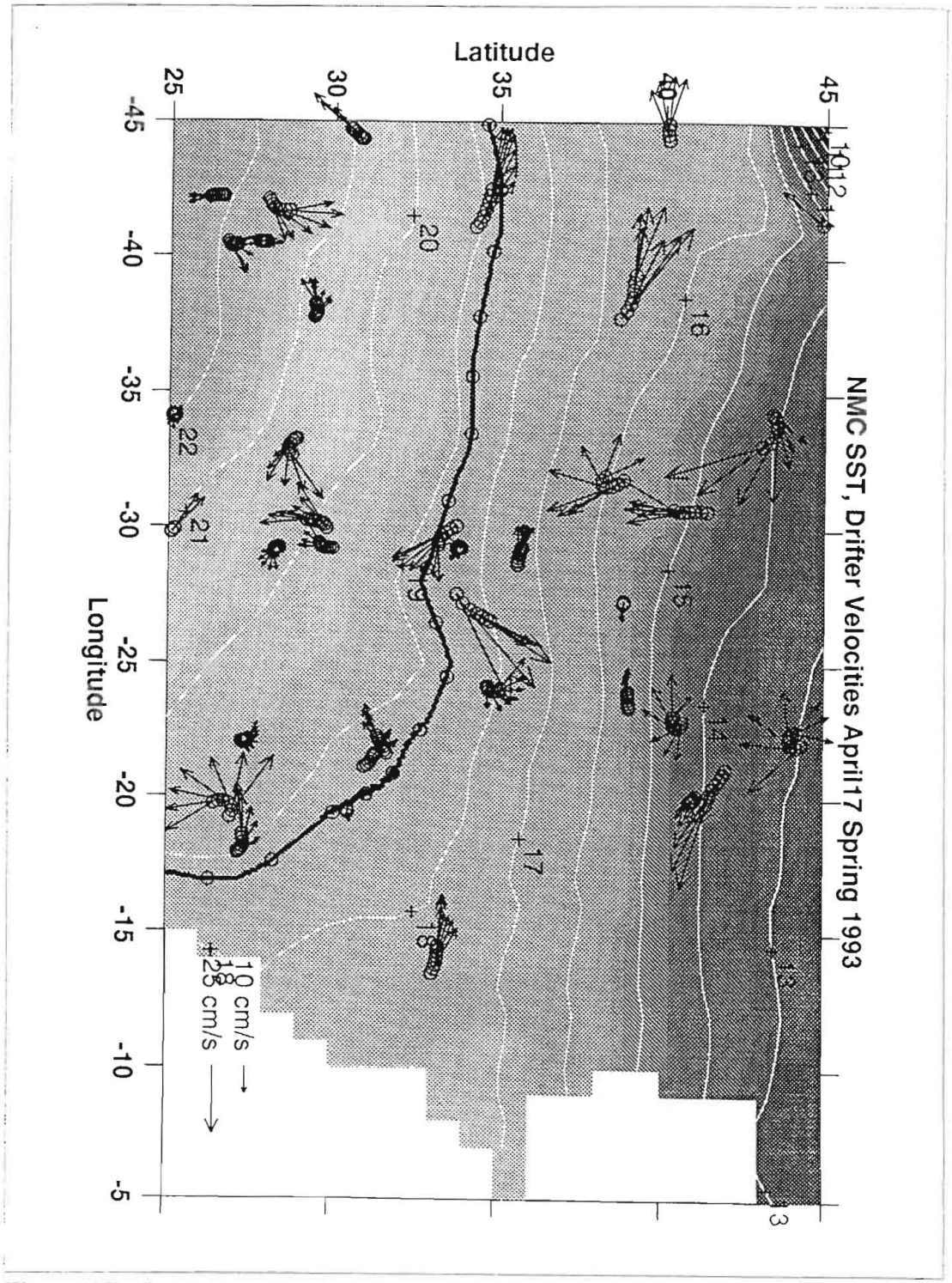

Figure 4.7 Contours of NMC SST with daily drifter velocities for the week of 17 April 1993. Bold line shows characteristic frontal temperature with symbols every 20 points.

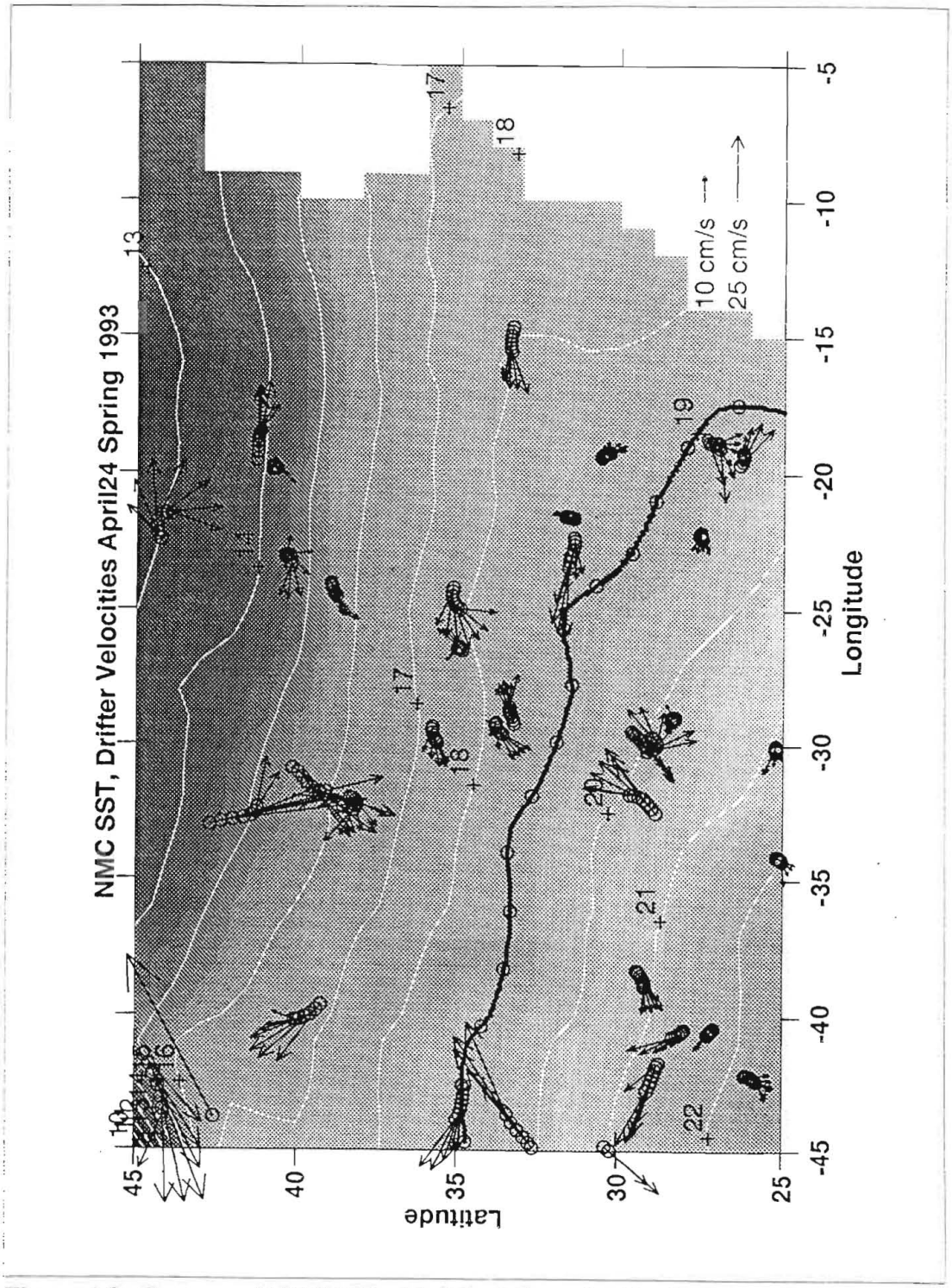

Figure 4.8 Contours of NMC SST with daily drifter velocities for the week of 24 April 1993. Bold line shows characteristic frontal temperature with symbols every 20 points.

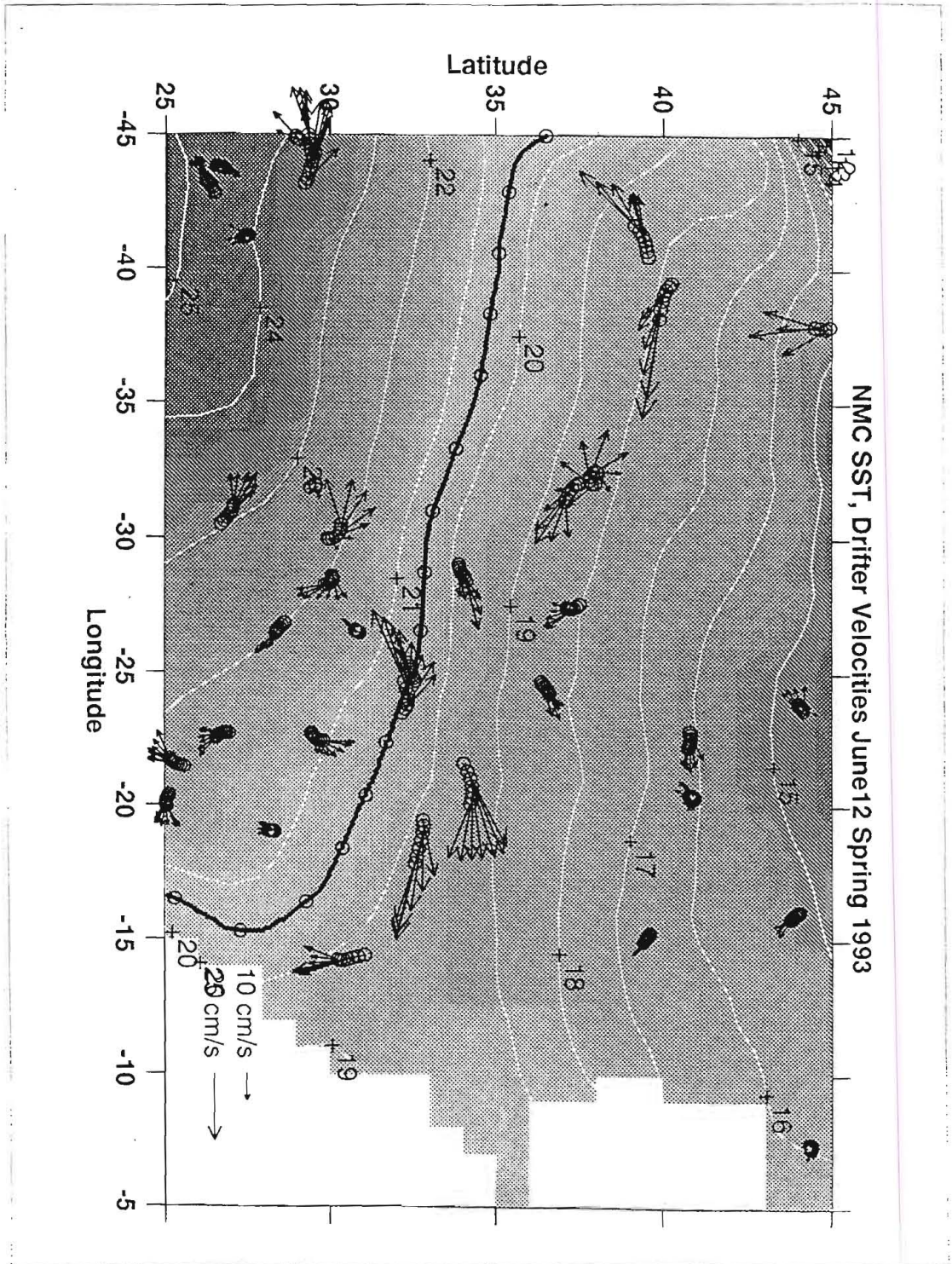

Figure 4.9 Contours of NMC SST with daily drifter velocities for the week of 12 June 1993. Bold line shows characteristic frontal temperature with symbols every 20 points.

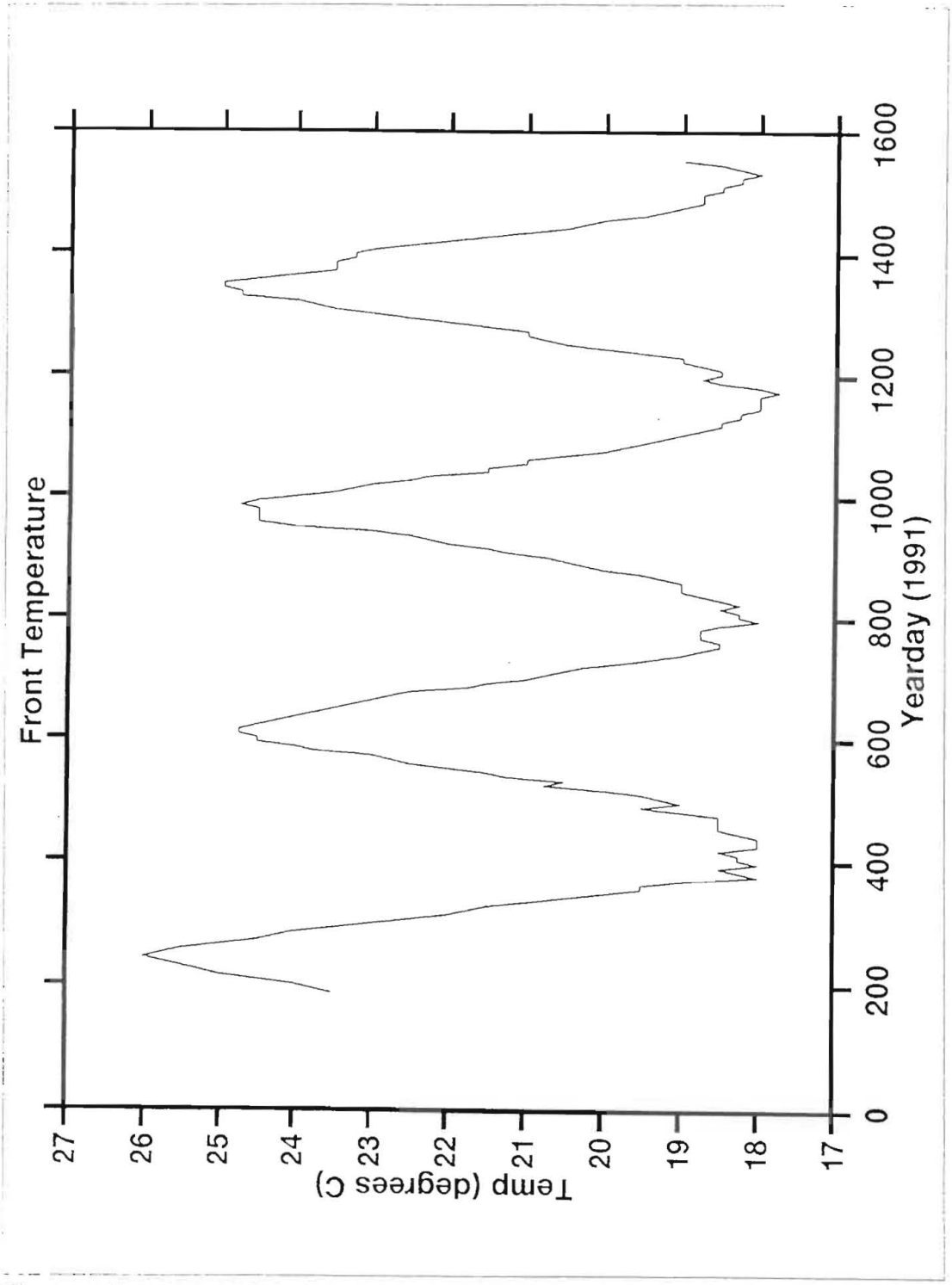

Figure 4.10 History of characteristic temperatures for the Azores Front based on weekly NMC SST analysis.

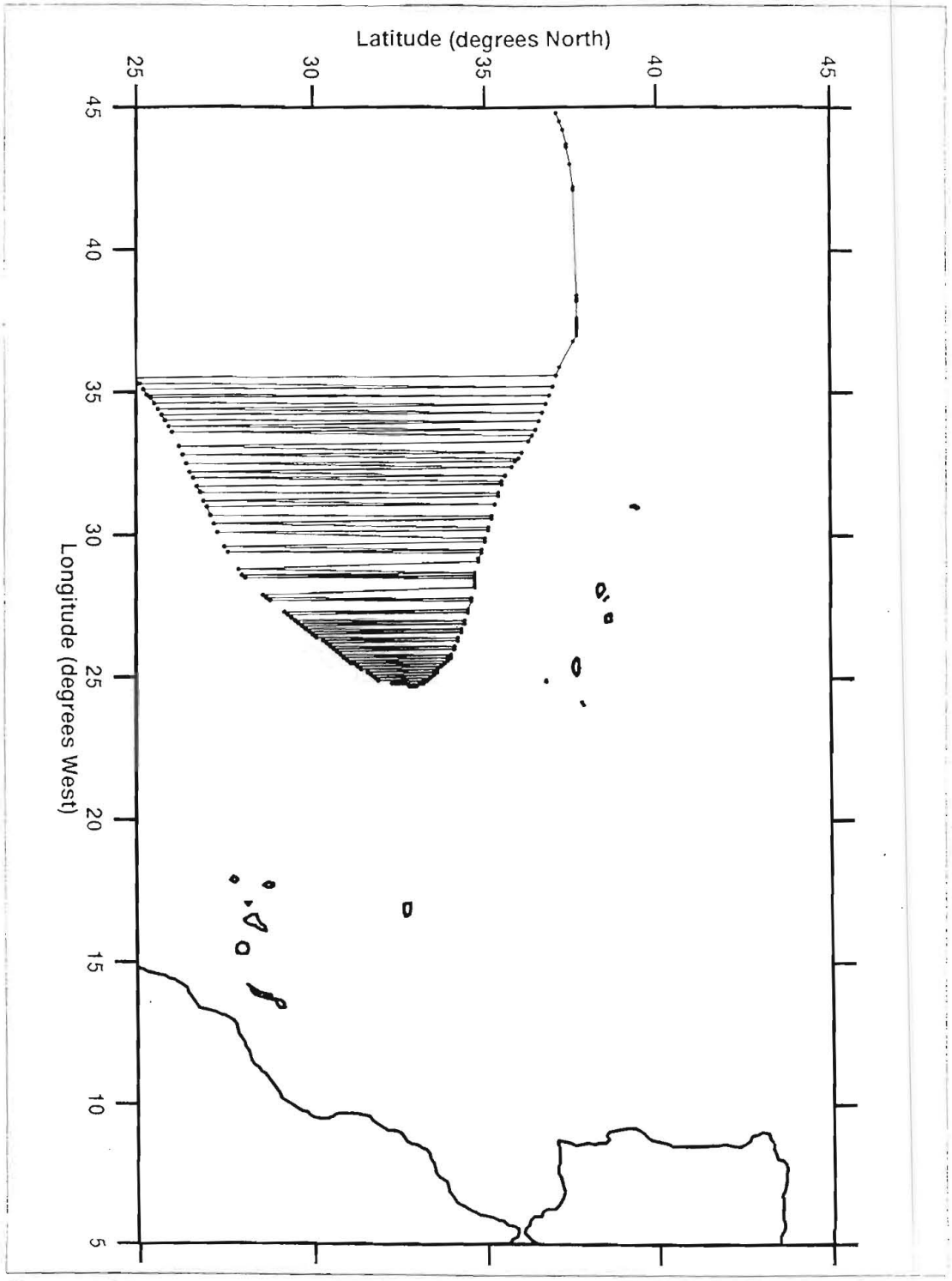

Figure 4.11 Sample jagged "sawtooth" front of unsorted positions for the week of 17 August 1991.

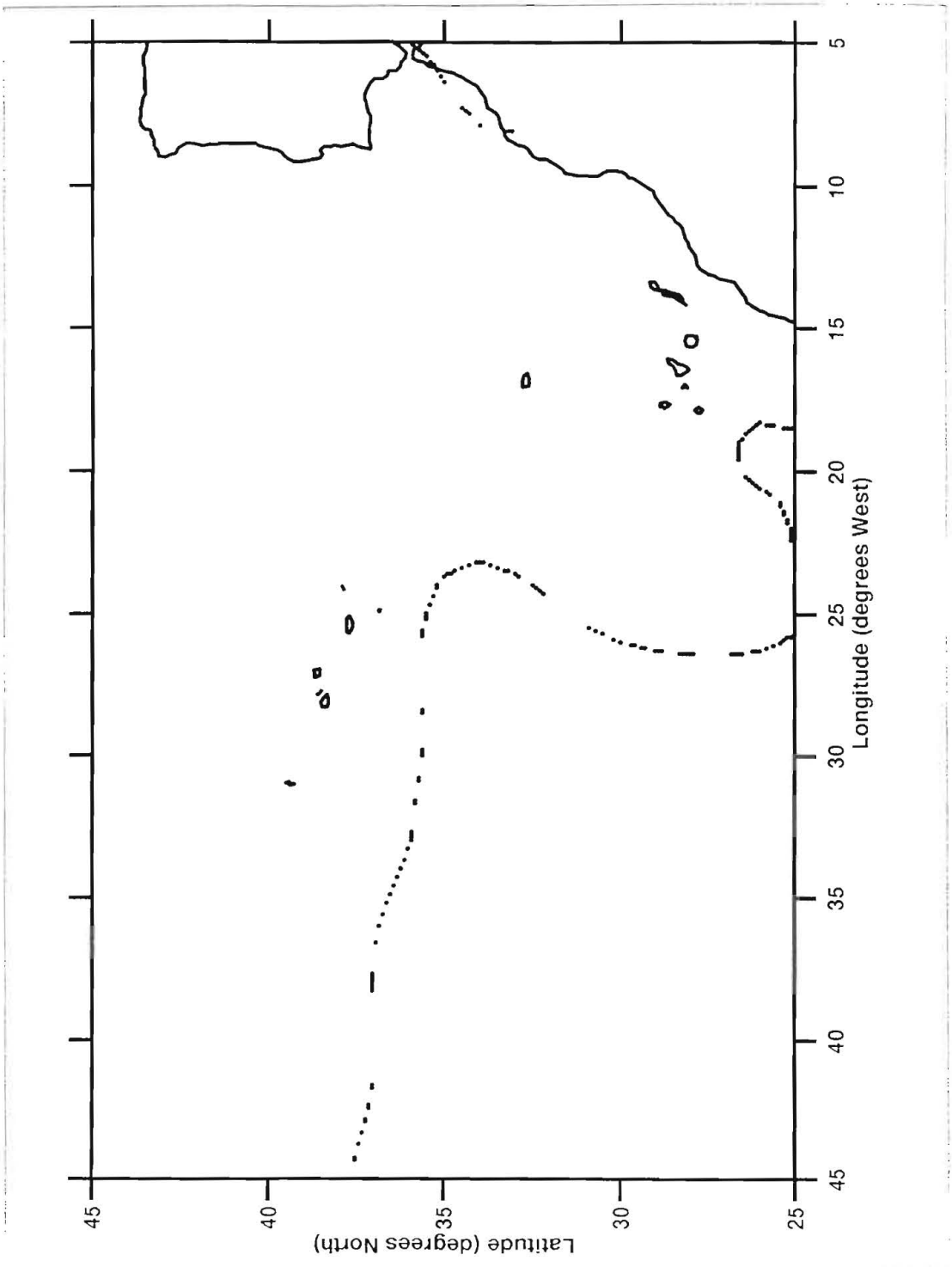

Figure 4.12 Sample of sorted frontal positions with large gaps for the week of 25 July 1992.

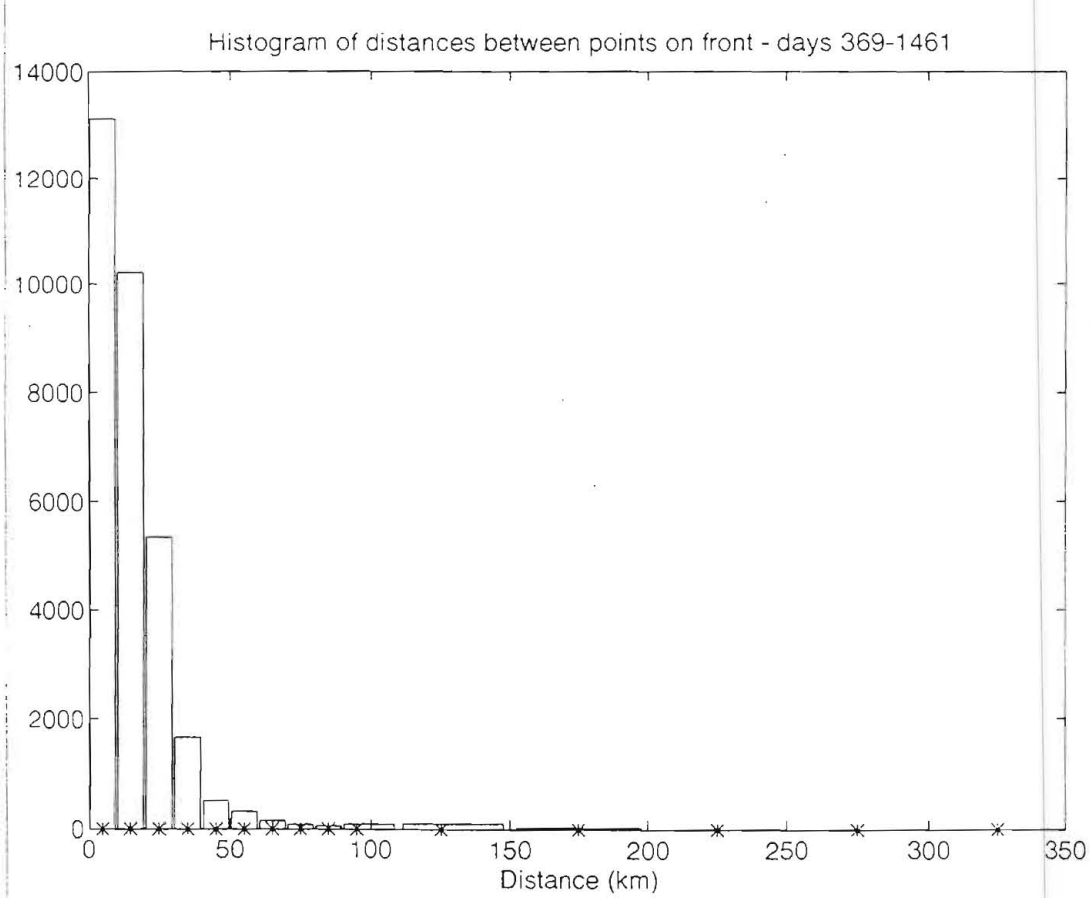

Figure 4.13 Histogram of distances between sorted points on the front before interpolation.

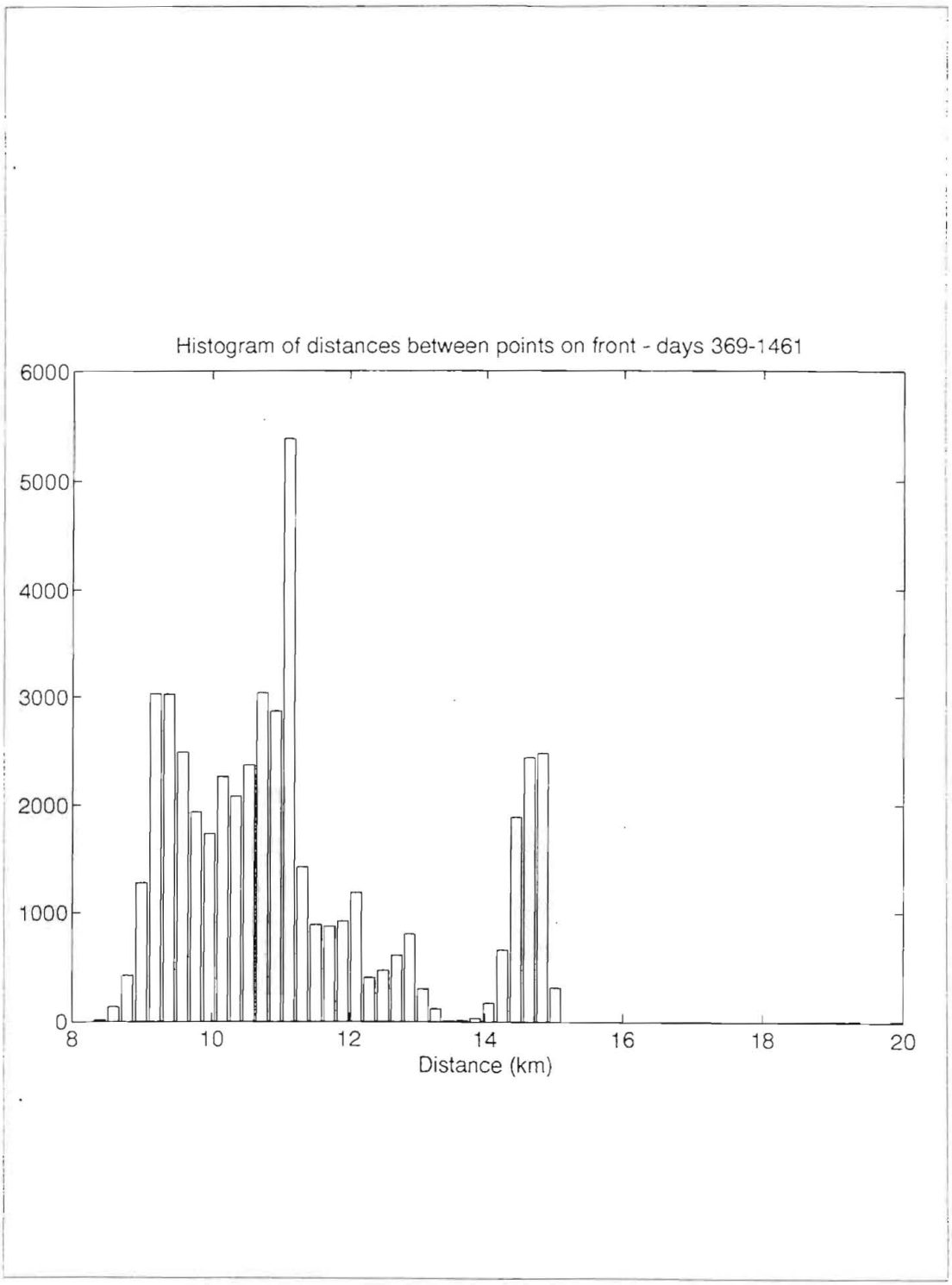

Figure 4.14 Histogram of distances between sorted points on the front after interpolation.

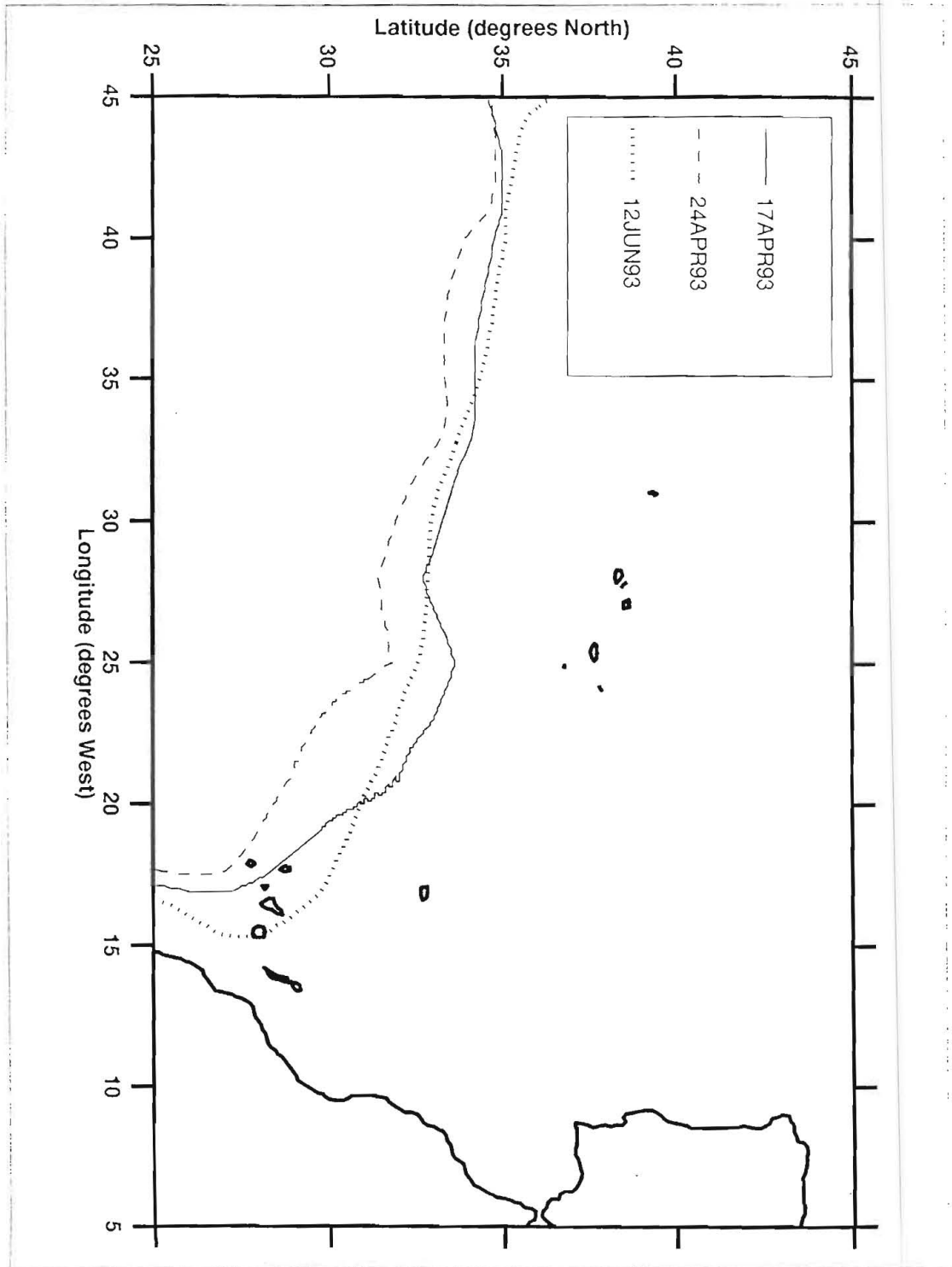

Figure 4.15 Sorted and interpolated SST fronts based on weekly NMC analysis. (cf high resolution fronts in Figures 4.2 - 4.4).

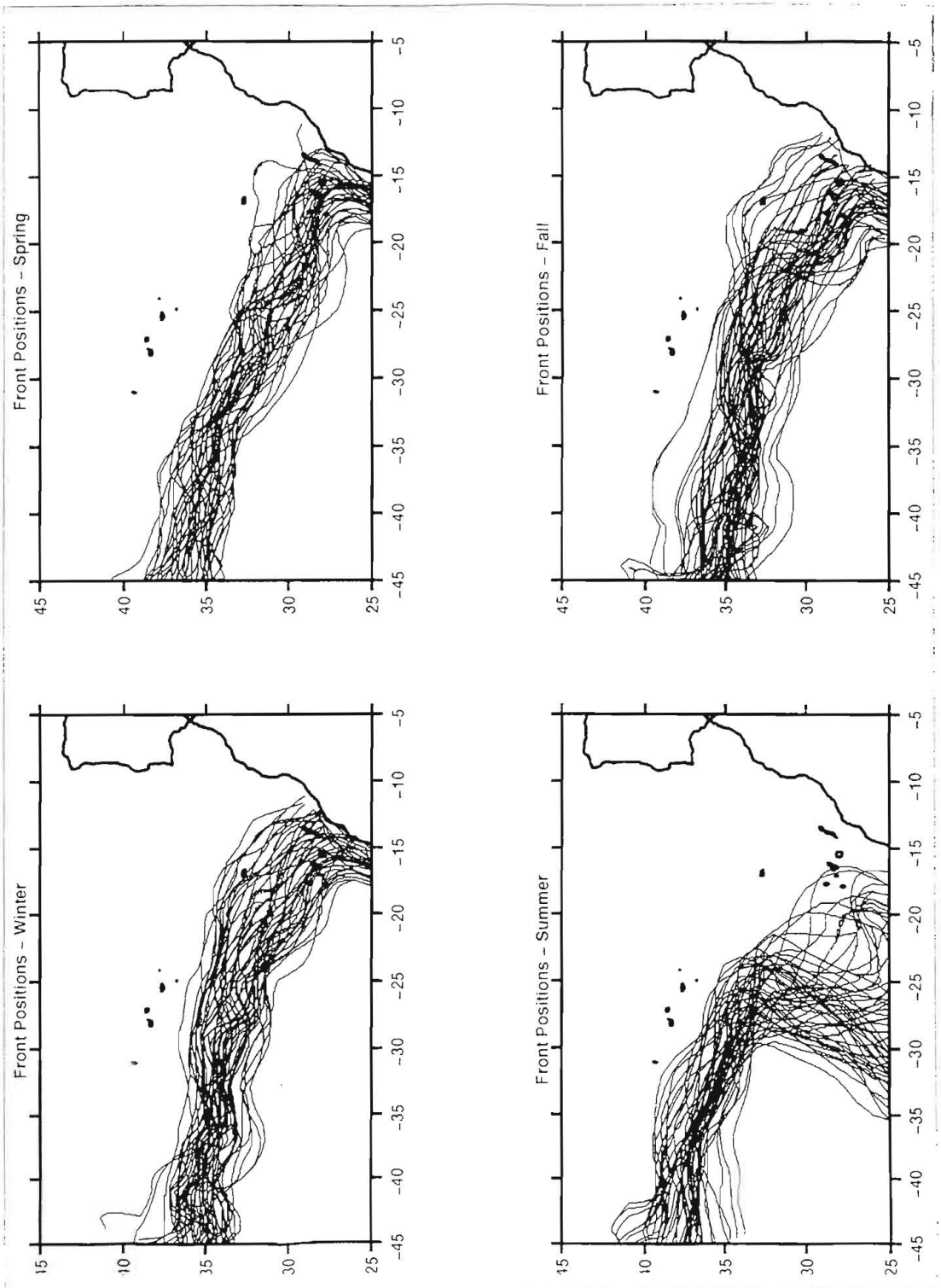

Figure 4.16 Seasonal composites of weekly SST fronts based on NMC analysis.

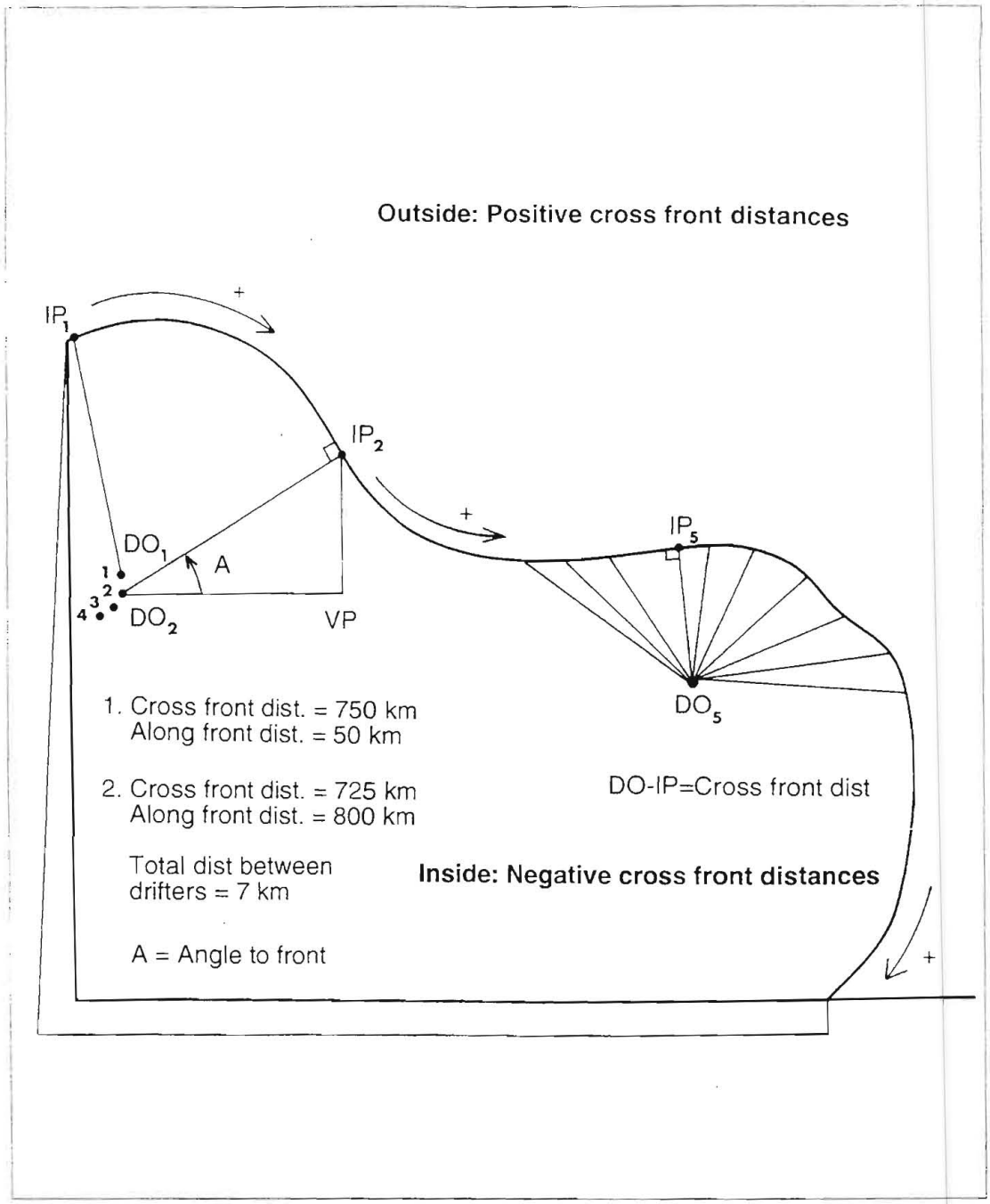

Figure 4.17 Schematic of drifter positions (DO) relative to location and orientation of a front. Intersection point (IP) determines distance to front. Along-front distance increases as shown. Vertex point (VP) is used to calculate angle to front (A). Bounding polygon is used to determine positive and negative cross-front values. Sample drifter trajectory with large jump in the intersection point for a small change in drifter position illustrates a potential problem for strongly curving fronts.

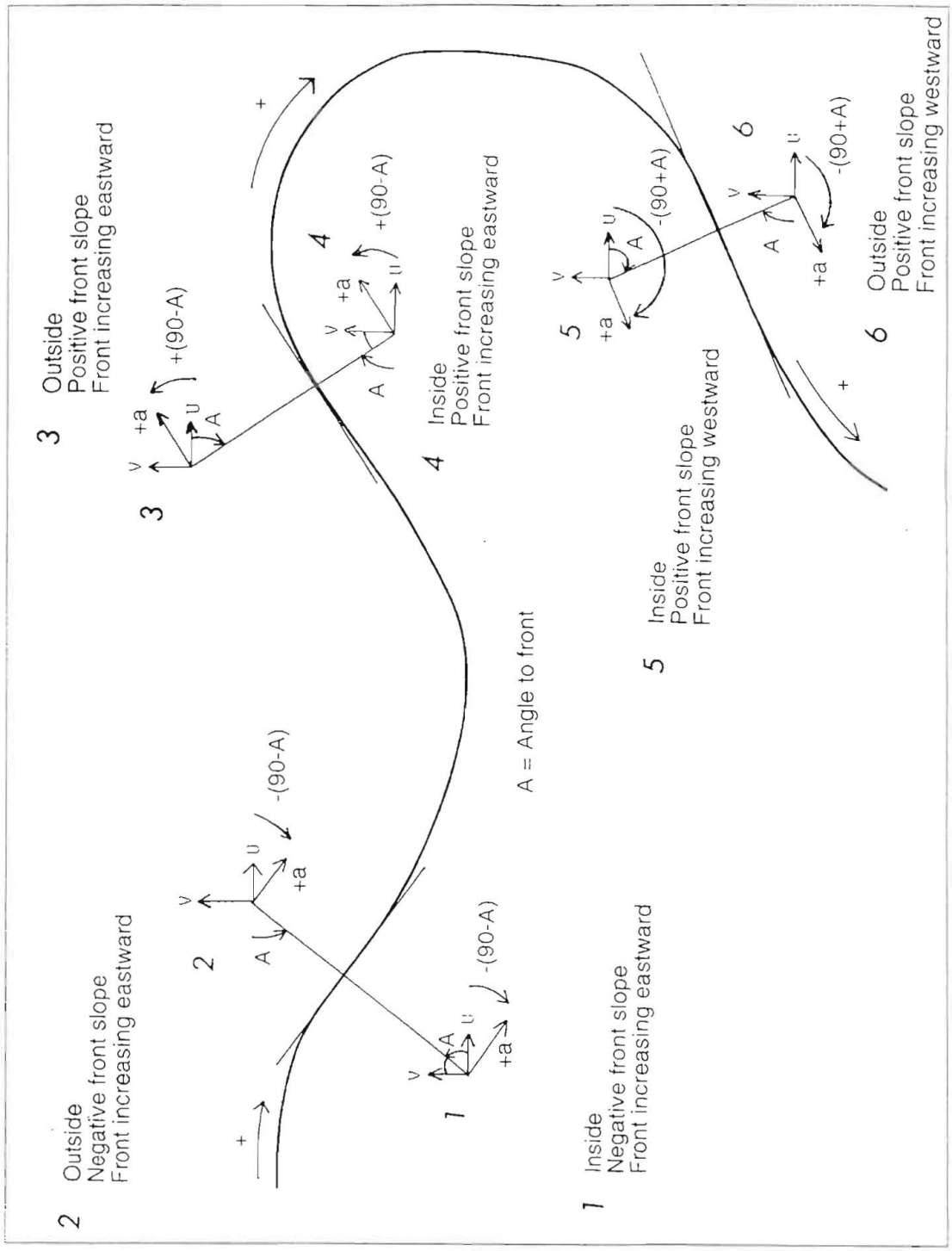

Figure 4.18 A few sample orientations of drifters relative to the front and the absolute rotation angles required to align velocity observations with the positive along-front direction.

V. STATISTICAL ANALYSIS AND RESULTS

In this chapter we present the results of statistical analyses showing mean currents, eddy kinetic energies (EKE) and standard errors. These values are given for both types of coordinate systems: latitude/longitude (Cartesian) coordinates and frontal coordinates. Cartesian coordinates used 1° latitude x 2° longitude boxes for averaging, while frontal coordinates used 150 km x 150 km boxes. Divergence is not numerically calculated due to the high noise level, but is qualitatively described using our the one degree zonal or along-front averages. Zonal or along-front averages were used to demonstrate the strength of the "east-west" flow is near the front as well as strength of the "north-south" flow convergence and divergence near the front. Regional divisions were also made. This reflects the intended focus on the large scale Ekman convergence in the north-south direction.

Seasonal averages were examined for trends and features. Spatial coverage for the four seasons can be seen in Figure 2.8. Although sufficient data are not available to characterize any distinguishing features from the four seasons, we do see that two seasons highlight the greatest differences in the velocity fields: summer (July - September) and winter (January - March). The seasons of spring (April - June) and fall (October - December) are transition periods and are not described here.

Regional averages were computed following Giannetti (1993): 1) by combining data for the entire range of longitudes in large areas covering many degrees of latitude (large area averages) and 2) by combining data for the entire range of longitudes in successive latitude bands extending over 1 degree of latitude (zonal averages). In the former case, three large

regions were defined: the Southern region, which combined all data south of 33° N, the Northern region, which combined all data north of 35° N, and the Frontal Zone (FZ), which combined all data in the latitude range between 33° N and 35° N (Figure 2.4). The Southern region, FZ, and Northern region accounted for 51.6, 19.5, 28.9 percent of the data, respectively.

In this chapter the mean mixed layer velocity components in lat/long coordinates (u,v) and frontal coordinates (a, c), together with their standard errors, are presented for the complete dataset. It is also possible to compute average velocities and standard errors for the ensemble of drifters available each day, month, season, or year. All mean current estimates are treated with an Eulerian perspective; that is, the data were combined according to the time and location of the observation (in lat/long or along/cross coordinates) without considering the trajectories from which they were derived. Standard errors of the means for each coordinate system were also calculated. To perform these calculations, it is necessary to know the number of independent velocity estimates that went into a particular average. That number was obtained by dividing the number of daily interpolated velocity samples by the number of samples required to total one integral time scale. From Giannetti (1993) a conservative value of 7 days was used for the integral time scale.

All averages presented in this thesis are accompanied by the 95% standard error of the mean, which is calculated according to the following formula:

$$u_{err} = \frac{2\sqrt{\sigma^2}}{\sqrt{N^*}} \qquad (5.1)$$

where σ^2 is the variance of the data and N^* is the number of independent observations. For example, in the case of the average velocity based on N daily interpolated observations, N^* is equal to N/7. A similar formula holds for the north-south standard error, v_{err}. The standard errors are generally much smaller than the standard deviations due to the larger number of observations in certain areas. The "break even" point occurs with 28 observations in a box. We chose to be very conservative, thus, plots show arrows/values for only those boxes containing at least 80 observations.

A. LATITUDE/LONGITUDE (CARTESIAN) COORDINATES

1. Mean Currents

Given the lack of sufficient data north of the Azores Islands, we have replotted the mean currents on a domain extending only to 42° N. These mean values and their associated standard errors are presented for the entire four-year dataset in Figures 5.1 and 5.2, respectively. They are based on all available data from the time of the first observation until the final yearday in question. The current vectors have not been corrected for any array bias that could be due to variations in data concentration from the process of diffusion. These corrections are made in Paduan et al. (1995). Despite the factor of two change in concentration over much of the SUBDUCTION area, the maximum correction applied to the mean currents had a magnitude of 6 cm/s, while most of the array biases had corrections of less than 2 cm/s (Paduan et al., 1995). Giannetti (1993) calculated an array bias of 0.7 cm/s for zonally averaged meridional velocity components.

A few important features are readily identifiable from the large-scale domain mean values: 1) a noticeable eastward flow (~ 5 to 15 cm/s) between 33° N and 35° N — the Azores Current; 2) a significant southward flow (~ 10 to 20 cm/s) in the vicinity of 40° N, 40° W — the North Atlantic Current feeding the Azores Current; 3) return flow (~ 5 to 15 cm/s) curving southwestward along the North African continental slope — the Canary Current; 4) slow, but identifiable counter-currents to the immediate north (~ 35° N) and south (~ 32° N) of the Azores Current; 5) a relatively calm center, located at 31.5° N, 20° W — the Madeira Plateau; and 6) bifurcation of the Azores Current west of the Madeira Plateau near 23° W.

Significant mean values can also be found in the large-scale regional averages. In particular, the Frontal Zone has strong eastward currents of 4.8 cm/s. In the Southern region, the mean currents are southwestward at 2.2 cm/s. For the Northern region, the mean currents are southeastward at 1.2 cm/s. Over the entire domain outlined in Figure 1.2 the mean current is 0.8 cm/s in the south-southeast direction.

For seasonal averages, unfortunately, we do not yet have sufficient data for the whole frontal area to be displayed. What observations were available for the region covered did reveal a few interesting points. The winter season had a slightly higher density of drifter observations, mostly in an area south of 35° N. One remarkable feature was the apparent "eddy-like" velocity field. Five possible vorticity centers could be located. A high level of noise obscured the characteristic eastwardly flow indicative of the Azores Current. The return flow itself was also noticeably farther away from the North African coast than

described by the entire dataset. The summer season had a lower density of drifter observations, but its relatively sparse velocity field was clearly more organized. Immediately noticeable were the characteristic eastward flows we expected for the Azores Current. These flows were centered around 33° to 34° N. Two return flows could also be identified — one along the continental slope of North Africa, and the other (less intense) starting around 27° W and heading southwest to 39° W. Whether these features are artifacts of the sampling or climatological features will await further analysis after more drifter observations have been made. These results provide a glimpse of seasonal patterns that were not previously available (Giannetti, 1993).

2. Eddy Kinetic Energy

Variability about the mean currents observed in the drifter data is also a useful measure of the currents in this area. The large number of observations obtained in this study provide a good characterization of the current variances. Looking at EKE fields can help us identify the position of the front. From our conceptual model, we expect to see higher EKE values immediately to the south of the front, where eddies and meanders are generated. EKE, which is defined as the average of the east-west and north-south variance, can be compared with values from other oceanographic regions and with values obtained from numerical models of ocean circulation.

The EKE for the complete dataset is shown in Figure 5.3. One can immediately see that the frontal zone has high EKE with values exceeding 200 cm^2/s^2. Generally speaking,

there is greater EKE south of the front than there is to the north, although these results are not conclusive. Overall, our results are consistent with the earlier computations of Richardson (1983) who calculated EKE distribution for 2° squares in the North Atlantic from satellite-tracked drifters and found EKE in excess of 200 cm^2/s^2 for the area 32° - 34° W by 32° - 34° N, which is within the Frontal Zone of this study. One item to note is the low EKE values in the Canary Current. This suggests that the Canary Current is a steady feature with little meandering or generation of eddies.

The average EKE was 126 cm^2/s^2 for the entire dataset. Krauss and Käse (1984) found an average EKE of 100 cm^2/s^2 in the SUBDUCTION region, while Giannetti (1993) calculated a value of 102 cm^2/s^2. There is a noticeable change in average EKE for the different regional groupings. The Southern region has an EKE of 81 cm^2/s^2, the Northern region an EKE of 157 cm^2/s^2, while the EKE in the Frontal Zone averaged about 181 cm^2/s^2. The apparent inconsistency of the Southern region's EKE versus the Northern region's EKE can be explained by the regional distribution of data (mostly in the Southern region than in the Northern region). When one considers the lat/long box averages with at least 80 daily observations in them, then the higher EKE values become more apparent immediately south of the front.

Comparing the winter/summer seasons a generally higher EKE field covering the winter season is present compared to the summer season. A few isolated pockets of 200 cm^2/s^2 could still be found in both seasons.

3. Zonal Averages

A second type of regional average was performed using drifter data based on zonal averages over smaller bands. Averages of all daily interpolated velocity estimates spanning the range of longitudes in one degree increments of latitude were computed. The results for these 1 degree latitude "windows" are shown in Figure 5.4 for the latitude range from 25° N to 45° N. The north-south variability of the mean currents based on the drifter data is highlighted in these results.

The zonally averaged velocity components shown in Figure 5.4 represent the mean conditions based on observations of the four-year dataset. The success of the measurements — in terms of the goal to observe statistically significant mean currents in the SUBDUCTION region — has greatly improved since Giannetti (1993). Standard errors of the mean components are also shown in Figure 5.4 and they indicate that uncertainties are small for most latitude zones, which is expected given the large number of observations in this dataset. The number of daily interpolated observations in each zonal average is also shown in Figure 5.4.

The east-west velocity component is relatively well resolved in the dataset, particularly for the latitudes around the Azores Frontal Zone. The average eastward velocity shows a significant current to the east of about 5 cm/s over a band from 33° N to 35° N with a peak of 5.4 cm/s at 33° N. The standard errors are less than 1.1 cm/s for this velocity component. The drifter observations have clearly isolated the mean eastward velocity in the vicinity of the Azores Front.

Immediately to the north and south of the frontal latitude band (within 2°) there are slight westward counter-currents of 0.8 cm/s to 1.8 cm/s, opposed to the direction of the maximum currents. This is consistent with hydrographic observations of the Azores Front (Stramma and Müller, 1989), as well as recent satellite altimetry data (Cromwell et al., 1995). The fact that velocities are oppositely-directed in the Frontal Zone means that averaging over fixed latitude ranges over multiple years - as was done in this study - will produce mean values that are much lower than instantaneous values near the front. Further to the south of the Frontal Zone there are significant mean westward currents of 2.5 cm/s to 3.3 cm/s in a broader latitude band from 25° N to 30° N. These results show the return flow of the Azores Current and the Canary Current.

The zonally averaged north-south velocity component shows a stronger southward mean flow north of the frontal zone and a weaker southward flow south of the frontal zone. These results support our conceptual model of convergence on the north side of the front and divergence south of the front (Figure 1.3). The standard errors of the means are of the same order as the mean values for this component, but this convergence and divergence pattern is significant. The magnitude of the mean southward velocity is less than 1 cm/s for most of the latitude range investigated. Between 38° N and 43° N the value ranges from 1.2 cm/s to 3.4 cm/s to the south, but this is often less than the standard errors, which range from 1.8 to 3.9 cm/s. These results are encouraging, though, as we do not have northward mean flow anywhere in the zonal averages as in Giannetti (1993).

B. FRONTAL COORDINATES

1. Data Concentration

The number of daily observations contained in the 150 km x 150 km boxes in both the along and cross-front coordinates relative to weekly frontal positions from the NMC analyzed SST data are shown in Figure 5.5 for the entire four-year dataset. A maximum in data coverage occurs near 2000 km along front and 250 km cross front. Before describing the mean velocity vectors in this frontal coordinate system, we note the following points from the frontal calculations described in Chapter IV: 1) frontal locations are expected to be least accurate in the eastern portion of the domain where SST data unrealistically skew the locations southward, particulary in summer (Figure 4.16) and 2) frontal coordinate calculations are not meaningful several frontal meander lengths (e.g., a few hundred kilometers) away from the front. Ideally, we should restrict our view of the frontal statistics to small cross-front locations in the western portion of the domain. However, the data concentration is highest in the east. Therefore, we adopt a compromise view and focus on a subarea within 750 km of the front in the center of the domain between 500 km and 2000 km. The number of daily observations in this subarea are shown in Figure 5.6.

2. Mean Currents

Mean values for the four-year dataset in the frontal coordinate system are presented in Figure 5.7 for the above subarea. The associated standard errors are shown in Figure 5.8. With this new perspective we see how drifters moved in relation to our selected fronts. We can clearly see a definitive front-parallel flow with convergence towards and divergence away

from the front. Some interesting features to highlight are: 1) strong cross-front convergence north of the front; 2) strong along-front flow (5 cm/s - 10 cm/s); and 3) weaker cross-front divergence south of the front. At + 200 km cross-front distance we again see the fast, incoming feeder velocities of the North Atlantic Current. There is some evidence of a counter-current at -400 km cross-front distance.

The seasonal frontal coordinate data is much more confusing and so does not warrant the inclusion of a figure. Examination of this data did still manage to highlight the main activity we expected to see. The winter season had larger area coverage, but fewer observations in close proximity to the front than did the summer season. Strong along-front flow was found between 1000 km and 2000 km along the winter front. A significant southward moving convergent flow was evident for the first 500 km north of the front for this middle section. Surprisingly, there was a significant northward moving divergent flow above the 2000 km - 3000 km along-front section of the front. Perhaps the SEMAPHORE deployments were responsible for this result. South of the front good agreement was obtained with the Cartesian perspective of divergent flow. The summer season had generally weaker vectors. Front-parallel motion was found along the southern edge of the front. Motion was forward for the 1000 km - 2000 km along-front section and backward for the 2000 km - 3000 km along-front section. These backward, opposing motions were, however, in areas of low drifter observations. Where the winter season showed northward moving divergent flow north of the front, in the summer season a weaker southward moving convergent flow was seen.

3. Eddy Kinetic Energy

The eddy kinetic energy fields generally reinforced our findings from the Cartesian perspective. Eddy kinetic energy fields for the subarea are shown in Figure 5.9. EKE values > 200 cm^2/s^2 could be found only south of the front confirming the impression from the Cartesian averages. Low EKE values (< 100 cm^2/s^2) were found farther away from the front, particularly on the southern side.

Without presenting the figures, we comment on our preliminary analysis of the seasonal data. In winter areas of high drifter concentration showed EKE values ranging from 60 cm^2/s^2 to 160 cm^2/s^2, with a peak value of 170 cm^2/s^2 occuring at around the 2000 km point. Isolated pockets of > 200 cm^2/s^2 did exist in boxes containing between 50 and 100 observations. In summer season the EKE was generally less than in winter. A peak value of 174 cm^2/s^2 (131 observations) was found along the central spine of the front at 1650 km. For most boxes with more than 100 observations EKE values ranged between 100 and 130 cm^2/s^2. These two seasonal pictures did not have the necessary amounts and coverage of data to provide an unquestioned view of the seasonal variability around the Azores Front.

4. Along-Front Averages

For our frontal coordinates we also investigated along-front averages, which are analogous to the zonal averages of Cartesian coordinates. Strips of 150 km cross-front width were examined for the subarea. Mean currents are shown in Figure 5.10. These along-front averages were expected to help identify convergences to the immediate north (above) of the front and divergence away from the front to the south (below). These results were somewhat

mixed. From the along-front strip perspective very low mean velocities (< 5 cm/s) were found closest to front (Figure 5.10) where we expected to find faster velocities (~ 10 cm/s to 15 cm/s) comparable to those in the lat/long perspective. They do, however, confirm a net divergence south of the front. Examination of a smaller portion of the subarea, from 500 km to 1500 km along-front distance, revealed evidence of a net convergence north of the front. This is also reflected in the mean velocities pictured in Figure 5.7. These low values seem at odds with the lat/long coordinate system's mean values near the mean frontal position. This apparent paradox can be explained by the presence of weak westward counter-currents within the frontal zone (e.g., Figure 5.1). The Cartesian perspective showed these counter-currents occuring about 32° N and 35° N. This has implications for the frontal coordinate system's zonal mean values, since the box approach averages values within 150 km of the front — effectively including these opposing motions with the frontal Azores Current. Thus, any counter-currents present would cancel or at least reduce the strength of the main eastward flowing frontal current. A smaller box size could separate these currents, but then we would lose the data concentration required to quantify the significance of the means. The counter-currents do, however, set-up shears, which are possible mechanisms for the generation of eddies, providing another explanation for the higher EKE values found here.

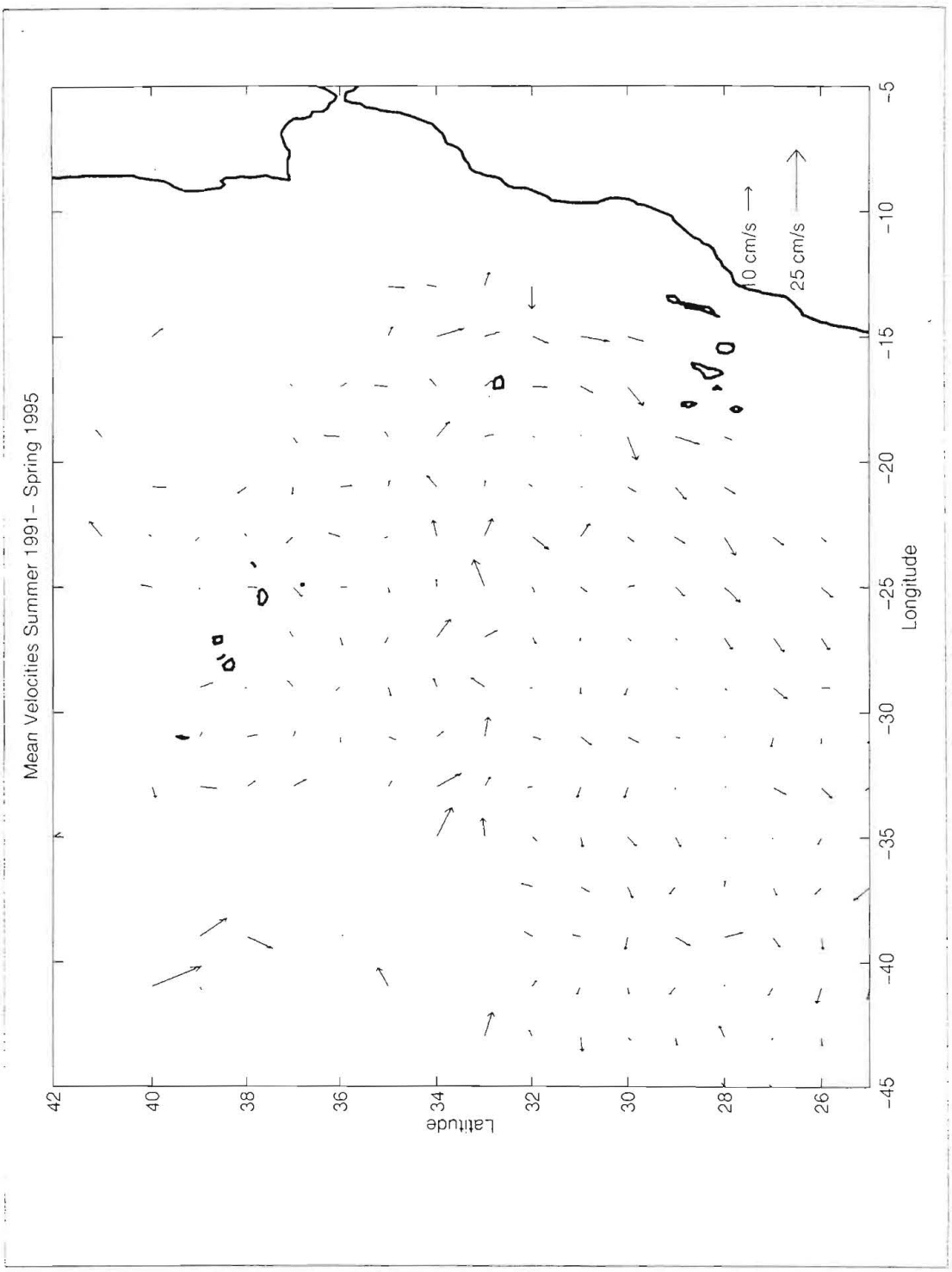

Figure 5.1 Mean velocities in 2° longitude by 1° latitude boxes with at least 80 daily observations for the period July 1991 through March 1995.

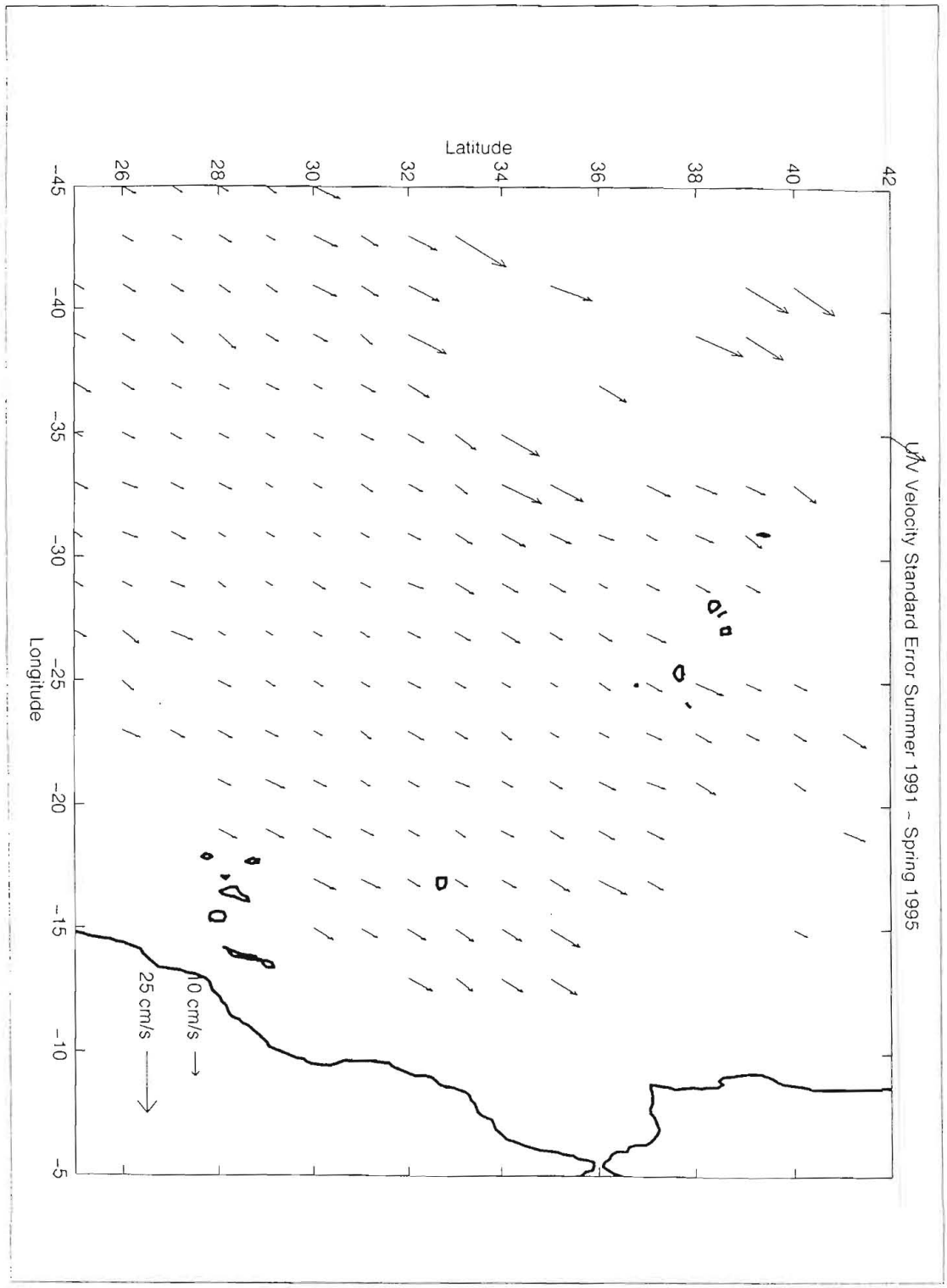

Figure 5.2 Ninety-five percent standard errors of the mean velocities from Figure 5.1.

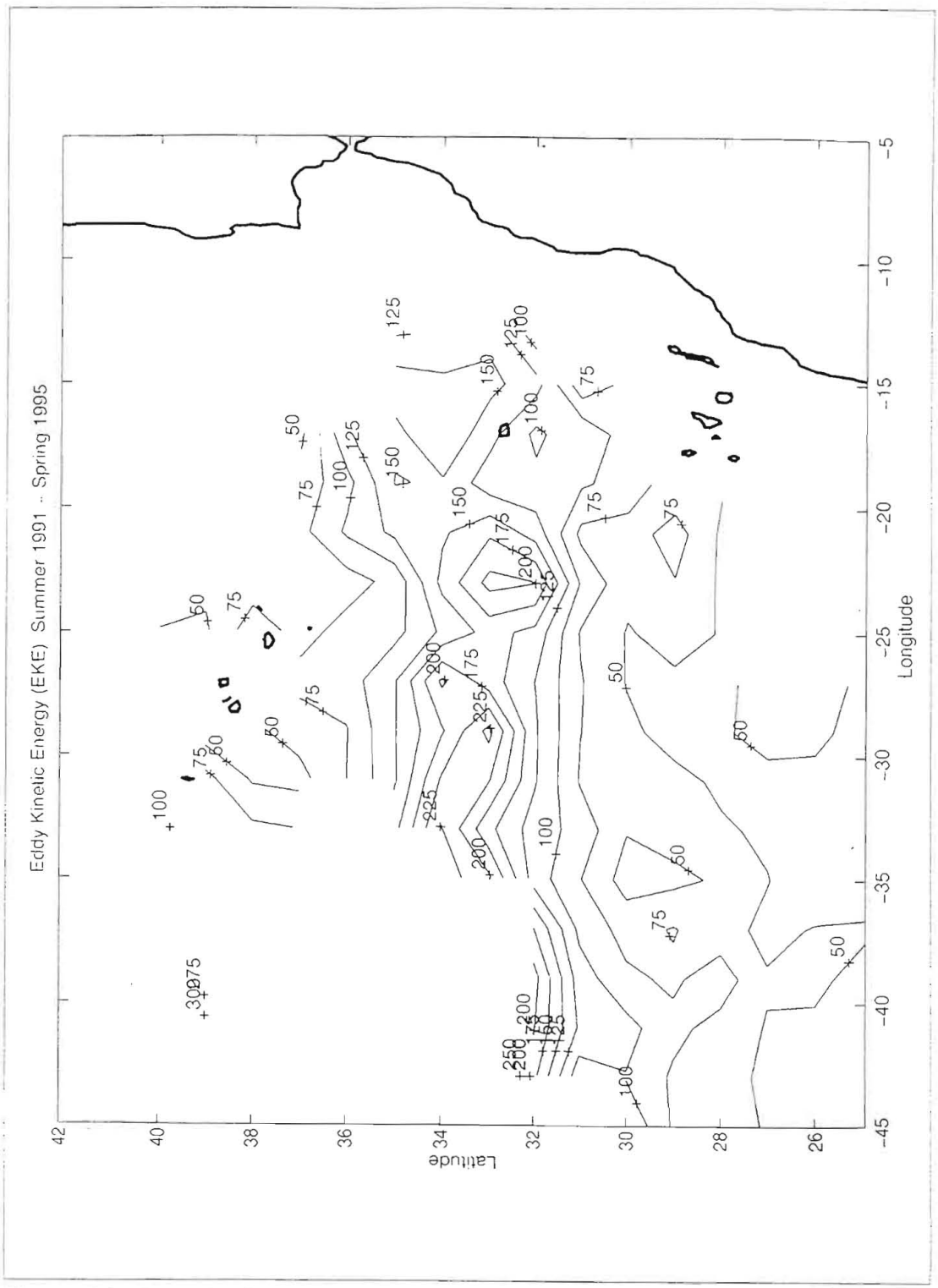

Figure 5.3 Eddy kinetic energy for velocity averages in Figure 5.1.

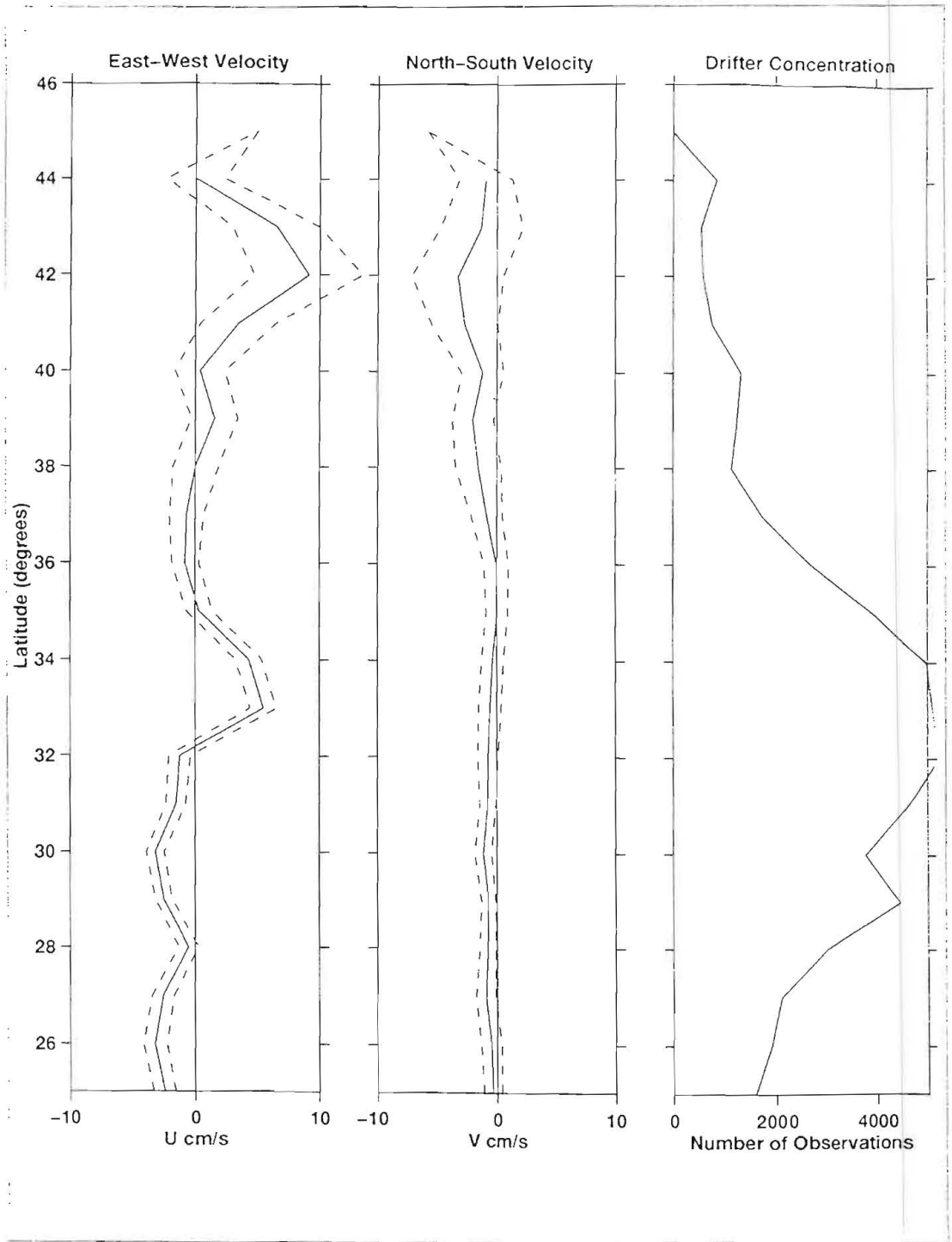

Figure 5.4 Zonal averages of data from July 1991 through March 1995. Eastward (left) and northward (middle) velocity and their standard errors (dashed) with the number of daily interpolated observations in 1 degree latitude bands (right) are shown.

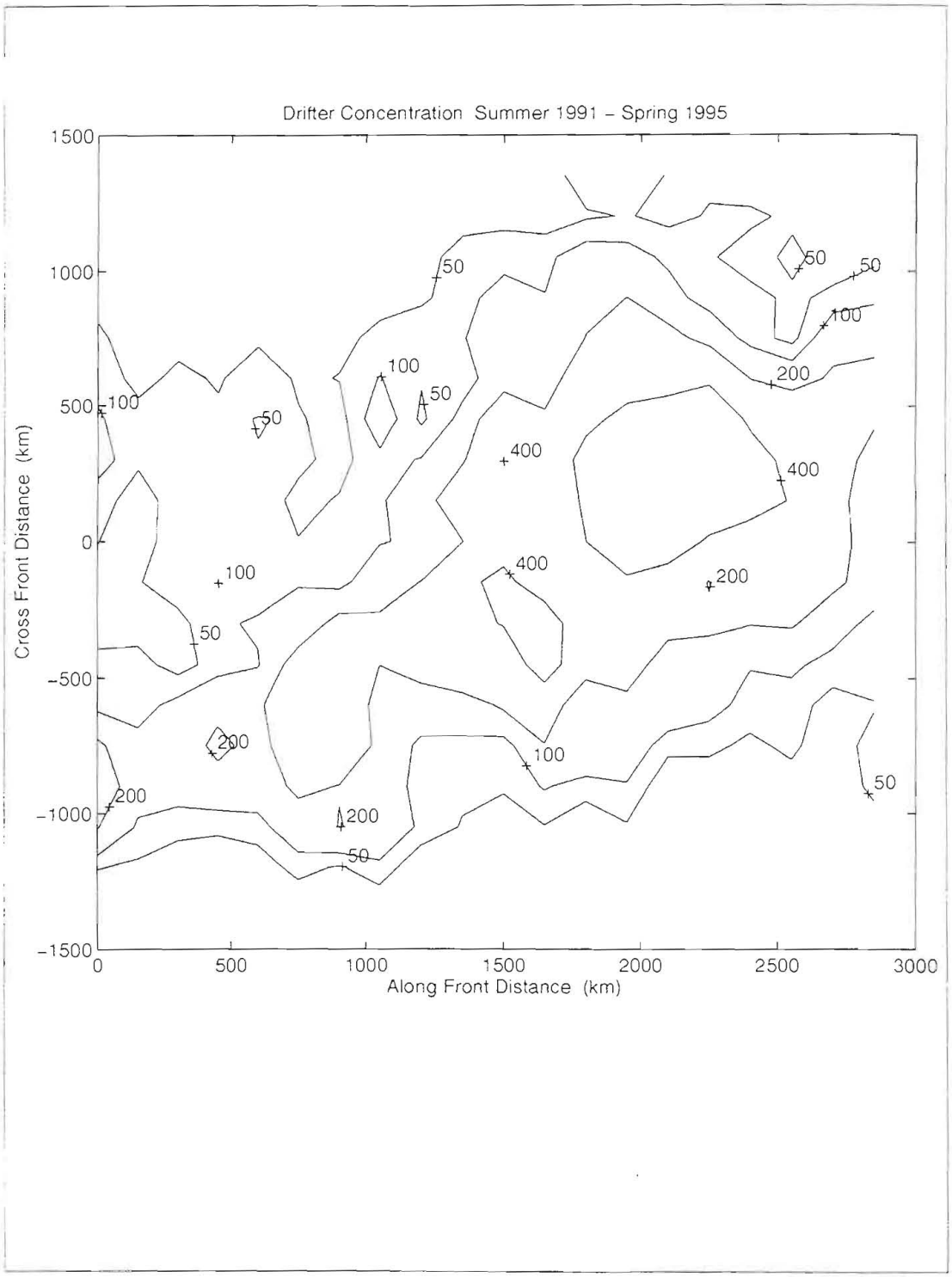

Figure 5.5 Density of daily drifter observations in 150 km by 150 km boxes for frontal coordinate locations from July 1991 through March 1995.

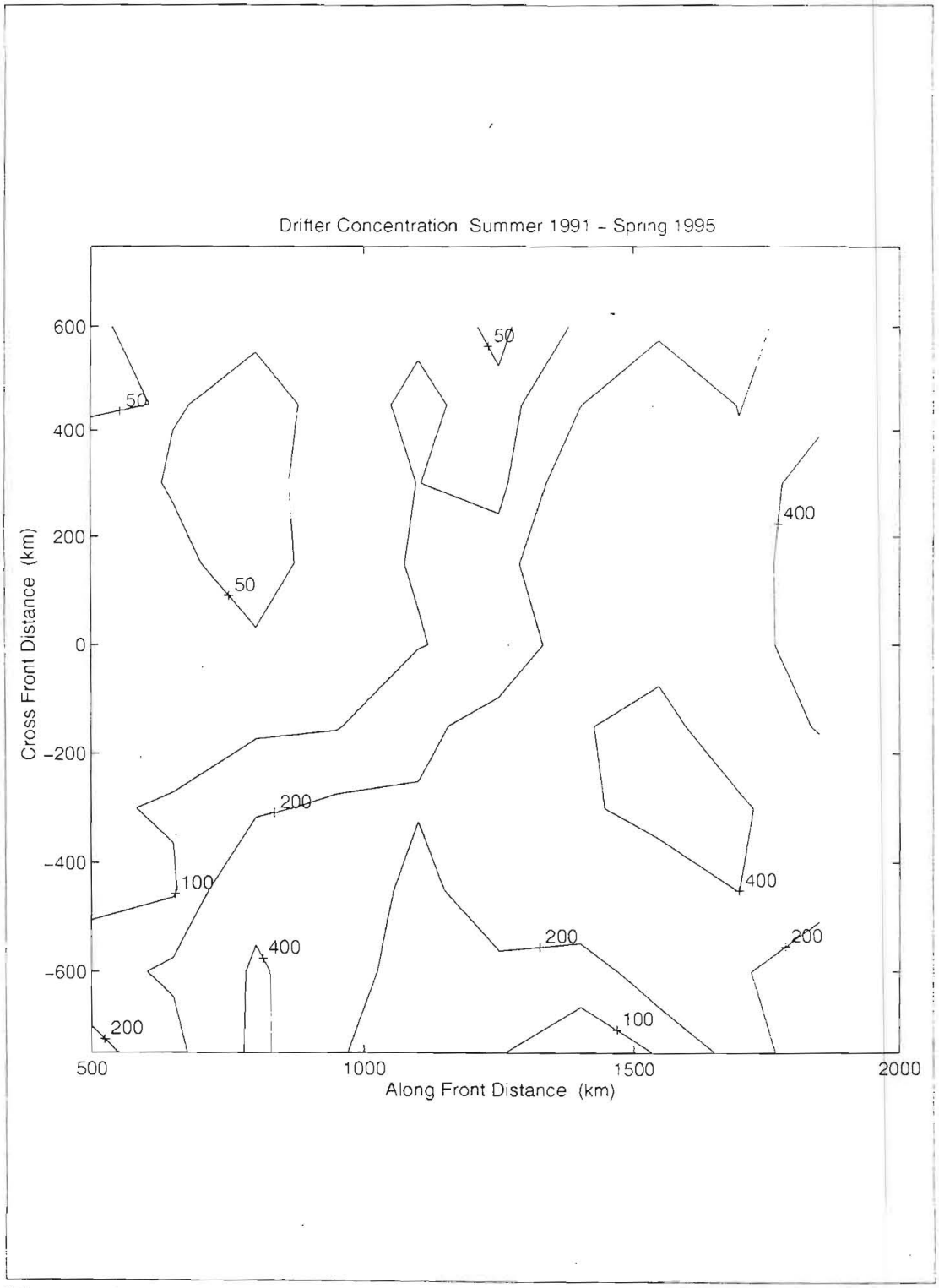

Figure 5.6 Density of daily drifter observations as in Figure 5.5 for targeted subarea.

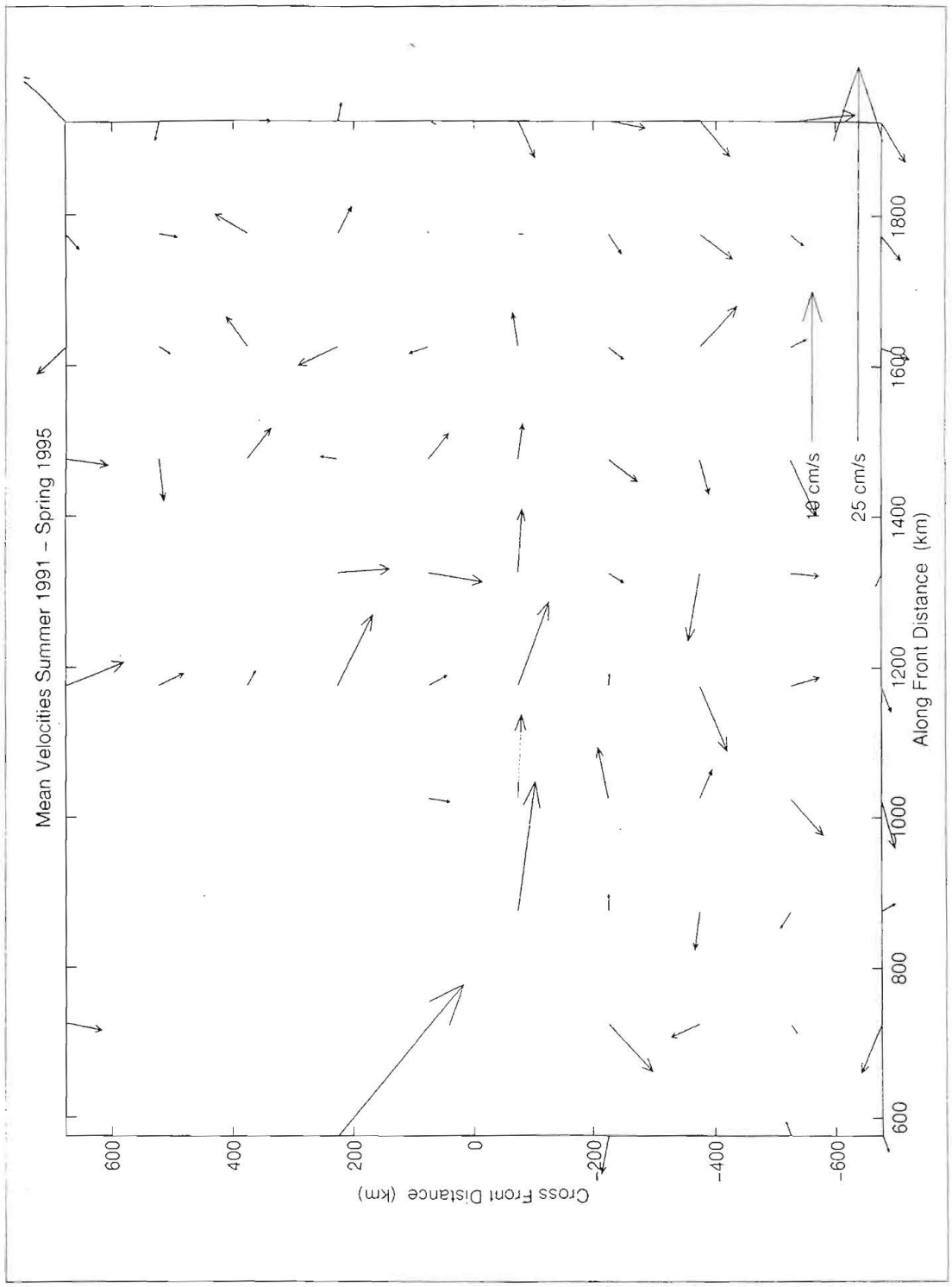

Figure 5.7 Mean velocities in 150 km by 150 km boxes with at least 80 daily observations for frontal coordinate positions for July 1991 through March 1995.

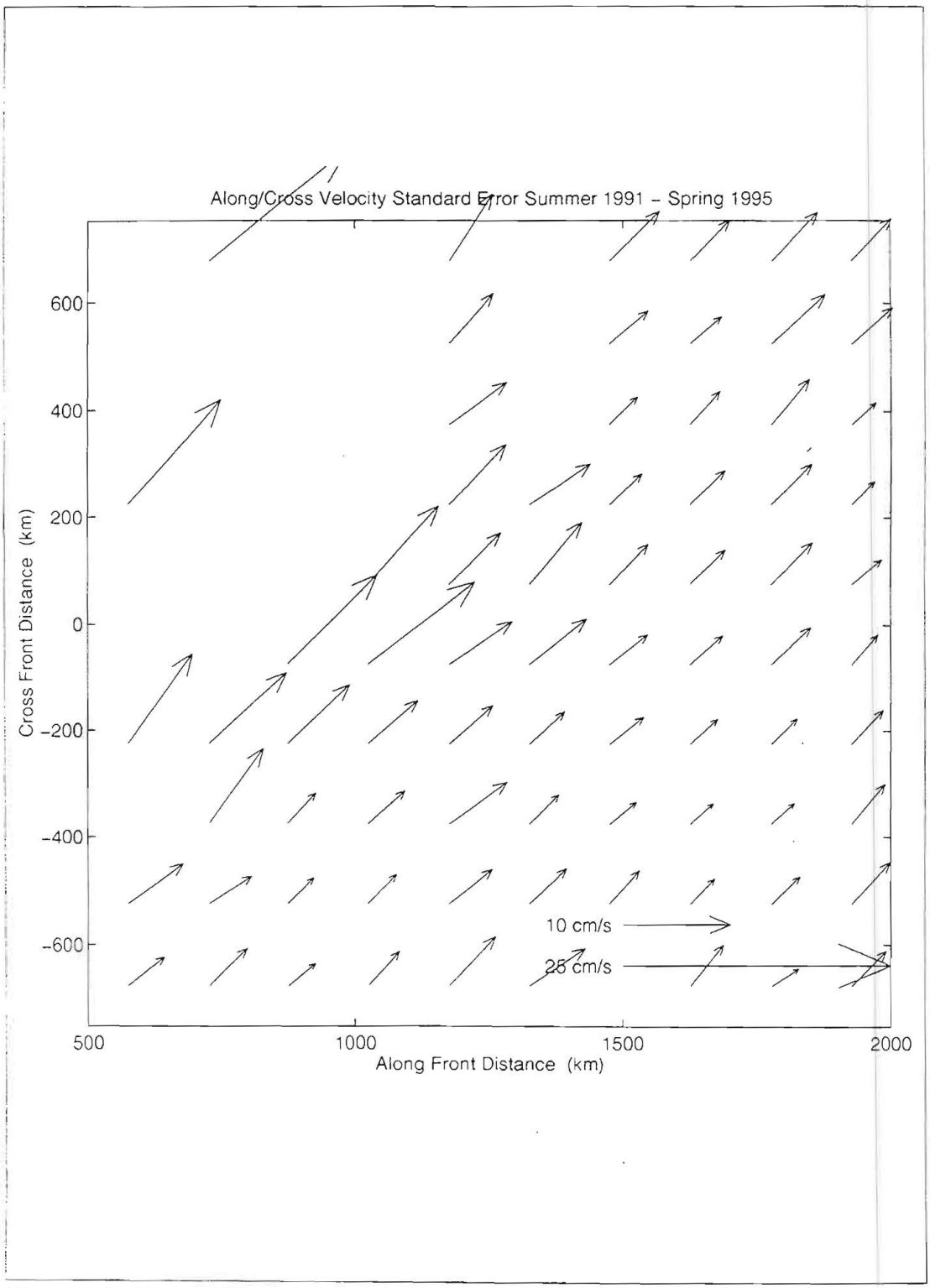

Figure 5.8 Ninety-five percent standard errors of the area velocities in Figure 5.7.

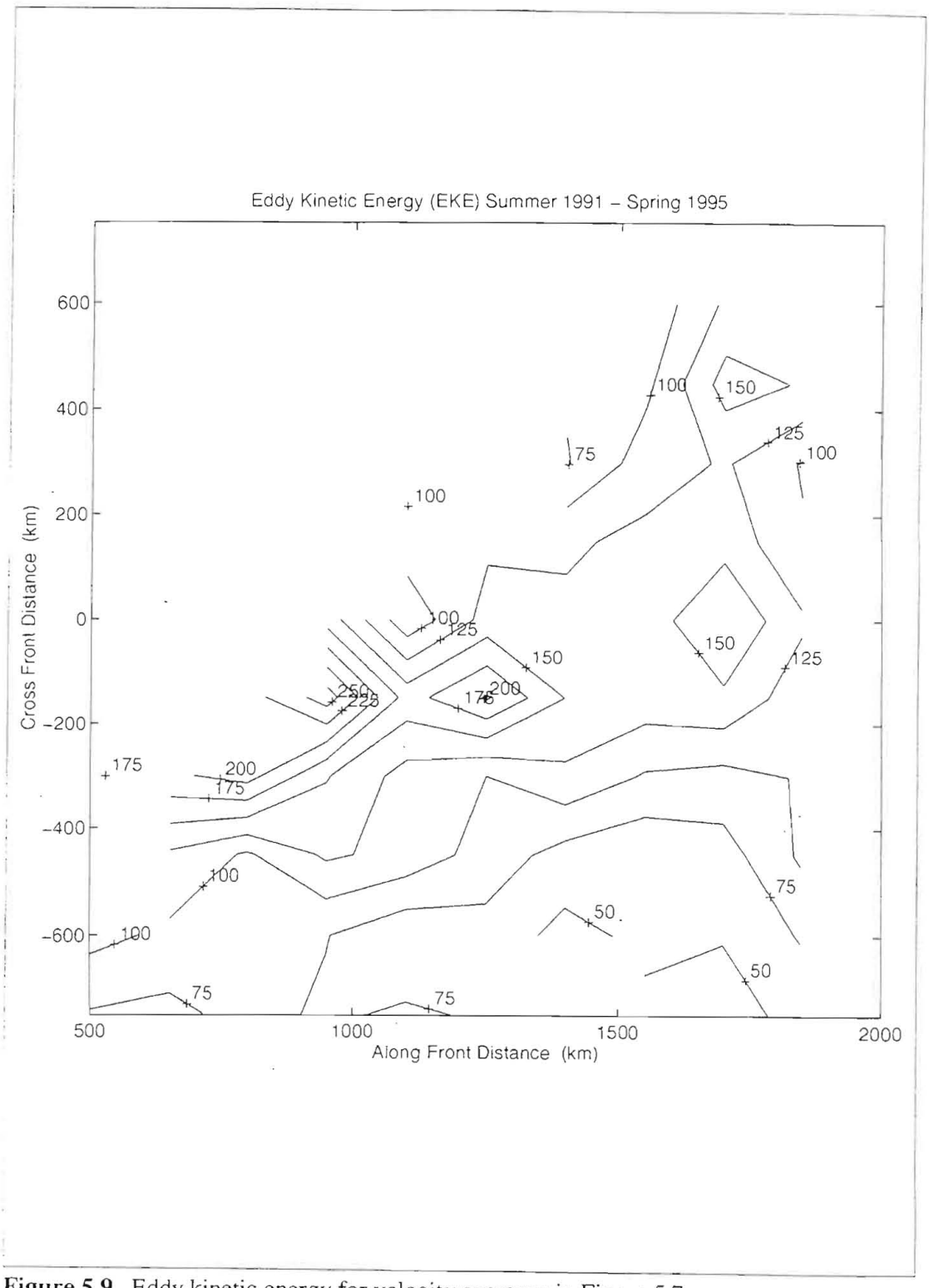

Figure 5.9 Eddy kinetic energy for velocity averages in Figure 5.7.

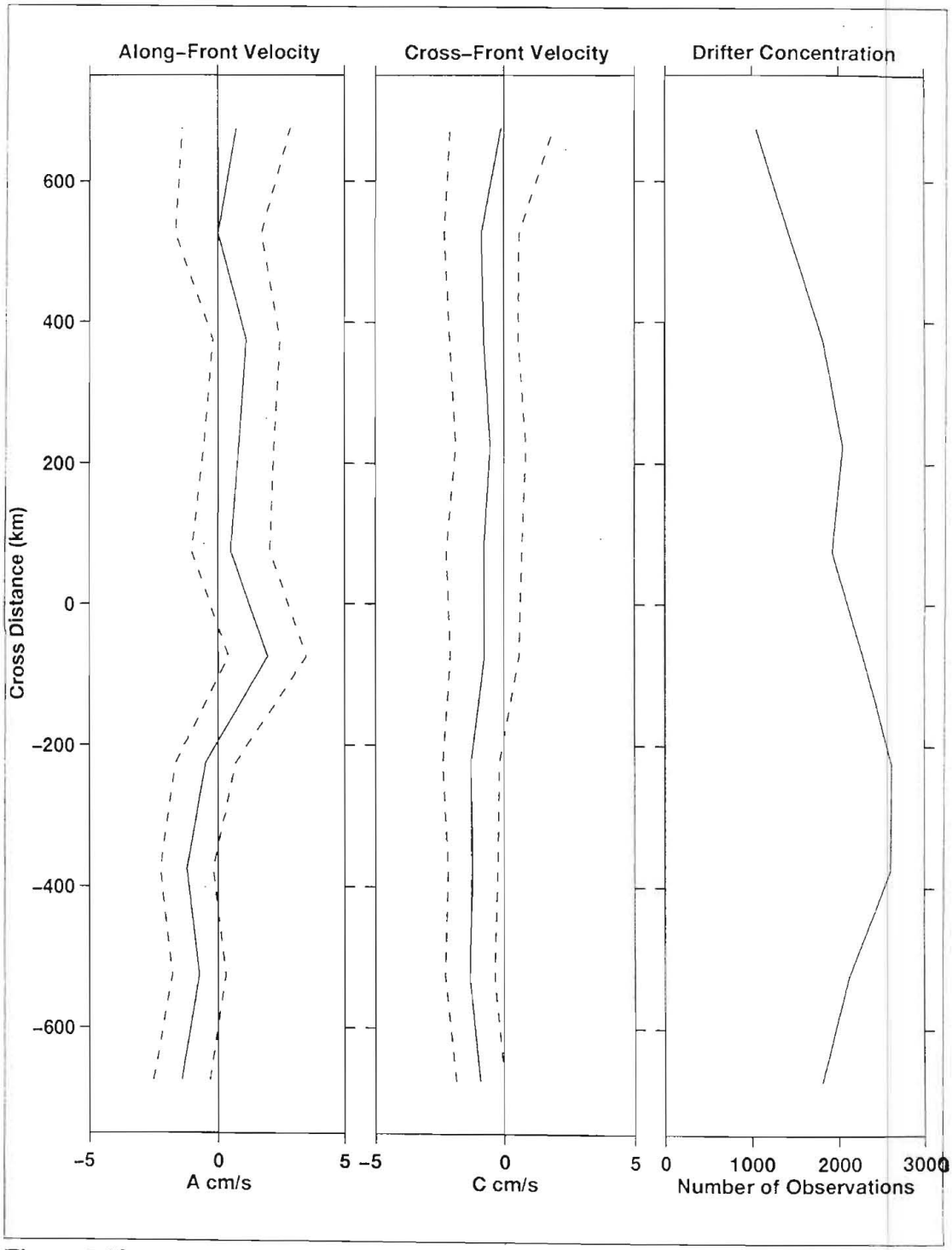

Figure 5.10 Along-front averages of front-parallel (left) and front-normal (middle) velocity and their standard errors (dashed) with the number of daily interpolated observations in 150 km bands (right).

VI. SUMMARY

A. DISCUSSION

One of the goals of the drifter observation program in the SUBDUCTION region was to measure the convergence of the mixed layer currents. This convergence is expected because of the climatologically convergent Ekman transport in the area. The primary contribution to wind stress curl in the area comes from the north-south variability of the east-west wind stress. Hence the dominant convergence in the mixed layer is expected to be in the north-south currents. It is also assumed that mean currents in the SUBDUCTION region are much weaker than the currents due to mesoscale eddies. Because of this, large numbers of observations are required to obtain a statistically significant measure of mean currents.

In Giannetti (1993), 14,000 plus drifter days from 36 separate drifters over a two-year period (1991 - 1993) were analyzed for mean currents, eddy kinetic energy, integral time and length scales, and diffusivities. His study attempted to improve over the results of Krauss and Käse (1984), who identified the main problem as being unable to separate the mean current from eddy motion. They recommended a much larger dataset to obtain statistically significant mean currents as a function of latitude. In contrast to our results, Giannetti (1993) computed weak mean meridional currents and divergence around the frontal latitudes. For comparison with our four-year results (Figure 5.4), the zonal averaged currents determined from his study are shown in Figure 6.1. Interannual variability is a possible explanation for differences between these two results. Although not investigated in this study, our data allows for such examination. However, given the results of Giannetti (1993), and the data concentrations for

the following years, we don't expect the averages to be significant over each of these single year periods. Thus, any interannual signal would not be resolvable above the level of noise.

A larger dataset is even more critical if one wants to examine seasonal variability and divergence patterns. With our four-year archive, consisting of over 52,000 drifter days from 155 individual drifters, we have approached the necessary amount of observations to definitively describe mean currents for the most critical areas of our study domain, namely the Azores Frontal Zone. This is based on our standard error vectors approaching the size of (or being smaller than) our mean velocity vectors. Seasonal variability can be seen in our dataset, but we are still lacking sufficient temporal and spatial coverage to statistically separate seasonal changes in the current patterns.

A clear view of the mean path of the Azores Current has emerged from this study. The meandering current flows eastward around 34° N essentially straight over to the continental slope off northwest Africa. There it joins the more steady flow of the southwestward flowing Canary Current. A significant bifurcation of the Azores Current occurs west of the Madeira Plateau near 23° W. Weak but persistent westward countercurrents are observed both north and south of the Azores Current.

One source of error, array bias due to non-uniform distribution of observations, was shown by Paduan et al. (1995) to be of minor importance for the four-year mean currents. They applied a maximum correction of 6 cm/s while most array biases were less than 2 cm/s. Our calculations, which did not include corrections for array bias, were in close agreement

with Paduan et al. (1995), varying only in the "sharpness" of the mean currents in the frontal zone to those outside the frontal zone.

The first major goal of the thesis was to examine and compile a time history of the Azores Front using composited satellite images of SST, drifter trajectories, and isolated hydrographic surveys. This goal remains elusive given the many areas where a subjective interpretation was made and the difficulty of identifying sub-surface features using primarily SST information. For certain time periods such as a few weeks or months, in the winter or spring, a definitive front could probably be mapped, but not consistently over a prolonged time period or entire frontal zone. High resolution imagery is subject to multiple expressions of surface temperature gradients which prevent identification of the main sub-surface dynamic front. Global Area Coverage (GAC) compositing is also poor during periods of prolonged cloudiness, leaving large areas void of useful data. High-speed drifter trajectories were found to be not only associated with the Azores Front, but also with propagating eddies, meanders, and the input source of the North Atlantic Current (NAC). Sensitivity of the high-speed trajectories and its window of applicability for an examined week did not produce enough trajectory data in the frontal region to be used with any consistency. Isolated hydrographic surveys were just that — isolated. Existing surveys, while being very precise and definitive, could only describe very small portions of the Azores Front and domain, and only for a few particular days. Frontal analysis could be "anchored" or fixed by these surveys, but the rest of the front could be skewed or displaced as a result. Low resolution imagery is only useful in generating a general picture of the large area and should be used only to fill in data void areas of the high resolution imagery. A very subjective frontal analysis conducted over the

entire four-year time period did, however, produce a quite reasonable climatological picture of the Azores Front in the western portion of the study area (Figure 4.16).

Despite these limitations, we can make a few conclusions from our case study using the high resolution GAC composite imagery: (1) The Azores Front fluctuates naturally over a range between 32° N and 36° N, (2) the Azores Front and other mesoscale phenomena such as eddies, jets, and meanders persist and vary slowly over a weekly time frame, (3) strong and variable currents occur north and west of the front, which are responsible for the higher EKE values obtained in our regional analysis, and (4) multiple SST fronts in the GAC data coupled with seasonal surface warming makes it nearly impossible to routinely detect the location of the sub-surface Azores Front using only this data source.

We have shown that we can definitively describe the mean currents of the Canary Basin using conventional Eulerian latitude/longitude box averaging, but this method cannot adequately describe the small-scale circulations in the immediate vicinity of the frontal zone. As the frontal feature is continuously moving and changing shape, its migration effectively "contaminates" data that specifically measure motion relative to the front. Derived parameters of convergence/divergence, vorticity, momentum and heat flux, and vertical motion need accurate horizontal current information that evolves as the Azores Front evolves. Thus, we have a strong requirement to evaluate the processes in terms of a frontal coordinate system.

The second main goal was to develop this frontal coordinate system. We accomplished this goal, producing an orthogonal curvilinear system which has been optimized to take advantage of the matrix handling capabilities of the MATLAB programming code.

This sytem was able to transform drifter positions and velocities in latitude/longitude space to front-normal/front-parallel space.

Given the subjective frontal history produced from the low resolution composite NMC SST data, we can only make basic conclusions about our drifter statistics using this new coordinate system. Improvement in frontal positioning can come from the Navy's Optimum Thermal Interpolation System (OTIS). OTIS is an ocean thermal analysis product developed for real-time operational use at the Fleet Numerical Meteorology and Oceanography Center (FNMOC). It has become the centerpiece of the Navy's analysis and prediction capabilities both ashore and afloat. OTIS Version 1 became operational at FNMOC on Northern Hemisphere and Southern Hemisphere 63 x 63 polar stereographic grids in July 1988. The system was subsequently upgraded to version 1.1 in July 1989, doubling the spatial resolution to 125 x 125 polar stereographic grids. This gives an effective resolution from about 100 km in the tropics to about 160 km in the midlatitudes. Details on the development and methodology of OTIS 1.0 can be found in Clancy et al. (1990). Details on the improvements made by OTIS 1.1 can be found in Clancy et al. (1992). A regional scale version (OTIS 3.0) was designed to resolve mesoscale features, such as fronts and eddies, in areas dominated by strong thermal gradients. Nominal grid spacing is 22 km. Two regions are currently in operational use: Gulf Stream and Kuroshio. The installation of a new supercomputer at FNMOC has enabled the extension of the regional eddy-resolving OTIS 3.0 of Cummings and Ignaszewski (1991) to basin-scale, and eventual global scale domains. The Azores Front is now routinely bogused as an extension of the Sargasso Front.

Analysis of the Azores Front using high-resolution (1.1 km) LAC AVHRR SST data has been done four times a week in support of OTIS since 1991 at the Naval Warfighting Support Center located at the Naval Oceanography Office (NAVOCEANO) in Bay St. Louis, Mississippi. Earlier analyses defined the front using on the order of 50 points (positions). Later analyses became more automated with less smoothing and kept smaller scale undulations longer. These later style analyses produce a frontal position containing on the order 150 - 200 points (Moshier, personal communication, 1995). Comparison of bogused Azores Front positions from the 1990 - 1993 time frame with the positions determined in this study shows the Navy product more closely follows the east-west path of the Azores Current than deduced from the drifter trajectories and SST, particularly in the summer.

Results from this section appear to support both schools of thought regarding the subduction process in the Canary Basin. Large area convergence is evident throughout the north side of the front, while there is also support for the type of frontal convergence/divergence hypothesized by Niiler and Reynolds, (1984) and observed in at least one location by Rudnick and Luyten (1995). Although the multi-year drifter statistics cannot definitively distinguish between competing theories of distributed versus frontal-based subduction, these results tend to confirm the latter hypothesis, particularly for the Cartesian zonal averages. The complete seasonal surface current pattern hypothesized by Niiler and Reynolds (1984; Figure 1.3) will require better seasonal distributions of drifter data. Seasonal variability was investigated in the sense that extreme summer versus winter

conditions were described, but the present dataset is not sufficient to map details of seasonal characteristics.

B. RECOMMENDATIONS

The primary recommendation for proceeding from this point is to improve the frontal detection and location. Given a more accurately located front, the frontal coordinate system could give a reliable picture of how drifters are moving in relation to the front. A highly accurate frontal position would in turn give us high confidence in the derived parameters. Progress in this arena is just now beginning to achieve this potential. The French group of Hernandez, Le Traon, and Morrow (1995) have shown good qualitative agreement between satellite altimetry taken from the TOPEX/Poseidon joint US/France mission and ERS-1, corresponding deep-drogued (150 m) drifters, and three hydrographic surveys. Satellite altimetry has the capability to resolve smaller scale structures and show the magnitudes and directions of the geostophic shears. They show agreement in dynamic height mapping from the above mentioned sensors (Hernandez et al., 1995). Drifter statistical analysis using the dataset described in this thesis should also be done using the Azores Front locations bogused into OTIS for comparison with our results.

Besides sea surface temperature and satellite altimetry, ocean color can also aid in the mapping of the Azores Front. Fronts are known to be locations of high biological productivity, providing us an opportunity to detect the mass of plankton and algae convergent there. Chlorophyll concentrations and other pigments will be measured in the near future when the SeaWifs ocean color satellite is launched sometime in 1996. In the near future all

the different in-situ data (hydrography, drifters, floats, current meters) will be combined to better estimate the dynamic topography. This, in turn, will provide good reference data for the precise validation for TOPEX/Poseidon and ERS-1 in the open ocean.

Other primary recommendations involve improvements to the frontal coordinate system processing used in this study. Improvements can be made to this system that account for the distance a drifter observation is away from the front and the positioning/orientation of the front. The closest drifters need to have a highly accurate picture of the front to record the nuances of the small-scale circulation, while far away drifters need only to know the general shape of the front to show their relative motion (Figure 4.17). This can be done with an incorporated decorrelation function and angle and distance formulas that vary with the distance to the front.

This topic of calculating drifter statistics using a frontal coordinate system should be applied to other regions. Highly accurate frontal positions are available for the Gulf Stream and Kuroshio Current. Calculating velocity statistics in frontal coordinates should help resolve secondary circulations around those important fronts.

Of course, a recommendation for continued deployments of drifters needs to be made. More data is a never-ending battle cry, but it is necessary to improve the statistical reliability of the averages calculated and to characterize the errors. In particular, the transmitter duty cycle used in the subduction drifters in order to reduce ARGOS tracking costs seriously impedes the accuracy of the drifter observations because of the inability to measure and filter out inertial motions. Additional hydrographic effort should be targeted at improving the

baseline knowledge of the Azores Front, which is mapped from the Mid-Atlantic Rise to the North African continental shelf.

Further dynamical insights will be gained by investigating the heat, momentum, and energy balances in the SUBDUCTION region from long-term drifter observations combined with improved surface temperature, dynamic height, and wind forcing data. These insights will lead us to the predictive link we seek between the mixed layer and the upper thermocline and to the goal of deep-ocean prediction using only surface data.

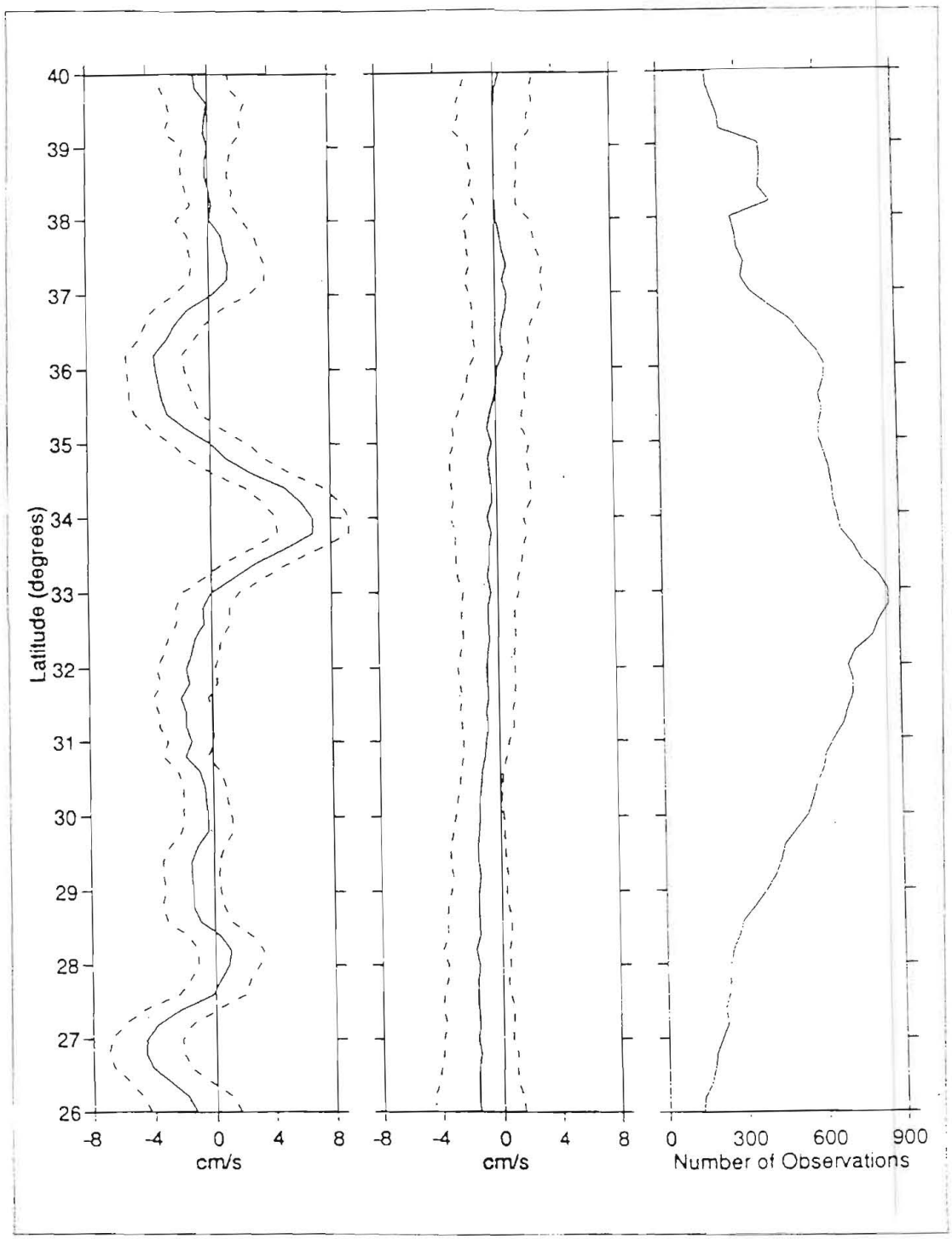

Figure 6.1 Zonal averages from Giannetti (1993) of data from July 1991 through May 1993. Eastward (left) and northward (middle) velocity and their standard errors (dashed) with the number of 2-day interpolated observations in 1 degree latitude bands (right).

APPENDIX A. THERMAL REMOTE SENSING OF THE OCEAN

A. ELECTROMAGNETIC (EM) EMISSION FROM THE SEA SURFACE

Thermal emission from the ocean surface covers the entire spectrum from the near IR to the MW and peaks near 10 μm. In the IR region the most appropriate spectral regions correspond to the 3-4 μm and 10-12 μm atmospheric windows. Though the emitted radiation at 10 μm is stronger than at 3 μm, the sensitivity to surface temperature variation is significantly larger at the shorter wavelength. The relative sensitivity is given by the ratio of the derivative of Planck's spectral brightness relative to temperature:

$$\frac{1}{S}\frac{\partial S}{\partial T} = \frac{c_2}{\lambda T^2}\frac{\exp(c_2/\lambda T)}{\exp(c_2/\lambda T) - 1} \quad , \tag{A.1}$$

$S(\lambda)$ = spectral radiant emittance in W/m^3 (watts per unit wavelength per unit area)
λ = radiation wavelength
h = Planck's constant 6.626×10^{-34} Ws^2
T = absolute temperature in °K
c = speed of light 2.9979×10^8 m/s
k = Boltzmann constant 1.38×10^{-23} Ws/°K
c_2 = ch/k 1.44×10^{-2} m °K

where S is the spectral distribution of radiation from a black body given by

$$S(\lambda) = \frac{2\pi hc^2}{\lambda^5}\frac{1}{e^{ch/\lambda kT} - 1} \quad . \tag{A.2}$$

In most of the near infrared region $c_2 >> \lambda T$; then,

$$\frac{1}{S}\frac{\partial S}{\partial T} \simeq \frac{c_2}{\lambda T^2} \quad . \tag{A.3}$$

For the near IR region then the relative sensitivity at 3 μm is about 3.3 times higher than the sensitivity at 10 μm. In addition, the error due to water vapor in the 3-4 μm region is significantly lower than in the 10 μm region. On the other hand, the error due to aerosol scattering is significantly higher at the shorter wavelengths (Rayleigh scattering). These facts have led to the use of multispectral observations to correct for humidity and aerosol effects (Elachi, 1987).

High-resolution IR radiometers have been flown on a number of NOAA satellites in polar orbits since 1966. In most cases the atmospheric window from 10.5 to 12.5 μm has been used, but its use for determining absolute sea surface temperature has often been secondary to its use for imaging of clouds and thermal fronts associated with ocean currents and upwelling (Legeckis, 1978). Radiometers of improved quality, such as the Advanced Very High Resolution Radiometer (AVHRR), with two and three atmospheric window channels, have permitted development of methods to retrieve absolute SST of far better accuracy than was possible with single window systems (Strong and McClain, 1984).

A technique for producing SST based on single window IR measurements was used from 1979 until 1981. This technique, called Global Operational Sea Surface Temperature Computation (GOSSTCOMP), did not permit adequate cloud filtering and water vapor

corrections (McClain, 1979; Strong and Pritchard, 1980). Correction for atmospheric attenuation, principally by water vapor, can amount up to 8 to 10 °C for warm, moist atmospheres in the 10.5 to 12.5 μm data (Maul, 1984). Empirical corrections have been generally unsatisfactory; even those based on moisture information from atmospheric sounders on the same spacecraft have been inadequate. Accurate corrections are possible with coincident in situ radiosonde measurements, a situation that is relatively rare over the open ocean (Rao et al., 1990).

B. MULTICHANNEL SEA SURFACE TEMPERATURE PROCESSING

In 1981, the Multichannel Sea Surface Temperature (MCSST) technique became operational. The technique makes use of various combinations of the five channels of AVHRR in the initial and critical cloud filtering stages of the procedure. (McClain et al., 1985). In the absence of clouds, ice, or relatively intense sun glint, the oceans appear quite dark compared with clouds, so appropriate thresholds have been established for the bidirectional reflectance in Channel 1 (0.58 to 0.68 μm) or Channel 2 (0.725 to 1.1 μm). Principal cloud tests, however, take advantage of the small-scale spatial uniformity of fields of ocean surface temperature and visible spectrum (VIS) reflectance, air mass moisture, and the low level of noise in the AVHRR data. In the daytime the cloud filter rejects those small scanspot arrays (2 x 2 or 3 x 3) with variabilities of more than about 0.3 % in reflectance. Nighttime cloud tests are based on temperature thresholds (many clouds are colder than the coldest ocean surface) and on temperature uniformity in the spatial sense. This is particularly

true for clouds that do not fill the radiometer field-of-view (FOV). The nighttime cloud filter rejects scanspot arrays whose IR temperature varies by more than 0.2 $^{\circ}$C (Rao et al., 1990).

Interchannel IR temperature comparisons are also useful for cloud detection, especially at night. Comparisons are also critical in those cases that fail spatial uniformity tests (e.g., an extremely uniform cloud that completely fills the radiometer FOV). Since the reflectivity of cloud water droplets is greater at 3.7 μm than it is at 11 or 12 μm, this significantly lowers the 3.7 μm temperature relative to either of the other window temperatures. This gives us another means of nighttime cloud detection (Rao et al., 1990).

The fundamental basis for making atmospheric attenuation corrections to satellite-based IR temperatures is differential absorption in the various atmospheric window regions of the spectrum (McMillin and Crosby, 1984). Differing IR temperatures measured by the AVHRR channels observing the same spot lead to highly linear relation between any pair of IR temperatures and the correction needed. Tests using substantial numbers of satellite and fixed-buoy measurements (matched to within 25 km and 24 hours) enabled the derivation of operational temperature dependent bias corrections for MCSST equations (Rao et al., 1990).

An example of operational MCSST equations is given below for the AVHRR on NOAA-9 (IR temperatures in Kelvin yield MCSST in Celsius):

$$T = 3.64 \times T_{11} - 2.66 \times T_{12} - 267.96 \qquad \text{(A.4)}$$

Daytime (using split-window channels)

$$T = 0.99 \times T_{3.7} + 1.01 \times T_{11} - 0.99 \times T_{12} - 273.28 \quad (A.5)$$

Nighttime (using three channels)

Measurements from MCSST 100 km and 50 km daily field analyses validated with drifting buoy data show biases within +/- 0.1 °C and accuracies from 0.4 to 0.6 °C (McClain et al., 1985).

The most serious limitation of the MCSST technique is that essentially cloud-free FOVs are required. Multi-day compositing permits satisfactory mapping of the temperature field in all but the most persistently cloud covered regions. Anomalously high concentrations of atmospheric aerosol, such as those associated with severe volcanic eruptions or intense dust storms, occasionally degrade IR-based SST, though progress has already been made with this problem (Walton, 1985; Reynolds, 1993).

APPENDIX B. FRONTAL COORDINATE SYSTEM MATLAB CODE

```
%
%   CURVIWINTER.M
%
%   Program loads in the Azores Front from a location file.
%   Front is determined by selecting a characteristic
%   temperature.  (Winter 1994)
%
%   Calculate along front and cross front distances to each
%   drifter observation during the time frame. Plot drifter
%   locations and their velocities. Plot the front.
%
%   Calculate Points of Intersection to the front and the
%   relative along front and cross front velocities.
%
%   Save new data to a file.
%

callstart

%   Open list of NMC SST weekly data files

listName = 'winter94.lst';

f1 = fopen(listName,'r');
if (f1 < 0)
  error([listName, ' not opened properly ... TERMINATED'])
end

%   Open list of interpolated Front position files

listName2 = 'winterfront2.lst';

f2 = fopen(listName2,'r');
if (f2 < 0)
  error([listName, ' not opened properly ... TERMINATED'])
end
```

```
%  Open new big file for transformed coordinates

f5 = fopen('Winter94','w');

counter = 0;

while 1

%  Read in NMC SST data file

pos_file = fgetl(f1);

%  This is what breaks out of the infinite while loop.
%  Breaks out when you reach end of listName file.

if ~isstr(pos_file), break, end;
counter = counter + 1;

disp(' ')
disp(['Processing ',pos_file])
disp(' ')

%  Decompose NMC temperature file

nameA = num2str(pos_file);
f3 = fopen(nameA,'r');
ip = findstr(pos_file,'.');

nameB = pos_file(1:ip-1);
yearname = pos_file(ip+1:length(nameA));
yearstop = 1900 + str2num(yearname);
dayname = (pos_file(ip-2:ip-1));
daystop = str2num(dayname);
monthname = num2str(pos_file(1:ip-3));

if (strcmp(monthname, 'January') == 1)
  monthstop = 1;
elseif (strcmp(monthname, 'February') == 1)
  monthstop = 2;
elseif (strcmp(monthname, 'March') == 1)
  monthstop = 3;
elseif (strcmp(monthname, 'April') == 1)
  monthstop = 4;
```

```
elseif (strcmp(monthname, 'May') == 1)
  monthstop = 5;
elseif (strcmp(monthname, 'June') == 1)
  monthstop = 6;
elseif (strcmp(monthname, 'July') == 1)
  monthstop = 7;
elseif (strcmp(monthname, 'August') == 1)
  monthstop = 8;
elseif (strcmp(monthname, 'September') == 1)
  monthstop = 9;
elseif (strcmp(monthname, 'October') == 1)
  monthstop = 10;
elseif (strcmp(monthname, 'November') == 1)
  monthstop = 11;
elseif (strcmp(monthname, 'December') == 1)
  monthstop = 12;
end

%  Read in NMC SST data into an array

dat = fscanf(f3,'%g',[41,21]);
dat = dat';
index = find(dat < 0.001);
dat(index) = NaN .* ones(length(index),1)

disp(' ')

%  Find Start and Stop dates to match
%  with Drifter Observations of the same period

if (yearstop < 1991 & yearstop > 1995)
  error(['Data unavailable.']);
end
if (monthstop < 1 | monthstop > 12)
  error(['Ending month not entered correctly']);
end
if (daystop < 1 | daystop > 31)
  error(['Ending day not entered correctly']);
end
if (monthstop == 2 & ...
  (yearstop == 1992 & daystop > 29))
  error(['Leap year February has only 29 days']);
end
```

```
if (monthstop == 2 & ...
  (yearstop ~= 1992 & daystop > 28))
  error(['Non Leap year February']);
end
if ((monthstop == 4 | ...
   monthstop == 6 | ...
   monthstop == 9 | ...
   monthstop == 11) & ...
   daystop > 30)
  error(['Days not matched to month']);
end

stopdate = 0.000;
yearstop = yearstop - 1900;
yearday = cal2yearday(yearstop,monthstop,daystop);
stopdate = yearday;
if (yearstop == 92)
 stopdate = stopdate +365;
end
if (yearstop == 93)
 stopdate = stopdate +365+366;
end
if (yearstop == 94)
 stopdate = stopdate +365+366+365;
end
if (yearstop == 95)
 stopdate = stopdate +365+366+365+365;
end

startdate = stopdate - 6;

%  Set Domain

minLat = 25;
if (minLat < 0 | minLat > 90)
  error(['Minimum latitude', minLat,' not entered correctly']);
end
disp(' ')
minLon = -45;
if (abs(minLon) > 180)
  error(['Minimum longitude', minLon,' not entered correctly']);
end
maxLat = 45;
```

```
if (maxLat < 0 | maxLat > 90 | maxLat < minLat)
  error(['Maximum latitude', maxLat,' not entered correctly']);
end
disp(' ')
maxLon = -5;
if (abs(maxLon) > 180 | maxLon < minLon)
  error(['Maximum longitude', maxLon,' not entered correctly']);
end
dtLat = 1;
disp(' ')
dtLon = 1;
disp(' ')

maxLat = maxLat + dtLat;
maxLon = maxLon + dtLon;

lonGrid = minLon:dtLon:maxLon;
latGrid = minLat:dtLat:maxLat;
gridlon = length(lonGrid);
lonlen = num2str(gridlon-1);
gridlat = length(latGrid);
latlen = num2str(gridlat-1);
width = abs(maxLon - minLon);
wide = num2str(width);
depth = abs(maxLat - minLat);
deep = num2str(depth);

disp(['The domain width is: ', wide,' deg'])
disp(' ')
disp(['The domain depth is: ', deep,' deg'])
disp(' ')
disp(['The gridded field is a: ', latlen,' by ', lonlen,' box'])
disp(' ')

%  Plot Temperature Field & Color Bar

figure(1)

coldest = finmin(dat);
warmest = finmax(dat);
levels = [ceil(coldest):1:floor(warmest)];
levlen=length(levels);
x =  -45:1:-5;
```

```
y = 25:1:45;
pcolorc(dat,x,y,[9,28],'2.0f')
shading interp
hold on

%  Contour Temperatures and Calculate Gradient

c = contour(x,y,dat,levels);
kids = get(gca,'Children');
kidlen = length(kids);
set(kids(1:kidlen-1),'color','k');
clabeld(c,0);
[px,py]=gradient(dat);
%quiver(x,y,px,py,3,'k')

%  Label Plot

title(['NMC SST, Drifter Velocities ',nameB,' Winter 1994']);
xlabel('Longitude');
ylabel('Latitude');

%  Overlay Interpolated Drifter Observations which match the
%  the NMC coverage

addpath('/home/usr4/brownj/thesis/');

values3 = [];
outs3 = [];
counter3 = 1;
ALLDRIF = [];
longO = [];
latO = [];
DATO = [];
timeO = [];
TIMEO = [];
CRITOBS = [];

%  Load Master drifter file with the daily interpolated
%  positions and u, v velocities.

disp(' ')
disp(['Processing C.mat'])
disp(' ')
```

```
load C.mat

DAT3 = C;

critobs4 = 0;

%  Find all drifters that match the selection criteria

index3 = find(DAT3(:,5) >= minLon  & ...
          DAT3(:,5) <= maxLon  & ...
          DAT3(:,4) >= minLat  & ...
          DAT3(:,4) <= maxLat  & ...
          DAT3(:,8) >= startdate & ...
          DAT3(:,8) <= stopdate);

values3 = [values3; DAT3(index3,:);];
[r3,c3] = size(DAT3);
numobs3(counter3) = r3;
obs3 = num2str(r3);
disp(['Number of observations in this C.mat file is ', obs3])
disp(' ')
critobs3 = num2str(length(index3));
disp(['Observations meeting selection criteria: ', critobs3])
disp(' ')
critobs4 = 1:str2num(critobs3);
critobs4 = critobs4';
CRITOBS = [CRITOBS; critobs4;];

%  Plot Drifter Observations

plot(DAT3(index3,5), DAT3(index3,4), 'or')

%  Plot Drifter Velocities

[Ax,Sf] = mercat([-45,-5],[25,45]);
set(gca, 'AspectRatio', [Ax,Sf]);
uVel = DAT3(index3,6);
vVel = DAT3(index3,7);
h1 = arrowplot(DAT3(index3,5), DAT3(index3,4), ...
          DAT3(index3,6), DAT3(index3,7).*Sf, 1/10, 'w-');
set(h1, 'Clipping', 'off');
```

```
% Plot Scale Arrows

xS1 = -10;
yS1 = 27.5;
uS1 = 10;
vS1 = 0;
arrowplot(xS1, yS1, uS1, vS1, 1/10, 'w-');
text(xS1,yS1,'10 cm/s ','HorizontalAlignment','right');
xS2 = -10;
yS2 = 26.5;
uS2 = 25;
vS2 = 0;
arrowplot(xS2, yS2, uS2, vS2, 1/10, 'w-');
text(xS2,yS2,'25 cm/s ','HorizontalAlignment','right');

timeO = [DAT3(index3,8)];
TIMEO = [TIMEO; timeO;];

DATO = [DAT3(index3,5), DAT3(index3,4)];
ALLDRIF = [ALLDRIF; DATO;];

% Criteria Observations

longO = ALLDRIF(:,1);
latO  = ALLDRIF(:,2);
[rO,cO] = size(ALLDRIF);

% Read in Sorted, Interpolated Front Location data file

addpath('/home/u1/cook/Brown/InterpSort/');

front_file = fgetl(f2);

% This is what breaks out of the infinite while loop.
% Breaks out when you reach end of listName file.

if ~isstr(front_file), break, end;

disp(' ')
disp(['Processing ',front_file])
disp(' ')

frontname = num2str(front_file);
```

```
ip2 = findstr(front_file,'.');
frontdate = num2str(stopdate);
frontttemp = front_file(ip2+1:length(frontname));

f4 = fopen(frontname,'r');

DATF = fscanf(f4,'%g %g %g %g',[4, inf]);
DATF = DATF';
longF = DATF(:,1);
latF = DATF(:,2);
[rF,cF] = size(DATF);

%   Plot Azores Front

plot(longF(:), latF(:), '.m')
plot(longF(1:20:length(longF)),latF(1:20:length(latF)), 'om')

orient landscape

hold off

%  Calculate  Cross Front Distances

disttofront = [rO,rF];
for i = 1:rO
 for j = 1:rF

 disttofront(i,j) = greatcircle(latO(i),longO(i),latF(j),longF(j));

 end
end

NORMDIST = [];
ALLDRIFNORM = [];
normindex = zeros(1,rO);
normdist = zeros(1,rO);

for k = 1:rO
 mindist1 = [i,min(disttofront(k,:))];
 [mindist2, minindex] =  min(disttofront(k,:));
 NORMDIST = [NORMDIST; mindist1];
 normindex(k) = minindex;
 normdist(k) = mindist2;
```

```
 ALLDRIFNORM = [ALLDRIFNORM; [mindist2, minindex];];
end

% Calculate Along Front Distances

alongdist = 0.0;
ALONGFRONT = [0,1];

for l = 2:rF
  incrdist = greatcircle(latF(l-1),longF(l-1),latF(l),longF(l));
  alongdist = incrdist + alongdist;

  ALONGFRONT = [ALONGFRONT; [alongdist,l];];

end

% Construct Polygon

longP = [longF', longF(rF), -46, longF(1)];
latP = [latF', 24, 24, latF(1)];
longP = longP';
latP = latP';

% Check whether Drifters are "Inside" or "Outside"
% the Front

polyindex = inside1(longO, latO, longP, latP);

signchange = find(polyindex == 1);
normdist(signchange) = -1 .* normdist(signchange);

% Perform Drifter Calculations

drifterdata = [];
frontdata = [];
intersectdata = [];
rotatedata = [];
longI = [];
latI = [];
longV = [];
latV = [];
VERTFRONT = [];
DRIFTVERT = [];
```

```
east = 1;
streast = 'east ';
west = 2;
strwest = 'west ';
south = 3;
strsouth = 'south';
north = 4;
strnorth = 'north';
cosA = zeros(1,rO);
RangleA = zeros(1,rO);
DangleA = zeros(1,rO);
slope = zeros(1,rO);
direction = zeros(1,rO);
pointer = [];
Rotangle = zeros(1,rO);
alpha = zeros(1,rO);
alongvel1 = zeros(1,rO);
crossvel1 = zeros(1,rO);

for m = 1:rO

%  Find Points of Intersection

 longI = [longI; longF(normindex(m));];
 latI = [latI; latF(normindex(m));];

%  Find Vertex Points for the Right Spherical Triangle

 longV = [longV; longF(normindex(m));];
 latV = [latV; latO(m);];

%  Calculate Front to Vertex Point Distances

vertdist = greatcircle(latI(m),longI(m),latV(m),longV(m));
VERTFRONT = [VERTFRONT; [vertdist,m];];

%  Calculate Drifter to Vertex Point Distances

basedist = greatcircle(latO(m),longO(m),latV(m),longV(m));
DRIFTVERT = [DRIFTVERT; [basedist,m];];

%  Calculate Angle between Drifter Latitude
%  and Front Intersection Point
```

```
cosA(m) = (basedist.^2 + normdist(m).^2 - vertdist.^2)/...
        (2 .* basedist .* abs(normdist(m)));

RangleA(m) = acos(cosA(m));
DangleA(m) = RangleA(m) .* (180/pi);

%  Calculate Front Slopes at the Intersection Points

if (normindex(m) == 1)
 slope(m)=(latF(normindex(m)+1) - latF(normindex(m))) /...
        (longF(normindex(m)+1) - longF(normindex(m)));
elseif (normindex(m) == rF)
 slope(m)=(latF(normindex(m)) - latF(normindex(m)-1))/...
         (longF(normindex(m)) - longF(normindex(m)-1));
else
 slope(m)=(latF(normindex(m)+1) - latF(normindex(m)-1))/...
        (longF(normindex(m)+1) - longF(normindex(m)-1));
end

%  Test for Degenerate Cases

if (slope(m) == Inf)
   slope(m) = 1e10;
elseif (slope(m) == -Inf)
   slope(m) = -1e10;
elseif (slope(m) == NaN)
   slope(m) = 0;
else
   slope(m) = slope(m);
end

%  Check whether Along Front distances are increasing
%  to the East or West

if (normindex(m) ~= rF)
 if (longF(normindex(m)+1) > longF(normindex(m)))
   direction(m) = east;
   pointer(m,:) = streast;
 elseif (longF(normindex(m)+1) < longF(normindex(m)))
   direction(m) = west;
   pointer(m,:) = strwest;
 elseif (latF(normindex(m)+1) <= latF(normindex(m)))
```

```
  direction(m) = south;
  pointer(m,:) = strsouth;
 else
  direction(m) = north;
  pointer(m,:) = strnorth;
 end
else
 if (longF(normindex(m)) > longF(normindex(m)-1))
  direction(m) = east;
  pointer(m,:) = streast;
 elseif (longF(normindex(m)) < longF(normindex(m)-1))
  direction(m) = west;
  pointer(m,:) = strwest;
 elseif (latF(normindex(m)) <= latF(normindex(m)-1))
  direction(m) = south;
  pointer(m,:) = strsouth;
 else
  direction(m) = north;
  pointer(m,:) = strnorth;
 end
end

%  Calculate Rotation Angle For Change to
%  Curvilinear Orthogonal Coordinates

if (direction(m) == east)
  if (latO(m) > latI(m))
    if (slope(m) < 0)
      Rotangle(m) = -(90 - DangleA(m));
    elseif (slope(m) > 0)
      Rotangle(m) =  (90 - DangleA(m));
    else
      Rotangle(m) = 0;
    end
  elseif (latO(m) < latI(m))
      if (slope(m) < 0)
        Rotangle(m) = -(90 - DangleA(m));
      elseif (slope(m) > 0)
        Rotangle(m) =  (90 - DangleA(m));
      else
        Rotangle(m) = 0;
      end
  else
```

```
    Rotangle(m) = 0;
   end
elseif (direction(m) == west)
   if (latO(m) > latI(m))
     if (slope(m) < 0)
       Rotangle(m) =  (90 + DangleA(m));
     elseif (slope(m) > 0)
       Rotangle(m) =  -(90 + DangleA(m));
     else
       Rotangle(m) = -180;
     end
    elseif (latO(m) < latI(m))
       if (slope(m) < 0)
         Rotangle(m) = (90 + DangleA(m));
       elseif (slope(m) > 0)
         Rotangle(m) = -(90 + DangleA(m));
       else
         Rotangle(m) = 180;
       end
     else
      Rotangle(m) = 0;
     end
elseif (direction(m) == south)
   if (longO(m) > longI(m))
     Rotangle(m) = -90;
   elseif (longO(m) < longI(m))
     Rotangle(m) = -90;
   else
     Rotangle(m) = 0;
   end
elseif (direction(m) == north)
   if (longO(m) > longI(m))
     Rotangle(m) = 90;
   elseif (longO(m) < longI(m))
     Rotangle(m) = 90;
   else
     Rotangle(m) = 0;
   end
end

alpha(m) = Rotangle(m) .* pi/180;
```

```
%  Calculate Along Front Velocities and
%  Cross Front Velocities

alongvel1(m) =  uVel(m) .* cos(alpha(m)) + ...
            vVel(m) .* sin(alpha(m));

crossvel1(m) = -uVel(m) .* sin(alpha(m)) + ...
            vVel(m) .* cos(alpha(m));

%  Collect All Data

 drifterdata = [drifterdata; [longO(m), latO(m), ...
             uVel(m), vVel(m)];];
 frontdata = [frontdata; [ALONGFRONT(normindex(m),1),...
  normdist(m), DangleA(m), alongvel1(m), crossvel1(m)];];

 intersectdata = [intersectdata; [longI(m), latI(m)];];

 rotatedata = [rotatedata; [direction(m), slope(m), Rotangle(m)];];


end

%  Display Data

disp(' ')
disp('Drifter Data')
disp('Drifter LON,  LAT,  U VEL,  V VEL')
disp(' ')
fprintf('%9.3f % 9.3f %8.4f %8.4f \n', drifterdata')
disp(' ')
disp('Frontal Data')
disp('ALONG DIST, NORM DIST, ANGLE to FRONT, ALONG VEL1, NORM VEL1')
disp(' ')
fprintf('%12.4f  %10.4f  %10.4f  %10.4f  %10.4f \n',...
      frontdata')
disp(' ')
disp('Intersection Data')
disp('Intersect LON,  LAT')
disp(' ')
fprintf('%9.3f  %9.3f  \n', intersectdata')
disp(' ')
disp('Rotation Data')
```

```
disp('Dir Code: 1 = east, 2= west, 3 = south, 4 = north')
disp('Direction Code, Front Slope, Rotation Angle')
disp(' ')
fprintf('%4.1f  %8.4f  %8.4f\n',  rotatedata')
disp(' ')
disp('Pausing to look at the Data and Figure')
disp(' ')

print

%  Write New Data to Big File

everything = [DAT3(index3,1), DAT3(index3,2), DAT3(index3,3), ...
        DAT3(index3,5), DAT3(index3,4), uVel, vVel, ...
        ALONGFRONT(normindex,1), normdist', alongvel1', ...
        crossvel1', DAT3(index3,8)];
everything = everything';
fprintf(f5, ' %g  %g  %g  %g  %g  %g  %g  %g  %g  %g  %g  %g  %g \n',...
     everything);

%  Close all files

fclose(f3)
fclose(f4)

end

fclose(f1)
fclose(f2)
fclose(f5)
```

LIST OF REFERENCES

Beyer, W. H., 1991: *CRC Standard Mathematical Tables and Formulae*. 29th ed. CRC Press, 609 pp.

Brink, K. H., R. C. Beardsley, P.P. Niiler, M. Abbott, A. Huyer, S. Ramp, T. Stanton, and D. Stuart, 1991: Statistical properties of near-surface flow in the California Coastal Transition Zone. *J. Geophys. Res.*, **96**, 14693-14706.

Bushnell, M., 1995: The global lagrangian drifter data assembly center at NOAA/AOML. *Intl. WOCE Newsletter*, **20**, 36-37.

Clancy, R. M., P. A. Phoebus, and K. D. Pollack, 1990: An operational global-scale ocean thermal analysis system. *J. Atmos. Oceanic Tech.*, **7**, 233-254.

Clancy, R. M., J. M. Harding, K. D. Pollack, and P. May, 1992: Quantification of improvements in an operational global-scale ocean thermal analysis system. *J. Atmos. Oceanic Tech.*, **9**, 55-66.

Cotter, D. J., 1990: The United States operational polar and geostationary satellites. *Weather Satellites: systems, data, and environmental applications*. P. K. Rao, S. J. Holmes, R. K. Anderson, J. S. Winston, and P. E. Lehr, Eds., American Meteorlogical Society, 51-59.

Cromwell, D., P. G. Challenor, and A. L. New, 1995: Does the Azores current flow west at 35° N ? *SIGMA: The UK WOCE Newsletter*, **17**, 10-11.

Cummings, J. A., and M. Ignaszewski, 1991: The Fleet Numerical Oceanography Center regional ocean analysis system. MTS '91 Proc. Marine Technology Society, 1123-1129.

Davis, R.E., 1983: Oceanic property transport, Lagrangian particle statistics, and their prediction. *J. Marine Res.*, **41**, 163-194.

Davis, R. E., 1993: Observing the general circulation with floats. *Deep-Sea Res.*, **38**, Suppl 1, S531-S571.

Davis, R. E., R. A. DeSzoeke, D. R. Halpern, and P.P. Niiler, 1981: Variability in the upper ocean during MILE. Part I: The heat and momentum balances. *Deep-Sea Res.*, **28**, 1427-1451.

DSP User's Manual, 1990, University of Miami/RSMAS Remote Sensing Group.

Elachi, C., 1987: *Introduction to the Physics and Techniques of Remote Sensing*, John Wiley & Sons, pp vii, 1, 267-270.

Gianetti, P., 1993: The velocity field in the northeast Atlantic from satellite-tracked drifting buoys. M.S. thesis, Department of Oceanography, Naval Postgraduate School, 76 pp.

Gould, W. J., 1985: Physical oceanography of the Azores Front, *Prog. Oceanog.*, **14**, 167-190.

Hansen, D. V., and A. Herman, 1989: Temporal sampling requirements for surface drifting buoys in the tropical Pacific. *J. Atmos. Oceanic Tech.*, **6**, 599-607.

Hansen, D. V., and P. M. Poulain, 1995: Quality control and interpolations of WOCE/TOGA drifter data. *J. Atmos. Oceanic Tech.*, submitted.

Hernandez, F., P. Y. Le Traon, and R. Morrow, 1995: Comparison of TOPEX/Poseidon and ERS-1 altimetric data with SEMAPHORE in-situ data. *J. Geophys. Res.*, submitted.

Kadko, D. C., and L. Washburn, 1991: Evidence of subduction within cold filaments of the northern California coastal transition zone. *J. Geophys. Res.*, **96**, 14909-14926.

Käse, R. H., W. Zenk, T. B. Sanford, and W. Hiller, 1985: Currents, fronts and eddy fluxes in the Canary basin. *Prog. Oceanog.*, **14**, 231-257.

Käse, R. H. J. F. Price, P. Richardson, and W. Zenk, 1986: A quasi-synoptic survey of the thermocline circulation and water masses distribution within the Canary Basin. *J. Geophys. Res.*, **91**, 9739-9748.

Käse, R. H., and G. Siedler, 1982: Meandering of the subtropical front south-east of the Azores, *Nature*, **300**, 245-246.

Kielmann, J., and R. H. Käse, 1987: Numerical modeling of meander and eddy formation in the Azores current frontal zone. *J. Phys. Oceanogr.*, **17**, 529-541.

Kirwan, A. D., Jr., G. J. McNally, and J. Coehlo, 1976: Gulf stream kinematics inferred from a satellite tracked drifter. *J. Phys. Oceanogr.*, **6**, 750-755.

Kirwan, A. D., Jr., G. J. McNally, E. Reyna, and W.J. Merrell, Jr., 1978: The near-surface circulation of the eastern north Pacific. *J. Phys. Oceanogr.*, **8**, 937-945.

Klein, B., and G. Siedler, 1989: On the origins of the Azores Current. *J. Geophys. Res.*, **94**, 6159-6168.

Kort, V. G., 1981: 31st Cruise of the R/V *Akademik Kurchatov* (Principal Scientific Results). *Oceanology*, **21** (1), 183-187.

Kort, V. G., A. Yu. Krasnopevtsev, and I. F. Shadrin, 1983: The evolution of mesoscale oceanic eddies southwest of the Azores. *Oceanology*, **23** (1), 5-12.

Kraus, E. B., and J. S. Turner, 1967: A one-dimensional model of the seasonal thermocline: II, The general theory and its consequences. *Tellus*, **19**, 98-106.

Krauss, W.,and C. W. Böning, 1987: Lagrangian properties of eddy fields in the northern North Atlantic as deduced from satellite-tracked buoys. *J. Marine Res.*, **45**, 259-291.

Krauss, W., and R. H. Käse, 1984: Mean circulation and eddy kinetic energy in the eastern North Atlantic. *J. Geophys. Res.*, **89**, 3407-3415.

Legeckis, R., 1978: A survey of worldwide sea surface temperature fronts detected by environmental satellites. *J. Geophys. Res.*, **83**, 4501-4522.

Le Traon, P.-Y., and P. De Mey, 1994: The eddy field associated with the Azores Front east of the Mid-Atlantic Ridge as observed by the Geosat altimeter. *J. Geophys. Res.*, **99**, 9907-9923.

Luyten, J. R., J. Pedlosky, and H. Stommel, 1983: The ventilated thermocline. *J. Phys. Oceanogr.*, 13, 292-309.

Maul, G. A., 1984: *Introduction to Satellite Oceanography*. Martinis Nijoff Publ., Kluwer Academic Publ., Norwell, MA, 606 pp.

McClain, E. P., 1979: Satelitte-derived earth surface temperature, Chapter 3. J. S. Winston (ed.), Quantitative Meteorological Data from Satellites, *Technical Note 166, WMO-No 531*, World Meteor. Organ., Geneva, Switzerland, 60-68.

McClain, E. P., W. G. Pichel, and C. C. Walton, 1985: Comparative performance of AVHRR-based multichannel sea surface temperatures. *J. Geophys. Res.*, **90**, 11587-11601.

McNally, G. J., 1981: Satellite-tracked buoy observations of the near-surface flow in the eastern mid-latitude north Pacific. *J. Geophys. Res.*, **86**, 8022-8030.

McNally, G. J., D. S. Luther, and W. B. White, 1989; subinertial frequency response of wind-driven currents in the mixed layer measured by drifting buoys in the mid-latitude north Pacific. *J. Phys. Oceanogr.*, **19**, 290-300.

McMillin, L. M., and D. S. Crosby, 1984: Theory and validation of the multiple window sea surface temperature technique. *J. Geophys. Res.*, **89**, 3655-3661.

Niiler, P. P., R. E. Davis, and H. J. White, 1987: Water-following characteristics of a mixed layer drifter. *Deep-Sea Res.*, **34**, 1867-1881.

Niiler, P. P., and E. B. Kraus, 1977: One dimensional models of the upper ocean in *Modeling and Prediction of the Upper Layers of the Ocean*, Pergamon, 143-172.

Niiler, P. P., and J. D. Paduan, 1995: Wind-driven motions in the northeast Pacific as measured by Lagrangian drifters. *J. Phys. Oceanogr.*, **25**, 2819-2830.

Niiler, P. P., A. S. Sybrandy, K. Bi, P-M. Poulain, and D. Bitterman, 1995: Measurements of the water-following capability of Holey-sock and TRISTAR drifters. *Deep-Sea Res.*, in press.

Niiler, P. P., 1995: Global drifter program: Measurements of velocity, SST, and atmospheric pressure. *Intl. WOCE Newsletter*, **20**, 3-6.

Ollitrault, M., 1995: The general circulation of the subtropical North Atlantic, near 700m depth, revealed by the TOPOGULF SOFAR floats. *Intl. WOCE Newsletter*, **20**, 15-18.

Paduan, J. D., and R. A. deSzoeke, 1986: Heat and energy balancess in the upper ocean at 50° N, 140° W during November 1980 (STREX). *J. Phys. Oceanogr.*, **16**, 25-38.

Paduan, J. D., and P. P. Niiler, 1990: A Lagrangian description of motion in northern California Coastal Transition Filaments. *J. Geophys. Res.*, **95**, 18095-18110.

Paduan, J. D., and P. P. Niiler, 1993: Structure of velocity and temperature in the northeast Pacific as measured with Lagrangian drifters in Fall 1987. *J. Phys. Oceanogr.*, **23**, 585-600.

Paduan, J. D., M. Zhou, and P. P. Niiler, 1995: Surface currents in the Canary basin from drifter observations. *Intl. WOCE Newsletter*, **20**, 13 - 15.

Parfit, M., 1995: Diminishing returns - Exploiting the ocean's bounty. *National Geographic*, **Vol. 188 No. 5**, 2-37.

Pollard, R. T., R. B. Rhines, and R.O.R.Y. Thompson, 1973: The deepening of the wind mixed layer. *Geophys. Fluid Dyn.*, **3**, 381-404.

Pollard, R. T., and L. Regier, 1990: Large variations in potential vorticity at small spatial scales in the upper ocean. *Nature*, **348**, 227-229.

Pollard, R. T., and L. A. Regier, 1992: Vorticity and vertical circulation at an ocean front. *J. Phys. Oceanogr.*, **22**, 609-625.

Poulain, P. M., and P. P. Niiler, 1989: Statistical analysis of the surface circulation in the California Current System using satellite-tracked drifters. *J. Phys. Oceanogr.*, **19**, 1588-1603.

Price, J. F., R. A. Weller, and R. Pinkel, 1986: Diurnal cycling: Observations and models of the upper ocean response to diurnal heating, cooling, and wind mixing. *J. Geophys. Res.*, **91**, 8411-8427.

Qiu, B., and R. X. Huang, 1995: Ventilation of the North Atlantic and North Pacific: Subduction versus obduction. *J. Phys. Oceanogr.*, **25**, 2374-2390.

Rao, P. K., S. J. Holmes, R. K. Anderson, J. S. Winston, P. E. Lehr, 1990: *Weather Satellites: Systems, Data, and Environmental Applications*, American Meteorological Society, pp 53, 378-386.

Reynolds, R. W., 1988: A real-time global sea surface temperature analysis. *J. Climate*, **1**, 75-86.

Reynolds, R. W., 1993: Impact of Mount Pinatubo aerosols on satellite-derived sea surface temperatures. *J. Climate*, **6**, 768-774.

Reynolds, R. W., and D. C. Marsico, 1993: An improved real-time global sea surface temperature analysis. *J. Climate*, **6**, 114-119.

Reynolds, R. W., and T. M. Smith, 1994: Improved global sea surface temperature analyses. *J. Climate*, **7**, 929-948.

Reynolds, R. W., and D. C. Stokes, 1994: Update Information (18 May 1994) for use of the NMC SST analyzed fields. [Available on-line from FTP nic.fb4.noaa.gov or FTP 140.90.50.22 in /pub/nws/nmc/ocean. Data description file is oiinfo.asc in the oisst directory.]

Richardson, P. H., and C. M. Wooding, 1985: Surface drifter measurements in the North Equatorial Countercurrent 1983-1985. Woods Hole Oceanographic Institution 31-85, 117pp.

Richardson, P. H., 1983: Eddy kinetic energy in the North Atlantic from surface drifters. *J. Geophys. Res.*, **88**, 4355-4367.

Robinson, M. K., R. A. Bauer, and E. H. Schroeder, 1979: Atlas of North Atlantic-Indian Ocean monthly mean temperatures and mean salinities of the surface layer. Naval Oceanographic Office Reference Publication 18. Dept. of the Navy Washington DC 20373.

Rudnick, D. L., and J. R. Luyten, 1995: Intensive surveys of the Azores Front. Part I: Tracers and dynamics. *J. Geophys. Res.*, in press.

Rudnick, D. L., 1995: Intensive surveys of the Azores Front. Part II: Inferring the geostrophic and vertical velocity fields. *J. Geophys. Res.*, submitted.

Sevice Argos System Guide, 1989: Version 1. Service Argos, Inc., 1801 Mc Cormick Drive, Suite 10, Landover, MD 20785. 138 pp.

Spall, M. A., 1990: Circulation in the Canary Basin: A model/data analysis. *J. Geophys. Res.*, **95**, 9611-9628.

Stramma, L., and T. J. Muller, 1989: Some observations of the Azores Current and the North Equatorial Current. *J. Geophys. Res.*, **94**, 3181-3186.

Stramma, L., and G. Siedler, 1988: Seasonal changes in the North Atlantic subtropical gyre. *J. Geophys. Res.*, **93**, 8111-8118.

Strong, A. E., and E. P. McClain, 1984: Improved ocean surface temperatures from space-comparisons with drifting buoys. *Bull. Am. Meteor. Soc.*, **65**, 138-142.

Strong, A. E., and J. A. Pritchard, 1980: Regular monthly mean temperatures of earth's oceans from satellites. *Bull. Am. Meteor. Soc.*, **61**, 553-559.

Sybrandy, A. L., and P. P. Niiler, 1991: WOCE/TOGA Lagrangian Drifter Construction Manual, SIO Reference 91/6, Scripps Institution of Oceanography, University of California, San Diego, WOCE Report Number 63.

Tabata, S., 1965: Variability of oceanographic conditions at Ocean Station "P" in the northeast Pacific Ocean. *Trans. Roy Soc. Can., Ser 4*, **3**, 367-418.

Talley, L. D., 1985: Ventilation of the subtropical north Pacific: The shallow salinity minimum. *J. Phys. Oceanogr.*, **15**, 633-649.

Taylor, G. I., 1921: Diffusion by continuous movements. *Proc. London Math. Soc.*, **20**, 196-212.

Thomas Jr., G. B., 1972: *Calculus and Analytic Geometry*. Alternate Edition. Addison-Welsey, 1034 pp.

Walton, C. C., 1985: Satellite measurement of sea surface temperature in the presence of volcanic aerosol. *J. Climat. Appl. Meteor.*, **24**, 501-507.

Washburn, L., D. C. Kadko, B. H. Jones, T. Hayward, P. M. Kosro, T. P. Stanton, S. Ramp, and T. Cowles, 1991: Water mass subduction and the transport of phytoplankton in a coastal upwelling system. *J. Geophys. Res.*, **96**, 14927-14945.

Weller, R. A., and R. E. Davis, 1980: A vector measuring current meter. *Deep-Sea Res.*, **27**, 565-582.

INITIAL DISTRIBUTION LIST

		No. Copies
1.	Defense Technical Information Center 8725 John J. Kingman Rd., STE 0944 Ft. Belvoir, VA 22060-6218	2
2.	Library, Code 013 Naval Postgraduate School Monterey, CA 93943-5101	2
3.	Dr. Robert H. Bourke (Code OC/Bf) Department of Oceanography Naval Postgraduate School Monterey , CA 93943-5000	1
4.	Dr. Jeffrey Paduan (Code OC/Pd) Department of Oceanography Naval Postgraduate School Monterey, CA 93943-5000	1
5.	LT John E.M. Brown, USN Naval European Meteorology and Oceanography Center PSC 819 Box 31 FPO AE 09645-3200	1
6.	Meteorology Department Code Mr/Hy Naval Postgraduate School 589 Dyer Rd., Rm 252 Monterey, CA 93943-5114	1
7.	Commanding Officer FLENUMMETOCEANCEN 7 Grace Hopper Ave., Stop 4 Monterey, CA 93943-0001-0120	1
8.	Technical Director Naval Research Laboratory 7 Grace Hopper Ave., Stop 2 Monterey, CA 93943-5502	1

9.	Director, Naval Oceanography Division Naval Observatory 34th and Massachusettes Avenue NW Washington, DC 20390	1
10.	Commander Naval Meteorlogy and Oceanography Command Stennis Space Ctr, MS 39529-5000	1
11.	Technical Director Naval Research Laboratory Stennis Space Center, MS 39529-5004	1
12.	Commanding Officer Naval Oceanographic Office Stennis Space Ctr Bay St. Louis, MS 39522-5001	1
13.	Library Scripps Institution of Oceanography P.O. Box 2367 La Jolla, CA 92307	1
14.	Professor Pearn P. Niiler Code 0230, Scripps Institution of Oceanography University of California, San Diego La Jolla, CA 92093-0230	1
15.	Library Moss Landing Marine Lab California State Colleges Sandholdt Road Moss Landing, CA 95039	1
16.	Library Hopkins Marine Station Stanford University Pacific Grove, CA 93950	1

17. Dr. Jean Rolland — 1
Centre de Meteorologie Marine
BP70
29263 Plouzane Cedex
FRANCE

18. Dr. Steve Ramp — 1
Office of Naval Research
Code 332PO
800 N. Quincy Street
Arlington, VA 22217-5660

19. Dr. Mark Swenson — 1
NOAA/AOML
4301 Rickenbacker Causeway
Miami, FL 33149

20. Director Naval Oceanography Division — 1
Naval Observatory
34th and Massachusetts Avenue, NW
Washington, DC 20390

21. Chief of Naval Research — 1
800 N. Quincy Street
Arlington, VA 22217

22. Library — 1
Department of Oceanography
University of Washington
Seattle, WA 98105

23. NOAA Library — 1
7600 Sand Point Way, NE
Building 3
Seattle, WA 98115

24. Library — 1
CICESE
P.O. Box 4803
San Ysidro, CA 92073

25. Library 1
College of Oceanography
Oceanography Admin. Bldg. 104
Oregon State University
Corvallis, OR 97331

26. Commander 1
International Ice Patrol
Avery Point
Groton, CT 06340

27. Commanding Officer 1
Naval European Meteorology and Oceanography Center
PSC 819 Box 31
FPO AE 09645-3200

28 Dr. Armando F. G. Fiusa 1
Grupo de Oceanografia
Faculdade de Ciencias da
Universidade de Lisboa
Rua da Escola Politechnica, 58
1200 Lisbon
PORTUGAL